# Application of Multiple Suppression Strategies in Glacially Overconsolidated Sediment margin in Weddell Sea Embayment.

Master Thesis MSc Marine Geosciences

Department of Geosciences

University of Bremen

By

Jude Castelino

Bremen,  2012

Universität  Bremen

AWI
Alfred-Wegener-Institut
für Polar- und Meeresforschung

**Supervisor** : Prof. Dr. Wilfried Jokat
Alfred Wegner Institute for Polar and Marine research

**Co-supervisor**: Dr. Benedict Preu
University of Bremen

**Declaration acc. to § 22 Abs. 9 Allg. Teil d. Master-PO**


I hereby declare that I wrote my Master thesis independently and that I did not use other sources and auxiliary means than the ones indicated.
I further declare that the Master thesis **might be / might not be**\* made available to the public in this version.




Place / Date : _____




Signature : _____

# Abstract

Several Multiple attenuation strategies have been developed over decades to improve the quality of marine seismic data images. This thesis presents the results of different multiple attenuation strategies in over-consolidated glacial sediment along the Antarctic coast in Weddell Sea region.

The shelf along the Weddell Sea is sediment filled basin that is several kilometers thick (Huebscher et al, 1996). The sediments are strongly over-consolidated due to glacial loading and erosional features from ice streams like furrows and lineations are visible (Stolldorf, 2012). The subsurface across the shelf is characterized by different geological features like strongly folded sediments, faults , dipping horizons, uniform and chaotic sedmentation.

In general, it is observed that methods based on move-out time depends on the maximum offset of the receiver. The far-offset distance should be at least four times the depth at which the multiples are to be suppressed.

F-K filtering is a very efficient method to suppress first and second order multiples at intermediate water depths (~500 m) but has to be accompanied by alpha-trim stacking in order to minimize contribution of strong amplitudes of multiples from far-offsets that are poorly suppressed. It is not very effective in suppressing subsurface multiples and higher order multiples because the distance of far-offsets is not enough to separate them, in addition to small signal to noise ratio (SNR). F-K filtering does not have a negative impact on other pre-stack processes like migration, which has been demonstrated in the strongly folded sections of the profile. If not, it would only improve the results of pre-stack migration.

Parabolic Radon transformation is very effective in suppressing multiples and significantly improves the signal to noise ratio giving excellent results at greater depths. The results can be further improved by a more accurate velocity model . However, this method is ineffective in suppressing very strong multiples from the seafloor due to imperfect inverse transform, besides being very expensive in terms of processing time, which limits the practical application of the method.

In a CDP gather with large offsets, predictive deconvolution method can be applied only in Radon domain because of lack of periodicty in time-offset domain. It works very well to suppress short period multiples related to ghost and 'bubble effect' although attenuation of multiple seafloor reflection is very weak owing to the distortion of the seismic signals propogating through long distances in large water depths. However, deconvolution prior to other multiple suppression methods gives improved results.

Wavefield extrapolation predicts the multiples very well however it lacks a good algorithm to adaptively subtract lower order multiples from the original data . The higher order multiples are almost completely suppressed. It may lack a good correlation to scale the predicted data to subtract it without affecting the primaries. Using a suitable gain function might improve the results. Another possiblity, is the approximations of acquisition geometry might significantly influence results in shallower depths.

A combination of methods improves the results where weakness of one method is compensated by the other. SRME applied to seismic data after predictive deconvolution provide the best results. With a 2600 m long streamer, multiple suppression in parabolic Radon domain provides the best results for depths up to 1500 m, where the move-out time of multiples can be distinguished from primaries.

Post multiple suppression, more subsurface structures can be delineated. On the flanks of the basin, sediment layers continue to dip towards the centre of the basin, while they are approximately horizontal in the centre of the basin. The eastern margin of the basin shows conclusive evidence of stress regime related to extensional tectonics of a stretched crust, in agreement to the geodynamic model proposed by Storey et al (1991), Huebscher et al (1996), Studinger & Miller (1999).

# Table of Contents

# Table of Figures

# Chapter 1.    Introduction

Seismic reflection surveys are a very efficient and and non-intrusive method of imaging the subsurface. A combination of sources and receivers record reflections at the interface of inhomogeneities. Seismic data processing strategies and results are strongly dependent on acquisition set up and environmental conditions. In addition to important geological information from the subsurface, it also records artifacts and other unwanted signals termed as noise. Seismic processing is aimed at focusing energy to its accurate position in space while at the same time minimising the effects of noise to give a superior image of the underlying features. While some artifacts can be removed with standard processing techniques, some others like multiple reflection events need specialized procedures and experience that are location specific. Although several strategies have been designed to suppress multiples, they are very specific in nature and cannot be applied in every situation. The objective of this work is to provide results of multiple suppression on seismic profiles acquired along a glacially consolidated sediment margin in the Weddell sea region. Surface velocities up to 2800 m/s have been measured at the seafloor and underlain by several kilometers thick sediments that have been subjected to different tectonic and geological processes. The primary aim of this thesis is to find an optimal method using a combination of different seismic data processing methods to obtain a true represention of the subsurface at the maximum depth without compromising on quality and reliability of the dataset.

## 1.1. Problem of Multiples in marine seismic acquisition:

Standard seismic data processing assumes that only upward propagating scattered energy that has been reflected only once in the subsurface is recorded by the receiver (Fig 1.1a). In practice this assumption does not hold true as every interface acts as a reflector irrespective of the direction of propagation. In other words, a propagating wave undergoes several reflections at every interface, most of which is recorded by a hydrophone.

Multiple reflected events can be classified into different categories as described by Verschuur (2006). Some of the important types of multiples briefly described in the following sections.
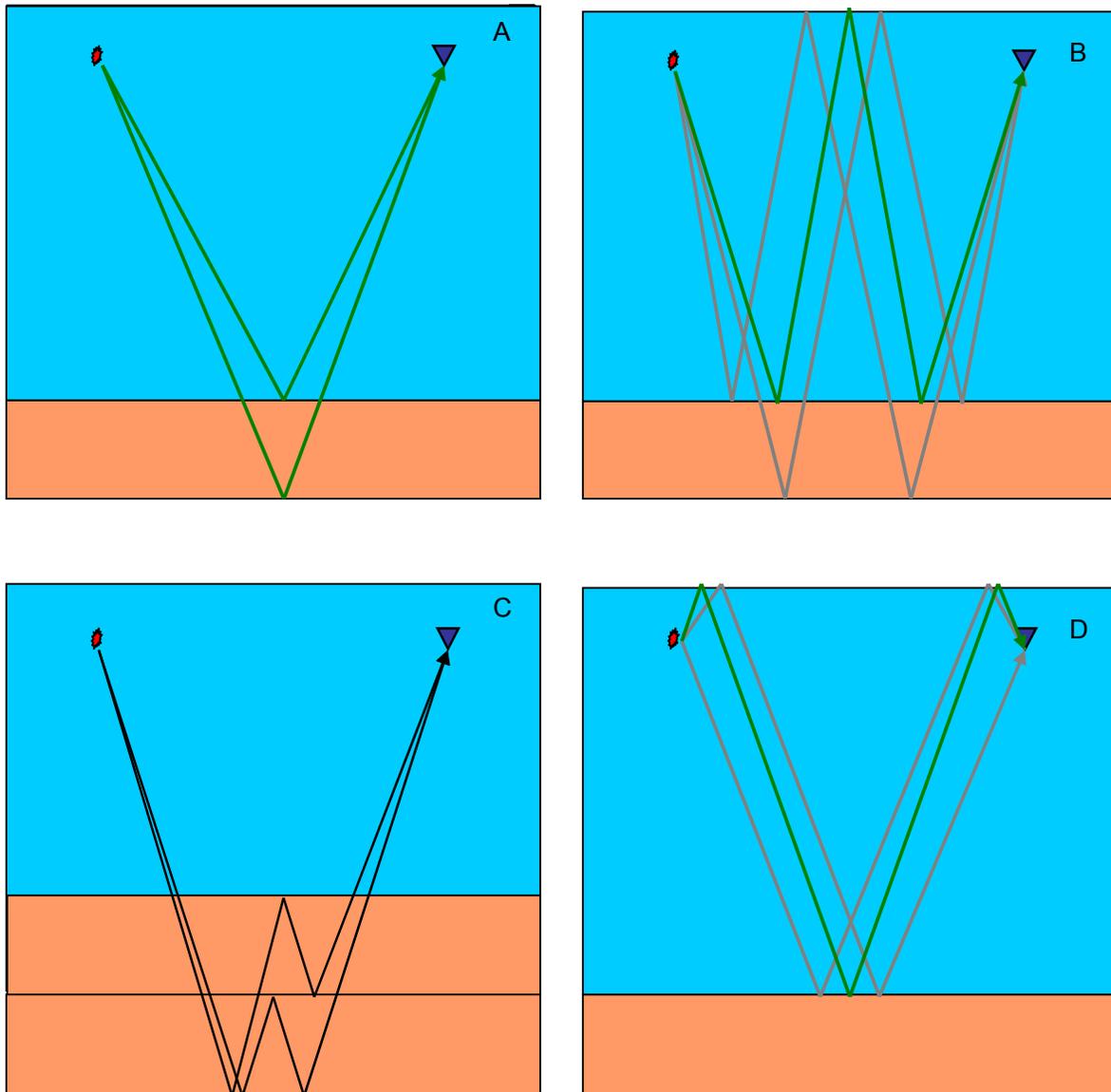
Figure 1.1: Reflections of sound waves travelling through different media in seismic acquisition setup. a) Primary reflections have only one upward reflection. b) Surface related multiple reflection are reflected at least once at a given surface (in this case seafloor). c) Internal multiples reflect downwards in the subsurface. d) Ghosts reflect at least once at the sea surface either close to source or receiver(grey) or both(green).

### 1.1.2. Surface related multiples (SRM) :

Surface related multiples are reverberations between two interfaces of homogenous layers. One of the most common and strongest form of noise in marine seismic data are multiples produced by reverberations in the water layer. Primary signals are reflected at least once at the sea surface where the phase of the signal is reversed and followed by a reflection at the sea floor (Fig 1.1b). The signals maybe be reflected multiple times between the sea surface and seafloor. It can be easily recognized in a CDP gather as events with velocities similar to the water layer and occur at constant intervals of the seafloor depth in a stacked profile. A generalized concept can be extended

to any layer below the seafloor and is, therefore, termed as surface related multiple. In the course of this thesis, SRM shall refer to subsurface events with water layer reverberations only (grey coloured travel path in Fig 1.1b) . To distinguish SRM  from pure water layer reverberations (sea surface – seafloor), it shall be referred to as sea-bottom multiples (green colour travel path in Fig 1.1b). Other kinds of surface related multiples produce minimal or no contributions and are therefore not discussed further.

### 1.1.3. Internal multiples

Internal multiples are generally short period multiples that undergo multiple reflections in the subsurface (Fig 1.1c). They are also sometimes refered to as inter-bed multiples. The problem of internal multiples are not observed in the dataset used in the thesis but they are commonly observed in presence of salt domes. Higher order multiples are too weak and, therefore, the problem does not need to be addressed here.

### 1.1.4. Ghosts

These multiples are observed with a short time lag, in the order of a few milliseconds,  after the primary. It travels directly from the source to the sea surface, where it is reflected. Sea surface is almost an ideal reflector. Energy propogating through the water column has a density of 0.996 g/cc while the air above the sea is 0.0013 g/cc. This sharp density contrast results in a reflection coefficient of -0.994 at normal incidence for sound traveling with a velocity of 1500 m/s and 340 m/s through water and air respectively, in other words almost everything is reflected with a phase reversal (Fig 1.1d). Ghost signals can be used to an advantage by lowering the source  below the sea surface in a way that the convolution of primary and ghost amplifies the reflection events. For frequency of 30 hz and water velocity of 1500 m/s, a source located at a depth of 12.5 m positively convolves with the primaries.

### 1.1.5. Bubble pulse

The seismic source in marine data is produced by a sudden release of highly compressed air released into water. The compressed air released in the water, undergoes a sudden expansion and is followed by compression when the water pressure exceeds the pressure in the bubble,  in a oscillatory process. The oscillations produce additional signals that lags by a few tens of milliseconds creating multiple seismic source signals successively. The effect of bubble pulse is not a multiple reflection event in its true definition but has the characteristics of a multiple that needs to be addressed. In the Weddell Sea dataset, reflections from a bubble pulse follow with an approximate lag of 180 ms (Fig 1.2).
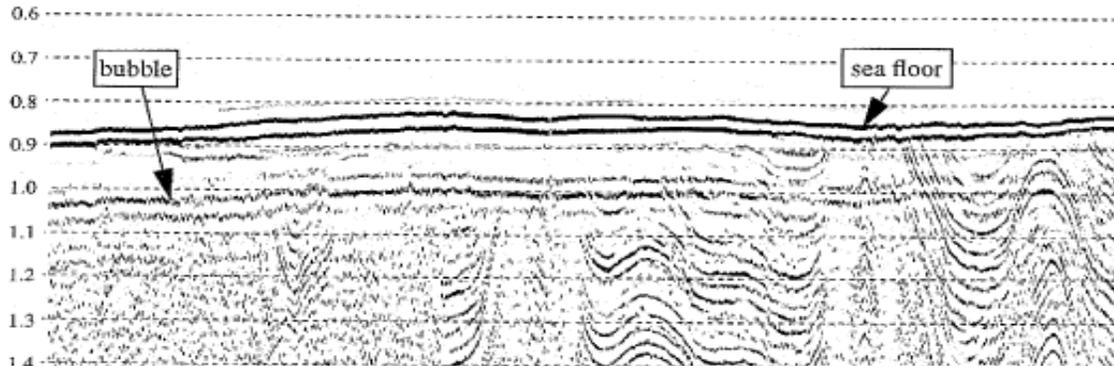
Figure 1.2: Seismic profile from Weddell Sea showing bubble pulse signature of the seafloor. Note the lag of 0.18 s of the bubble pulse after the seafloor.

## 1.2. State of the art

Multiple suppression methods can be categorized by the principle used in the algorithm applied. They can be broadly classified in to 3 groups: move-out time difference between primary reflections and secondary reflections, prediction of multiples based on the characteristic of periodicity and similarity of multiples and extrapolation of primary signals to reconstruct multiples recorded in subsequent traces and subtracting them from the original profile .

Understanding the need for suppressing multiples in the early days, multichannel processing was employed to discriminate noise from desired signals (Mayne, 1962). Since a simple stacking was not sufficient, processing strategies involved data transformation to alternative domains where it is possible to discriminate and filter noise from desired signals more efficiently and accurately.

The aforementioned methods based on move-out time difference, mostly, yield better results when performed in domains other than Time-Offset (X-T) domains. Some of the most commonly used domains are frequency- wave number (f-k) and Radon domains where primaries and multiples map to a different space because of their different move-out time.

Even earlier in 1950's , Robinson (1954) developed a filter to remove repetition effect of multiples by decomposition of recorded signals based on statistical methods. Although designed for a single fold seismic acqisition, this method has been developed further and adapted to work in multi-channel gather in different domains.

In recent years, wavefield extrapolation (SRME) has received a lot of attention as a very promising tool for multiple suppression. The advantage of SRME is that it needs no auxiliary data and that it uses the recorded data to predict multiples and adaptively subtract them from the original dataset.

Multiple suppression methods do not come without limitation. Each method makes some assumptions and is effective only when it is compatible to the preconditions. Acquisition parameters, geometry of the entire set up, physical properties of the medium and geological features, all play a very important role in the success or failure these methods.

## 1.3. Motivation

The paleopositions of micro plates in West Antarctica during the break up of Gondwana and their subsequent movement has been a subject of major controversy. While there is a good concensus on the geodynamic models that describe the separation of Antarctic from India, Africa and other masses, there is not much agreement on one single model that places microplates and smaller crustal blocks around the Weddell Sea region during the break-up of Gondwana (Grunow, 1987; Storey et al, 1996). Lack of constraint for the crustal structure and incoherent spreading anomalies makes the description of early break-up difficult (Jokat et al, 1996) . Being highly inaccessible with extreme weather conditions, geophysical measurements are few and restricted (Anderson et al, 1992, Sloan et al, 1995, Fechner and Jokat, 1995). During the Antarctic summer of 1994-95 , an expedition was organized to gather geophysical data to constrain support geodynamic models of the region. A rare sea-ice condition provided an opportunity to conduct a seismic reflection experiment along the Filchner- Ronne Iceshelf, very close to the ice-edge (Jokat and Oerter, 1997). Deeper sections of the profile are masked by strong multiples that prevents from providing more conclusive information on the crustal characteristics under the Filchner-Ronne Shelf ( Jokat et al, 1996).

Multiple suppression in glaciated margins, in general, is very challenging because of consolidated sediments that produce very strong multiples. Most studies try to ignore multiples in their interpretation whenever possible. With surface velocities in the range of 2.2 and 2.8 km/s and approximate densities of 2.2 g/cm$^3$ , the reflection coefficient at the water-sediment interface is approximately 0.66. In comparison to open ocean condition, the reflection coefficient would be approximately 0.3.

The primary objective of the thesis is to reveal new information, by suppressing multiples, that would contribute to the  constraints of geodynamic model of Weddell Sea. In addition, it would provide a guideline for future work to attenuate strong multiples in over-consolidated marine sediments.

## 1.4. Study Area

### 1.4.1. Geography

The Weddell Sea is a deep embayment of the Antarctic forming the extreme southern part of the Southern Ocean in the Atlantic sector. It is bounded by the eastern coast of the Antarctic Peninsula to the west,  Filchner-Ronne ice shelf to the south, by Coats Land and  Dronning Maud Land to the east and is separated from the Scotia Sea by South Scotia Ridge in the North. It is generally ice covered, extending several hundred kilometers to the north that makes ship navigation particularly difficult even during summer.

### 1.4.2. Glacial Setting

The Antarctic ice sheet comprises of $30 \times 10^6$ km$^3$ of ice that covers an area $13.6 \times 10^6$ km$^2$ (Denten et al, 1991) . The ice mass is divided in East Antarctic Ice Sheet (EAIS), which is a terrestrial ice sheet that is  more or less stable (Anderson, 1999).  West Antarctic Ice Sheet (WAIS) is mostly of marine ice sheet and very dynamic (Anderson, 1999). The drainage pattern of both EAIS and WAIS are convergent in the Filchner-Ronne and Ross ice shelves (Fig 1.3) creating rapidly flowing ice streams.  Three ice streams (denoted by A, B and C in Fig 1.3) flow into the Weddell Sea forming three troughs. The Ronne trough is juxtaposed with the Antarctic Peninsula while the Hughes and Filchner trough lie on either side of  Berkner Island (Fig 1.3).
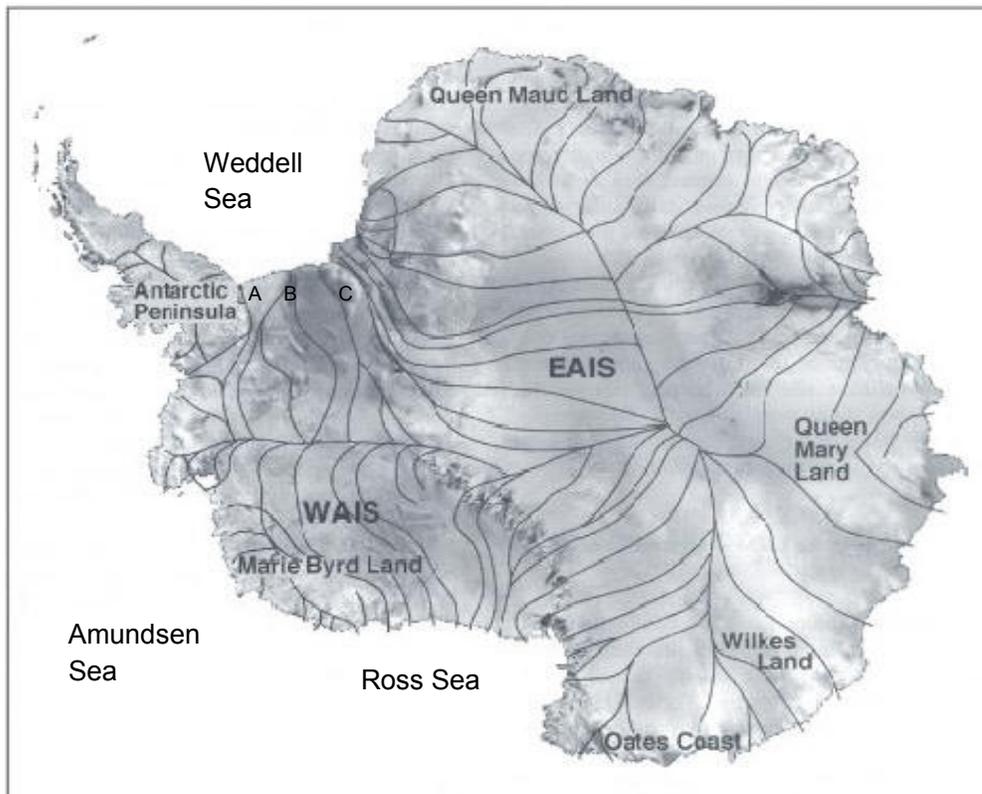
Figure 1.3: Drainage map for Antartica. Ice streams indicated by A, B and C debouch into Weddell Sea forming Ronne, Hughes and Filchner trough. Several ice scours are also observed on the seafloor besides the Filchner-Ronne ice shelf that were caused by flowing ice streams (modified from Bentley 1964)

The gentle subsurface profile of WAIS in comparison to the EAIS, might indicate that WAIS flows and ablates faster than its counterpart in EAIS. Basal sliding and 'wet based' glacial models (Hughes 1973,1977,1981) have been suggested that are supported by conditions in WAIS. Melt water might exist as a thin film under immense preesure at the base of ice sheets (Weertman, 1972) or there might be channelized water systems beneath the ice sheets (Hughes 1981). Alternatively, it could be accommodated in the sediments underlying the ice sheets. Geomorphological features and subglacial sediments could determine the relationship between ice sheets, ice streams, sea level that influence these features.

### 1.4.3. Geology and Tectonic setting

The prograding wedges of glaciogenic sediments along the entire margin, a major trough-mouth fan (Crary Fan) and numerous sediment drifts on the slope and in the deep basin are the main features in the Weddell Sea (Cooper et al, 2009). Ice-sheet flow pattern indicate that the EAIS and WAIS are the main source for drainage east and west of 45° W respectively (Cooper et al, 2009).

Sedimentary processes in the southern Weddell Sea are influenced by glacial-interglacial ice-shelf dynamics and the cyclonic circulation of the Weddell Gyre. The prograding shelf around the

Weddell Sea is more than a kilometer thick below the shelf ice and downlaps onto older units of uniform thickness (Cooper et al, 2009).
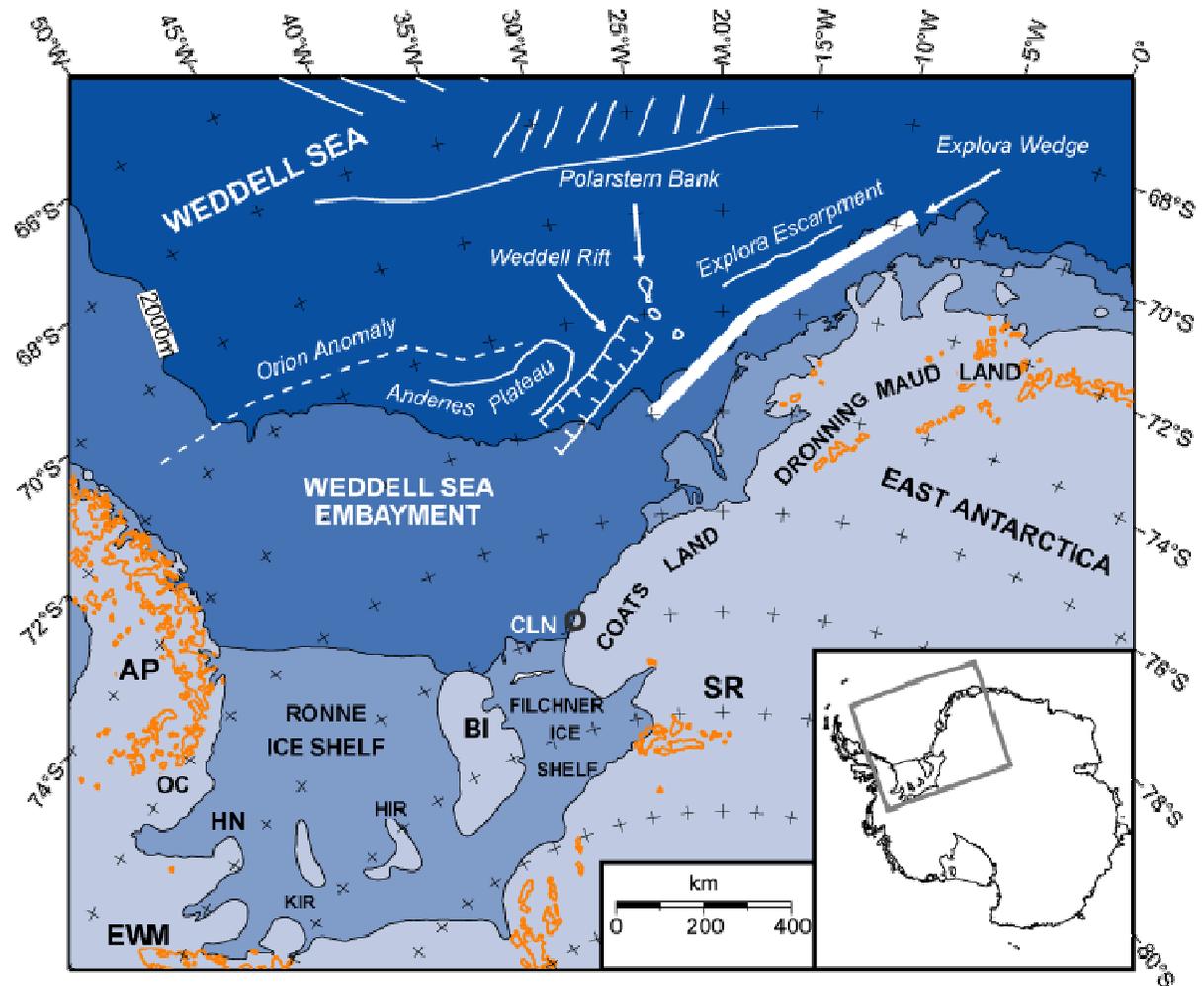


Figure 1.4: Tectonic feaures of the Weddell Sea and surrounding areas. Abbreviations are: AP, Antarctic Peninsula; BI, Berkner Island; CLN, Coats Land Nunataks; EWM, Ellsworth Whitmore Mountains; HN, Haag Nunataks. (modified from Studinger et al, 1999)

Antarctic Peninsula:

The Anatarctic Peninsula (AP) is  primarily a Mezozoic magmatic arc (Pankhurst, 1982) that was formed by the subduction of Pacific and proto-pacific ocean floor under the eastern margin of West Antarctica. There is a wide accretionary complex on the fore-arc side (Storey and Garrett 1985) and a thick sedimentart sequence in the back-arc region. The AP was deformed by a wide ductile shear zone related to the tectonic evolution of Weddell Sea region (Anderson, 1999).

Ellsworth- Whitmore mountains:

One of the five main crustal blocks, EWM is a 13km thick sedimentary succession of Cambrian - Permian origin folded during the Permian-Triassic Gondwanian orogeny (Webers, 1982) intruded by Mid-Jurassic break-up related granites (Millar and Pankhurst, 1987). Geophysical evidence

suggests that these mountains are a part of Gondwanian Cape fold belt of southern Africa (Schopf 1969, Dalziel and Grunow 1992). However, break up models of Gondwana suggesting transition of EWM to its present position is still debated.

Haag Nunataks:

This crustal block is formed of Proterozoic basement of Grenvillian Rb-Sr whole rock (Millar and Pankhurst 1987) that may extend into parts of the Weddell Sea region (Maslanyj and Storey, 1990).

East Antarctic craton

The East Antarctic craton can be divided in to 3 basement provinces viz., the Grunehogna province which consists of Archean granitic gneisses, the Maudheim province which consists of Proterozoic high grade metamorphic rocks and Shackleton Range that consists of Paleo to Mesoproterozoic magmatic and metamorphic rocks (Storey et al. 1994). The basement rocks are unconformably overlain by Devonian and younger sedimentary rocks and intruded by parts of middle Jurassic flood basalt province related to Gondwana break-up.

Gondwana Break-up Models

The Weddell Sea embayment lay at the centre during the break-up of Gondwana with concurrence of several Large Igneous Provinces (LIP). The position of microplates and their movements within the Weddell Sea region has very controversial, in particular, the paleoposition of EllsWorth Whitmore Mountains – Haagnunataks – Falkland Islands. While some scientists suggests rotational and large sinistral strike slip movement of the EWM block along East Antarctic craton (Grunow et al 1987 and Grunow 1993). This would imply that there should exist oceanic crust under the Weddell Sea and Filchner-Ronne Ice Shelf . King & Bell (1996) , Miller et al (1984), Jokat et al (1996) provide geophysical evidence of stretched continental crust that is in complete contrast to the existence of a subducted oceanic crust.

# Chapter 2.  Theoretical Background

## 2.1. Transformations and Domains

Seismic data are recorded in, what is known as, 'Time-Offset' (X-T) domain. The general purpose of transformation is to map the signals in a domain where different events can be clearly separated. In this case, multiples are separated from primaries followed by filtering algorithms that eliminate multiples. It should be noted that transforming back and forth has a smoothening effect and may introduce artifacts because approximations are used during the transformation process. In this section, transformations that are commonly used in seismic data processing are introduced and its advantages and limitations are briefly discussed.

### 2.1.1. Frequency – Wave number (F-K transform)

Fourier transform is a very widely used technique in signal processing. It is based on the principle that a complex signal can be synthesised by summing simple oscillatory functions of different frequencies, amplitude and phase. In short, seismic signals are transformed from X-T domain to frequency domain where it is separated into individual frequencies .

F-K transformation is also known as double Fourier transformation. As the name suggests, the signal is transformed twice. In the first step, the data are transformed  to a temporal frequency domain *(f)* defined by

$$D(x,f) = \int_{-\infty}^{\infty} d(x,t)e^{-j2\pi f}dt, \qquad\qquad 2.1$$

In the second step a fourier transform over spatial coordinate (K) is performed which is defined by

$$D(k_x,f) = \int_{-\infty}^{\infty} D(x,f)e^{+j2\pi k_x x} dx, \qquad\qquad 2.2$$

where f is temporal frequency and k is horizontal wave number or spatial frequency. F-K transform can be looked upon as decomposing a plane wave into monochromatic signals and angle of arrival. Figure 2.1 shows a monochromatic plane wave in X-T domain mapping to a single point in F-K domain. A broadband event like shown in Figure 2.2 maps to a line in F-K domain.  It is important to note that F-K transform is a reversible process, in other words, it is possible to map F-K events into X-T domain by simply using inverse transformation.
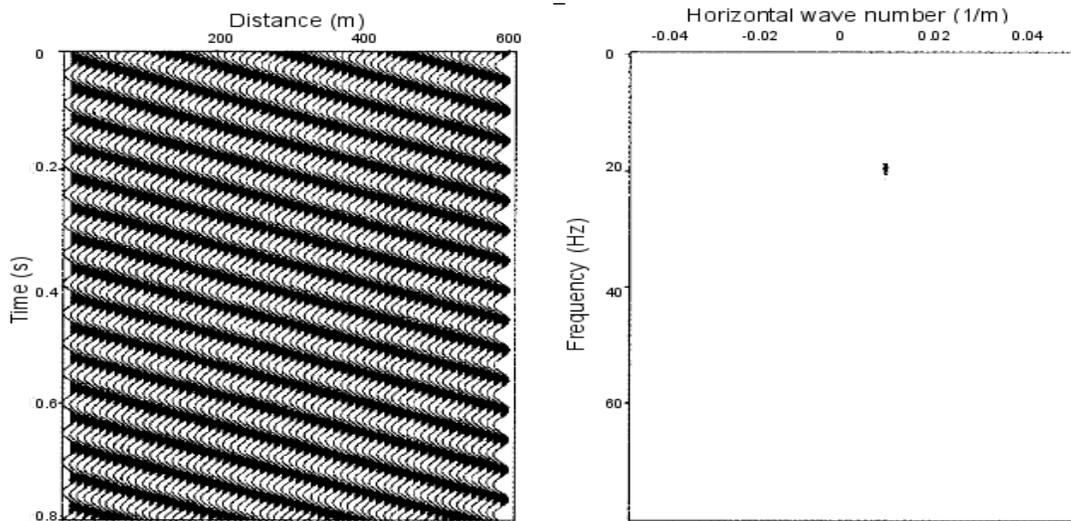
Figure 2.1: F-K tranformation of a monochromatic wave in X-T domain maps to a  in F-K domain. (a) is a uniform dipping event with a frequency of 20 Hz, (b) is a result of tranforming (a) to F-K domain.Note that a monochromatic signal with a constant dip maps to a single point  (modified from Verschuur 2006).
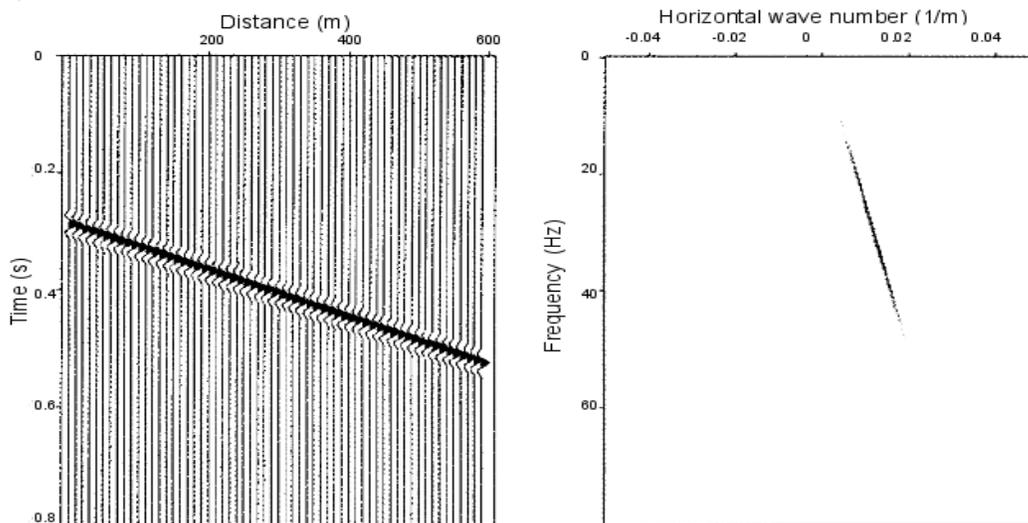


Figure 2.2:  F-K Transformation of a broadband wave with single dipping in the X-T domain  to F-K domain. Fig (a) is a uniform dipping event with a frequency range of 15 - 50 Hz and (b) is the result of the transformation. Note that a uniform dipping event maps to a straight line after a F-K transformation  (modified from Verschuur 2006)

## 2.1.2. Radon Domain

Radon transformations attempt to discretize input signals into individual events, similar to F-K transformation but using more complex relationships. The decomposition is based on propagation velocity differences and, therefore, is very effective in separating primary events from noise, in this case multiple reflection. Transformations can be achieved by both linear or non-linear relations. The amplitude is summed along the transformation function parameter 'p' against the intercept

time τ and the geometry of the output depends entirely on the type of transformation . The offset axis is replaced by ray parameter p axis and the time axis is replaced by new time axis τ which represents the summed up energy at that depth.

**Linear Radon Transformation.(Slant-stack or Tau-P)**
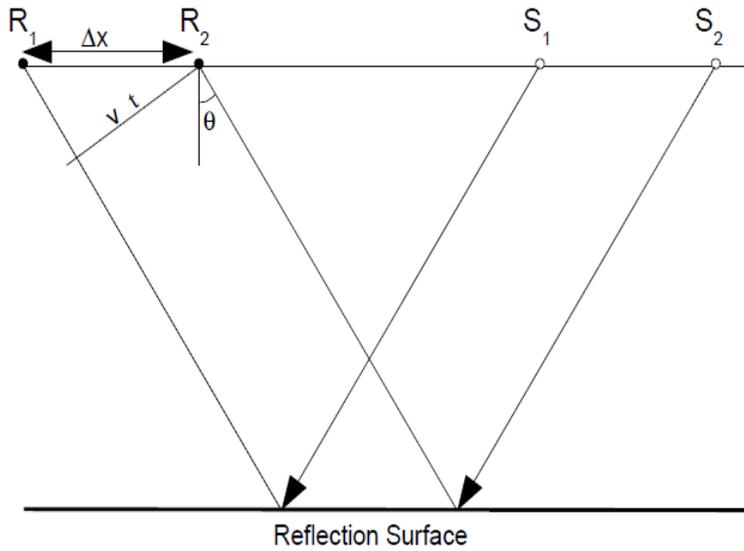


Figure 2.3: A plane wave traveling with a velocity v at angle θ. S1 and S2 are sources of seismic signals while R1 and R2 are receivers.

Each trace is reconstructed as plane wave that travels along a specific angle as described by the ray parameter. For near offsets, the angle of propagation is smaller as compared to the far offset, for example it is zero for zero-offset. Figure 2.3 shows the ray path for a wave propagating along an angle θ. If one imagines that each point source is activated at successively after time Δt then the inverse  horizontal phase velocity , i.e. , the ray parameter is given by the relationship.

$$p = \Delta t \, / \, \Delta x.$$  2.3

The Y-axis is plotted to intercept time which is defined by the relationship
$$\tau = t - px$$  2.4

To apply the above principal we consider a CDP gather with a single hyperbolic event. Points A and B map to an ellipse in the slant stack domain as can be seen in figure 2.4.
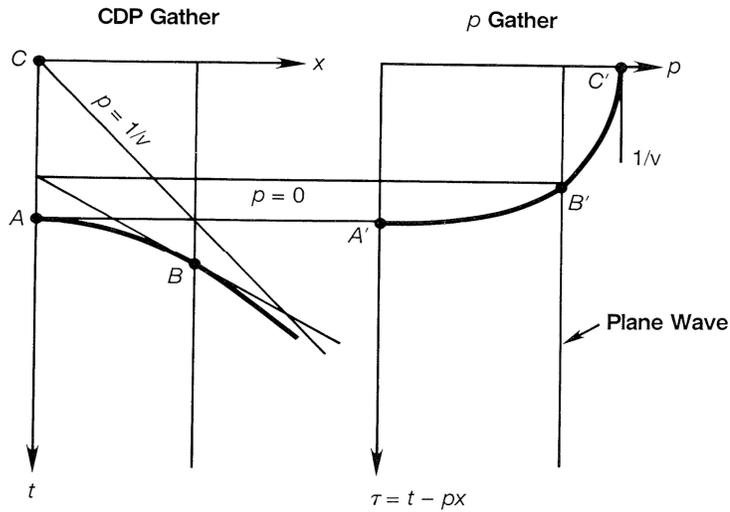
Figure 2.4: A single hyperbolic event in X-T domain transformed to slant stack domain maps to an ellipse.(modified from Yilmaz, 1987)

Mathematically , linear radon transformation function is given by :

$$m(p, \tau) \int_{-\infty}^{\infty} d(x, t = \tau + px) \, dx \qquad\qquad 2.5$$

where p defines the dip of the straight line along which the amplitude is summed along. It is important to note here that the seismic events mapped perfectly (p-intercept at 1/v) only if they are sampled for all offsets.  In practice, it is not possible to map all the offsets and therefore the ellipse ends abruptly depending on streamer length and depth of the seismic event.

**Parabolic and hyperbolic  Transformation:**

Instead of using linear functions, one can use curved functions to describe seismic events. The advantage of this method is that primaries and multiples map in different areas without overlap. One such method is describing the curve with a parabolic or hyperbolic function.

A parabolic shape can be described by

$$m\,(q, \tau) = \int_{-\infty}^{\infty} d(x, t = \tau + qx^2) dx \, , \qquad\qquad 2.6$$

or a hyperbolic function is described by

- 13 -

$$m(v, \tau) = \int\limits_{-\infty}^{\infty} d(x, t = \sqrt{\tau^2 + \frac{x^2}{v^2}}) dx \qquad\qquad 2.7$$

where q and ν is referred to as the parabolic and hyperbolic curvature parameter respectively.
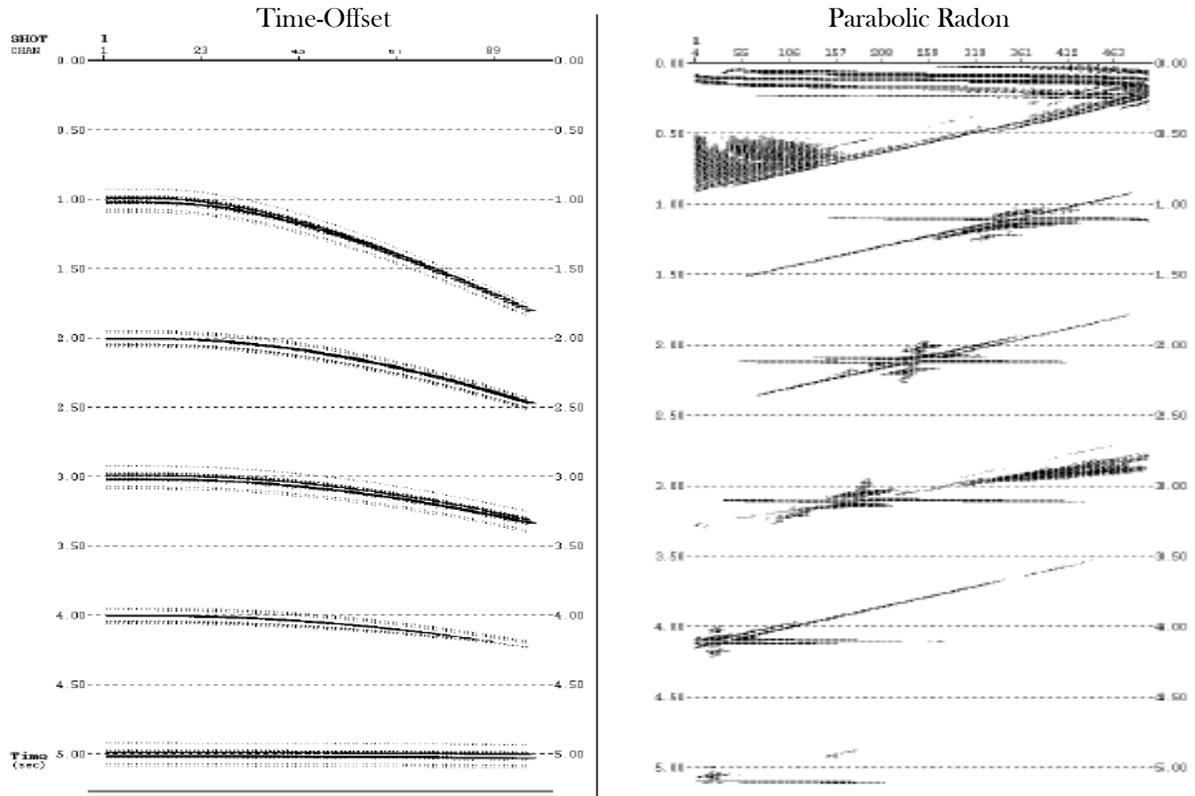


Figure 2.5: Transformation of seismic events from X-T to Parabolic radon transformation.

One of the major problems of Radon transformation is the inverse function , i.e., to map events back into the X-T domain. Inverse transformation creates artifacts that are not ideal. Hampson (1996) proposed a least-squares function to optimise the data in the parabolic Radon domain by reducing the difference between input and reconstructed data measured by rms values. For an efficient implementation, inversion is performed per frequency component as parabolic Radon transformation has an advantage that can apply inversion independently per frequency component.

## 2.2. Predictive Deconvolution

Mathematically, two or more signals can be combined to create a new signal and this process is know as convolution. The process of reversing the convolution process, i.e., decomposing a signal into its original components is known as deconvolution.

The problem with multiples in seismic data can be looked upon as superimposition of multiple events on primary events. Some of the  basic assumption made are

1.  Primary signals are not periodic like multiple events.
2.  Multiple events have a high correlation with its corresponding primary event.
3.  Multiples occur at constant intervals (integral multiples of water depth).
4.  The source wavelet is known.

These important assumptions are not always complied with and alternative solutions are used that minimize the error resulting from approximations.

To understand the process of deconvolution, it is important to observe the properties of convolving and correlating two signals. Convolution of two signals as a function of time  described by a(t) and b(t) is described by :

$$c(t)= \int_{-\infty}^{\infty} a(t)b(T-t)dt \qquad\qquad\qquad 2.8$$
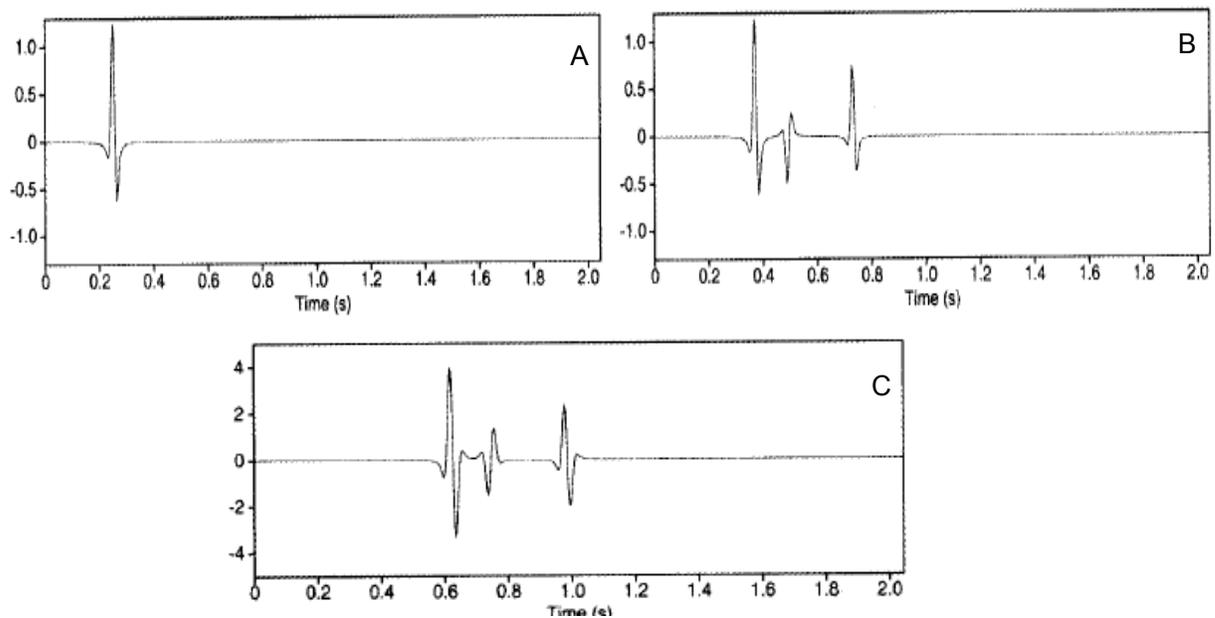


Figure 2.6: Convolution of two signals. A) is a signal with a single event B) is a signal with three events. C) is the result of convolution of A with B . Note that each event creates a new event at a time equal to the sum of the convolving event.  (modified from Verschuur, 2006)

In the frequency domain , it is a scalar muliplication

$$C(f) = A(f) \ B(f) \qquad\qquad\qquad 2.9$$

Therefore , convolution in frequency domain is commutative, i.ie. , the final product of convolution is independent of the order of the input signals. A new event is created from the combination of every event  from each input signal and the resultant source wavelet from a convolution of two signals does not resemble the input signals. . Figure 2.6 shows two signals with one and three events respectively and the result of convolution of the two signals. In terms of reflection seismic data, we consiser the seismic trace s(t) as a convolution of earth's reponse (primary signals)  e(t) with source wavelet (multiple reflected signals) w(t) , i.e.,

$$s(t) = w(t)*e(t) \hspace{8cm} 2.10$$

A noise component n(t) is added making the above equation

$$S(t) = w(t)*e(t) + n(t) \hspace{7cm} 2.11$$

To compute the earth's reflectivity from a seismic trace, an inverse method is applied. A function f(t) is designed to reduce the source wavelet to a zero-lag spike with zero width  d(t),

$$w(t)*f(t) = d(t) \hspace{8cm} 2.12$$

with a z-transform,

$$W(f) \, F(f) = 1 \hspace{8.5cm} 2.13$$

In other words eliminating it from the seismic trace leaving behind only the earth's primary response.

$$f(t)*s(t) = \; [f(t)*w(t)]*e(t) = e(t) \hspace{5.5cm} 2.14$$

Because of truncation, convolution of the truncated filter fn(t) with the wavelet will not give the desired output d(t), which is in this case $= \delta(t)$.
The actual output is

$$y(t) = f(t)*w(t) \hspace{8cm} 2.15$$

Wiener-Levinson Algorithm is used to design a filter such that there minimum error between the desired output and actual output.

**Wiener** optimum filtering involves designing a filter f(t) so that the error E between the actual output y(t) and the desired output d(t) is minimum:

$$E = \sum_i [d_i - y_i]^2 \qquad\qquad 2.16$$

$$E = \sum_i [d_i - [f(t)*w(t)]_i]^2 \qquad\qquad 2.17$$

The minimum error is attained by setting the variation of E with respect to $f_j$ to zero:

$$\partial E / \partial f_j = 0, \qquad\qquad j = 0, 1, 2, ..., (n-1) \qquad\qquad 2.18$$

Applying the last two relations we get

$$\sum_i r_{j-i} - f_i = g_i \qquad\qquad 2.19$$

Where *r* is the autocorrelation function derived from a wavelet seismogram relation . The above relation is a Toeplitz matrix and its inversion can be calculated using a Levinson procedure. In a given seismic exploration data, only the seismic trace is known and therefore we use a statistical approach based on seismogram-wavelet relation to design an optimum filter. The desired output is also unknown because of the random nature of the earth's response e(t). Hence, standard methods cannot be applied in this case . Instead, a time advanced version s(t+*a*) of the input s(t) is used where 'a' is called the prediction lag.

More information on predictive deconvolution can be found in Robinson,1954; Robinson 1957; Robinson and Treitel, 1980. Additional literature and application can be found in seismic data processing text books like Yilmaz, 1987; Brown, 1999; Sheriff, 1982.


## 2.3. Surface Related Multiple Elimination (SRME)

Figure 2.7 shows a ray-path of a surface related multiple ABC . This ray path can be split into two primary events AB and BC. Therefore, surface related multiples are nothing but convolution of two primary reflections with two constraints at point B; there is a phase reversal and Snell's law is not violated i.e., angle of emission (reflected) should be same as angle of arrival incidence.
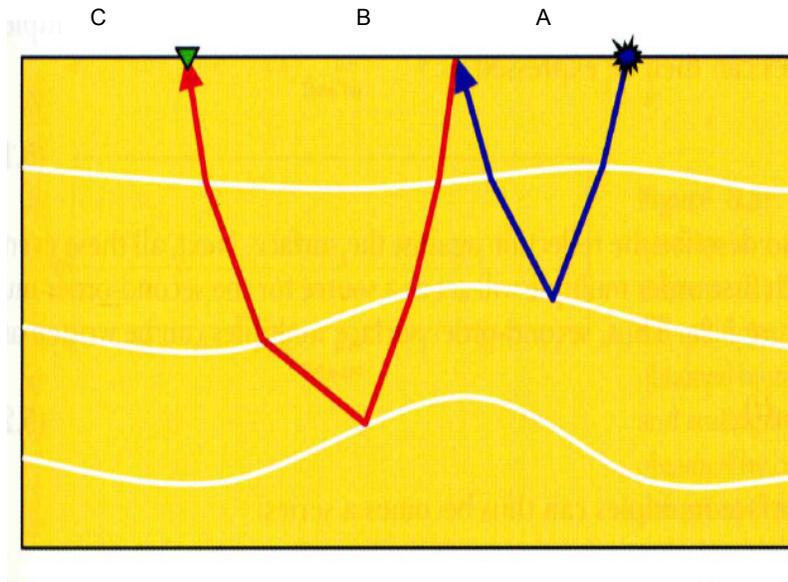
Figure 2.7: Ray path of a surface related multiple. The ray path is decomposed as combination of two primaries with first shot located at A (blue ray) and and second shot located at B (red ray) (modified from Verschuur, 2006)

To forward model all surface related multiple we consider a plane wave incident on a surface with an impulse response defined by $x_0(t)$ . If this wave is reflected from the free surface it acts as a source wave for the next roundtrip through the layer. The first order multiple is then expressed by

$$m_1(t) = - x_0(t)* x_0(t) \qquad\qquad 2.3.1$$

where the minus sign is introduce for phase reversal at air-water interface.

Extending this concept to higher order multiple , the all the events act as a source for the next round trip and is expressed by

$$m_2(t) = - x_0(t)*m_1(t) \qquad\qquad 2.3.2$$

or $\qquad\quad m_2(t)= - x_0(t)*- x_0(t)* x_0(t) \qquad\qquad 2.3.3$

The total response x(t) with all surface related multiple becomes a series .

$$x(t) = x_0(t) - x_0(t)* x_0(t) + x_0(t)* x_0(t) - \ldots. \qquad\qquad 2.3.4$$

From the above relation we can see that SRM can be constructed by convolving primary response with total response

$$x(t) = x_0(t) - x_0(t)*x(t) \qquad\qquad 2.3.5$$

In the frequncy domain it is a scalar multiplication.

$$X(f) = X_0(f) - X_0(f)X(f) \qquad\qquad 2.3.6$$

To subtract the multiples we rewrite equation 2.3.6 as

$$X_0(f) = X(f)[1-X(f)]^{-1} \qquad\qquad 2.3.7$$

The inversion term can be rewritten as a Taylor series

$$X_0(f) = X(f) + X^2(f) + X^3(f) + X^4(f) + \dots \qquad\qquad 2.3.8$$

Transforming back to the time domain gives summation of convolution.

$$x_0(t) = x(t) + x(t)*x(t) + x(t)*x(t)*x(t) + \dots \qquad\qquad 2.3.9$$

## Limitation of SRME method

Unequal source- receiver sample:

In practice, multiples are predicted by lateral convolution of seimic data with itself along the surface. It is assumed that the source and receiver have equal spacing. Irregular or coarse spacing introduces artifacts in the prediction.

Missing near-offsets:

In a typical marine seismic acquisition near-offsets are not recorded because of operational difficulties. In the dataset used here, the minimum offset is 219 m which implies 9 missing traces for a 25 m spacing. Dragoset and Jericevic (1998) have demonstrated the dramatic effect of missing near offsets in SRME.

3D effects:

SRME works on the principle of 2D extrapolation. What is not considered the contribution of geomorphic features that are not located in line with acquisition set up. Since the current dataset is a purely 2D acquisition, this problem has not solution unlike the previous problem that can be addressed by interpolation methods.

Detailed description of SRME and its application in seismic data processing can be found in Verschuur, 2006.

# Chapter 3.     Methods

## 3.1. Data Acquisition

Seismic and other data were recorded on Polarstern cruise ANT XII/3 from Cape Town to Punta Arenas during the Antarctic summer of 1994-95. The sea-ice conditions during the summer permitted ship navigation very close along the ice-edge (Jokat and Oerter, 1997). Fig 3.1 shows an overview map with recorded seismic profiles during the leg. A total of 2062 km of seismic reflection profile was recorded of which four profiles with a total length of 469 km (shown in red) along the ice edge have been processed for this thesis.
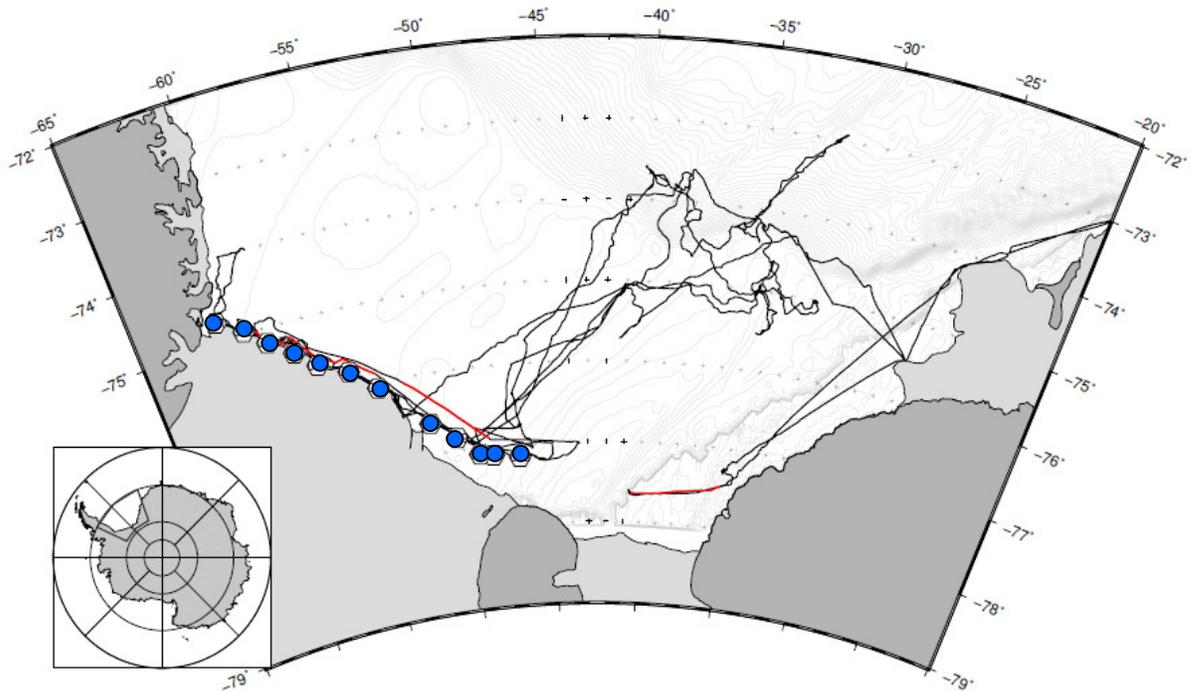


Figure 3.1:Ship trackline during Polarstern cruise ANTXII/3 (black line) . Processed seismic lines are shown in red and wide-angle refraction station in blue circle have been analysed in another thesis.   Inset: Overview map of Antarctica

| Profile number | 95060 | 95062 | 95070 | 95090 |
|---|---|---|---|---|
| **Start** | | | | |
| **Date** | 20.2.95 | 21.2.95 | 22.2.95 | 03.3.95 |
| **Time** | 23:17:45 | 14:40:00 | 14:30:00 | 00:13:15 |
| **End** | | | | |
| **Date** | 21.2.95 | 21.2.95 | 23.2.95 | 03.3.95 |
| **Time** | 13:40:00 | 22:00:00 | 06:00:00 | 13:00:00 |
| **Number of shots** | 3449 | 1759 | 3717 | 3107 |

| Length (km) | 131 | 71 | 142 | 125 |
|---|---|---|---|---|
| **Start** | | | | |
| **Lat** | 75.8873 S | 75.2075 S | 76.0559 S | 77.4720 S |
| **long** | 54.0348 W | 58.1015 W | 52.7232 W | 35.3665 W |
| **End** | | | | |
| **Lat** | 75.2023 S | 74.8496 S | 76.8870 S | 77.6328 S |
| **Long** | 57.8676 W | 59.9484 W | 48.5599 W | 40.5270 W |

Table 3.1 : Seismic profiles from leg ANT XII/3 that are to be processed.

An airgun cluster of 8 VLF-airguns with a total capacity of 24 l towed behind the ship was used as a seismic source. The airguns, controlled by the seismic recording unit, when triggered releases stored highly compressed air at 125 kP/cm³ into the water producing sound waves followed by oscillation caused by expansion-compression of the air bubble.

A 2400 m long streamer with 96 hydrophones (receivers) towed at a distance of 219 m behind the gun-array was used for recording multi-channel seismic data resulting in a maximum offset distance of 2594 m. The airguns were triggered every 15 seconds and recorded for 12 s with a sampling rate of 2 ms (Jokat and Oerter, 1997).
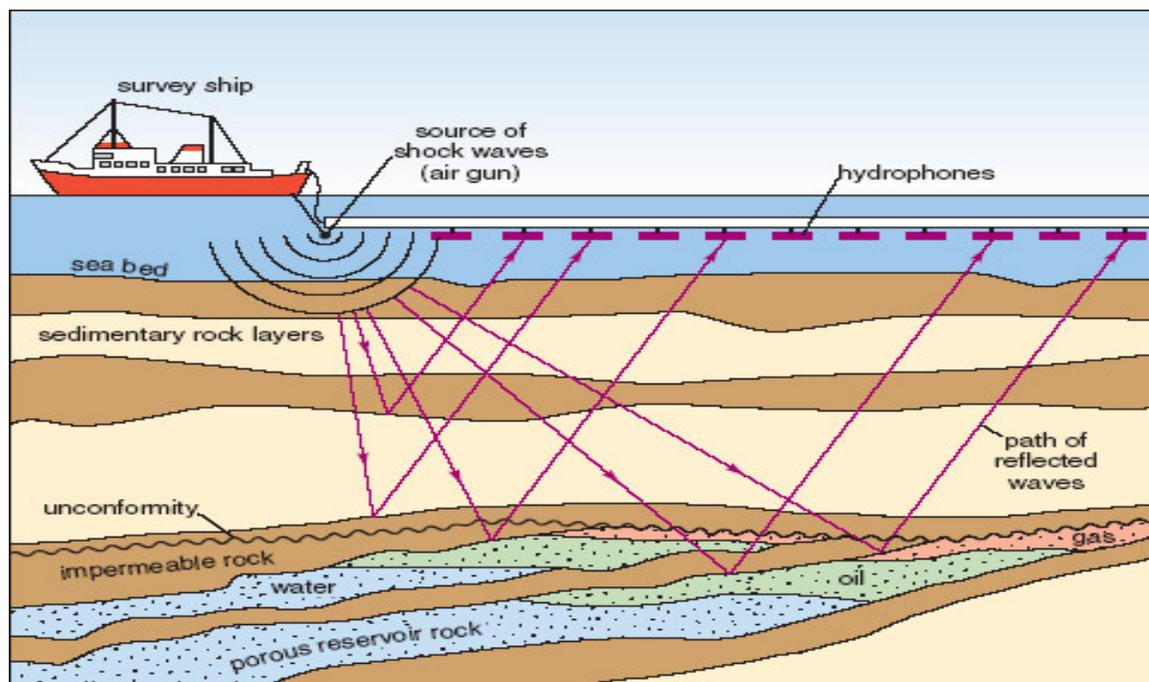


Figure 3.2 Illustration of marine seismic data acquisition. (Adapted from http://openlearn.open.ac.uk)

## 3.2. Seismic data processing

Seismic data recorded are stored in a raw format and have to be processed using standard routines before it can be used for interpretations. The data have been processed using the software 'Focus™' developed by Paradigm on 'Sun™' server. The seismic data used have been previously partly pre-processed for demultiplexing and sorted according to CDP (Common Depth Point) . However, it is briefly described in order to explain parameters selected during specific processing steps to suppress multiple events. Fig 3.3 shows standard processing flow.
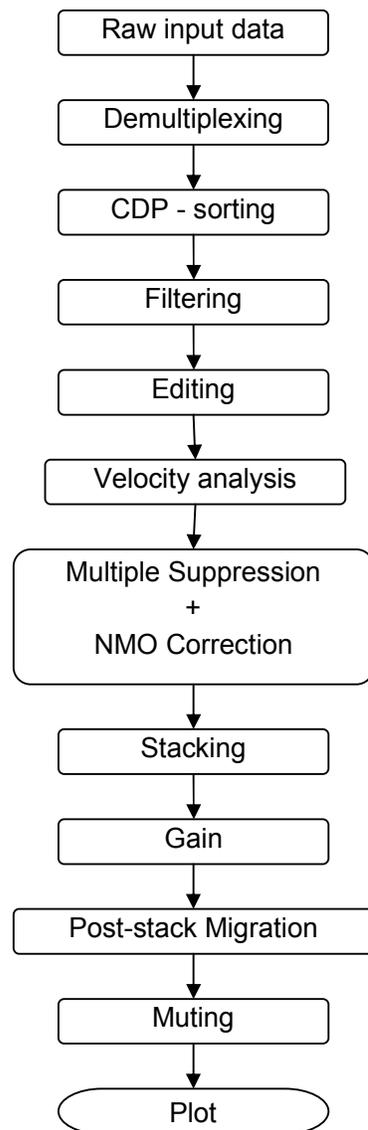


Figure 3.3: Generalized flow diagram of a standard seismic processing. Note: processes might interchanged or called more than once depending on the requirements of preceding processes like gain, muting, filtering and migration.

### 3.2.1. Demultiplexing

It is the first step in processing because field instruments samples each receiver channel successively, writing sample of each to a disktape before proceeding to the next sample in a multiplexed format. For processing seismic data it is required that they are reordered into into a more efficient sequence i.e. trace sequentional.

### 3.2.2. CDP Sorting

Once the data are demultiplexed, they have to be grouped into similar entities. Traces can be ordered in several ways such as shot number, channel number or common depth point. Most seismic routines across different software platforms require seismic data to be ordered according to their common depth point . The common reflection point is usually taken as half the distance between the source and the receiver where it is assumed that the reflecting surface is horizontal. Dipping reflectors  use different methods that are not discussed within the scope of this work. The position of the source and receiver can be calculated using the GPS locate on the ship since their relative position is more or less constant. The entire length of the profile is divided into smaller parts called bins. Each bin is considered as a single reflecting point on the surface. The dimension of the bin is based up on the number of traces 'fold' the user would like to include for further processing. The bin size is set to 25m which results in a fold of approximately 60 traces.
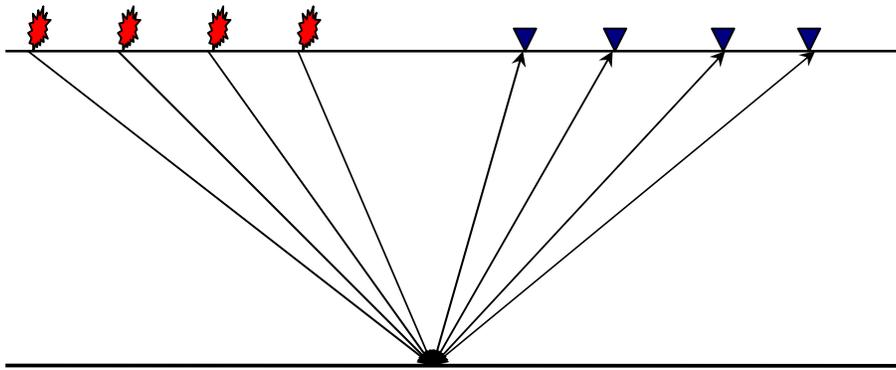


Figure 3.4. CDP gather with four traces . Reflections from the same point of successive shots (red) are recorded at different offsets

### 3.2.3. Filtering

Seismic signals contains a broad range of frequency some of which that does not originate from the source and results in a ringing effect. During the process of filtering, unwanted signal frequencies

that are recorded with the reflection events can be removed by allowing only a band of usable frequencies to pass. Frequency analysis of the signal shows that most of the energy lies between 10 and 60 hz with a peak in the range of 30-40 hz. The process of filtering already gives a more clear picture by removing high frequency noise. An Ormsby bandpass filter for 10-60 hz with 10 hz ramp on either sides used in most cases during the routine.

### 3.2.4. Velocity analysis and NMO-correction

The subsurface velocity modelling is extremely important as it plays a vital role in several seismic processing routines like multiple suppression, migration and stacking.

The arrival time of reflections from a single event from the subsurface depends on the travel path of the signals. For a reflection from a point located in the subsurface with a constant velocity, the time difference between a given offset and zero offset is called normal moveout (NMO) and can be calculated as

$$\Delta t = t(0) - t(x) = \frac{x^2}{v^2 t_0} \qquad\qquad 3.1$$

where       v = velocity through the layer

$t_0$ = total travel time for a round trip at zero offset

x = offset distance of receiver from source

For a wave travelling through multiple layer with different velocity , the root mean square (rms) is computed as

$$v_{rms} = \sqrt{\frac{v_1^2 t_1 + v_2^2 t_2 + ....}{t_1 + t_2 + ....}} \qquad\qquad 3.2$$

However, we make a simple assumption that the horizons are horizontal, i.e., the angle of incidence and reflection to the vertical are similar. This assumption would not work in case of strong dipping units and, hence, the method is not very optimal.

In Focus$^{TM}$, velocity analysis is performed using VELDEF module. It provides an interactive option to select best fitting hyperbola defined by rms velocity. Picking of velocity is assisted by a semblance of coherent trace energy (Fig 3.5).

Velocity analysis is done every 50 - 100 CDPs depending on topographic variations along the profile. The process was repeated in a iterative method where deeper reflectors could be identified after subsequent multiple suppression filters.
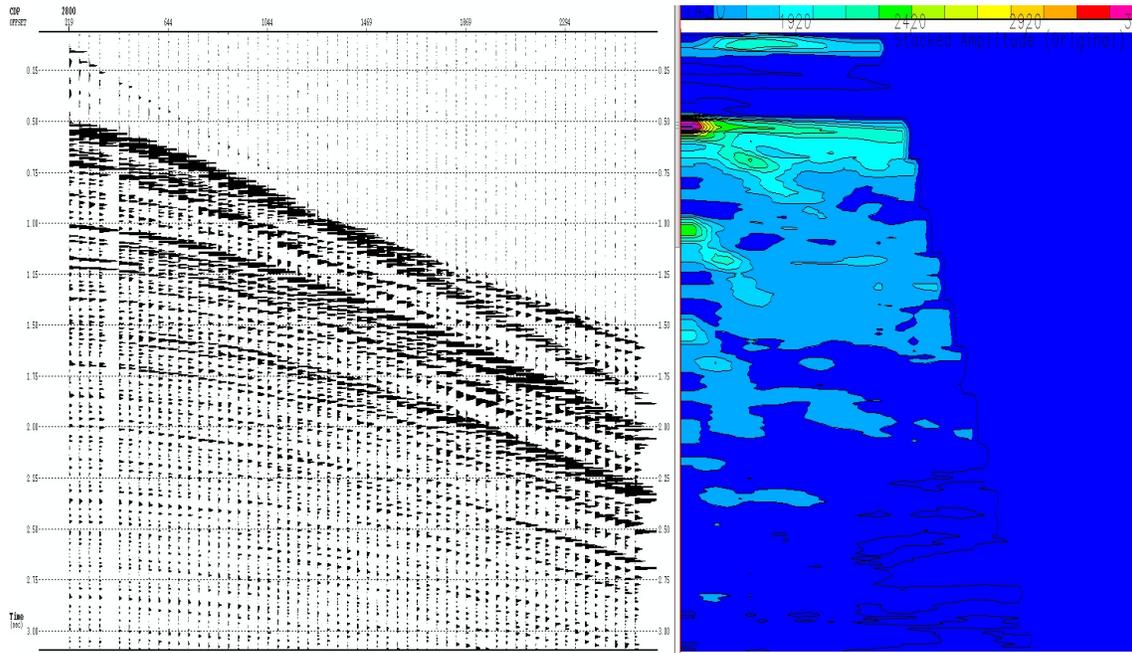


Figure 3.5: RMS velocity picking in Focus™. Single CDP 2000 from profile 95060 with applied Ornsby filter 10 – 60 Hz. Semblance window of magnitude of stacked traces against rms velocity.

## 3.2.5. Multiple Suppression

### A. F-K Domain Filtering

As mentioned in section 2.1 , F-K transformation plots dipping reflectors to points in the F-K domain using a double Fourier transform. Signals from a seismic reflector in a CDP gather, that do not have a dip, plot on the vertical axis, whereas upward dipping and downward dipping reflectors map on to negative and positive quadrant respectively. An NMO-corrected gather with velocity model that is in between primary and multiple velocity results in primary signals mapping to negative quadrant and multiple signals to positive quadrant.

In Focus™, the module ZMULT performs the F-K tranformation of the data and supresses undercorrected reflectors. Before seismic data are filtered using ZMULT it must be prepared such that the primaries are overcorrected and the multiples are undercorrected. An over-correction parameter (OVC) can be applied to the subsurface velocity model and is calculated from the mean move-out time for primaries ($t_p$) and multiples ($t_m$) (source: Focus™ manual).

$$OVC = (t_m - t_p)/2 \qquad\qquad 3.3$$

$$t(p,m) = t_0 + XV(p,m)$$

where,             $t_0$    = two way travel time

X    = reference offset

V(p,m) =  veloctiy of primaries and multiple

NMO corrected CDP is followed by a time variant OVC that is calculated using the above relation is well separated in F-K domain. The suppressed amplitude in the positive domain results in reduced multiples in the X-T domain.

Another important set of parameter is the filtering window size which identifies the dipping reflectors. Too small or too big windows hinders the process of correctly identifying reflectors. The window size is defined by the parameters NPT and NPX which is determines the number of traces to use and number of samples along a trace is to be used.

$$NPT = \frac{1}{DT}(\frac{1000}{F} + OVC)$$

$$NPX = \frac{(NTRS)}{0.002(OVC)(F)}$$

Where,             DT  = sample rate in milliseconds

F = Dominant frequency

NTRS= number of traces in a shot gather.

20-30 traces with 50-100 sample points is found to provide optimum results for the given dataset.

## B. Radon domain filtering

Parabolic Radon transformation uses a discrete Radon transform to model multiple energy in to parabolic events and subtract it using user specified parameters. An NMO corrected gather is forward transformed into the Radon domain where the flattened primaries can be easily separated from the multiples which exhibit residual moveout .

The range for parameter 'q' for minimum p-wave velocity of 1450 m/s and offset of 2594 is approximately 800. Therefore 450 p values with an increment of 2 should be sufficient for multiple suppression.

Toeplitz inversion is used for inversion method. It assumes that the parameter and noise has a Gaussian distribution in model space and the data space respectively that leads to a linear least-

squares inversion scheme. The operator matrix needs only one column to solve the system of linear equation using Levinson algorithm for model space parameters.

Seismic events in a CDP gather generally exhibit hyperbolic move-time and therefore it is corrected for NMO before the application of parabolic Radon transformation as it can be better approximated by a parabolic function. Parabolas are modelled for reflectors with a moveout difference range at maximum offset, which is the reference offset , between -20 ms and 1000 ms. The range is selected based on a visual interpretation of first order multiple. Multiples can be suppressed in two ways; only the reflectors that have a moveout range between -20 and 35 ms are not filtered out after processing, i.e., the original trace is replaced with primary reflectors. Alternately, the primaries are filtered out and the resultant trace, consisting of multiples and other noise, is subtracted from the original trace.

## C. Predictive deconvolution

Predictive deconvolution is based on the principle of periodicity. However, the multiples are periodic only in the near-offsets therefore predictive deconvolion is not as effective for far offsets. This problem can be solved by transforming it in the Tau-P domain. The angle of progagtion of multiples with respect to their corresponding primaries is preserved for a given parameter value. As explained in previous section, 450 p values with an increment of 2 has been used .

For predictive deconvolution, the window should be large enough to include both the primary and multiple .  The seismic traces exhibits ghosts and bubble pulse effect. This can hinder the process of correlation and hence the deconvolution module is run twice. First, to remove ghosts and bubble effect and then a second time to remove surface related  multiples. For the first module, the window is small to target only ghosts and bubbles, i.e. 200 ms ( operator length) + 60 ms (gap length). A  large operator length of 1200ms followed by a gap filter of 60 ms was chosen to target surface related multiples.

## D. Wavefield Extrapolation method (SRME)

SRME is a wavefield extrapoltion method where the multiples are estimated by extrapolating primary waves such that they act as a source. Extrapolation is achieved by convolving two traces from different shots, hence, it requires that traces are shot ordered. Multiple suppression is done in 3 phases.

Zero-offset Interpolation:

In order to compute the first order multiple for a specific offset distance, traces from half the offset distance are required and every one third of the distance of the offset for second order multiple. In practice, it is not posibble to have a zero-offest and the nearest offset is at a considerable distance away. In current dataset, it is 219 m which implies 9 missing traces. In such a case, multiples for traces up to 450 m cannot be reconstructed for the first order, 675 m for the second order and so on. Therefore, traces for the near offset has to be interpolated. This process regularizes traces and also accounts for traces that are required for extrapolating recorded multiples but lie in between two recorded traces.

The module does not use a seafloor topography model but extrapolates from the first recorded sample, therefore, it requires that the gather is precisely muted until the seafloor to remove water column noise and other interferences.

In the second phase, a Taylor series is generated that predicts multiples by method of extrapolation and phase reversal for multiples (Focus™ Help documents). Seismic traces convolves with itself along the surface.

In the last phase, the predicted multiples are correlated to the original trace, scaled in amplitude and subtracted from the original trace.

In Focus™, the above steps are achieved by two modules. The SMACTRM module interpolates traces to zero-offset and generates n terms of the Taylor series .

For computational resaons it is important to define shot intervals and receiver intervals such that every station has a shot and receiver. Missing receiver traces are interpolated using a velocity function defined by HANDVEL. Missing shots are determined using RATIO which copies nearest shot for missing stations. In order to be time efficient, only upto second order multiples are predicted to target only until depths where multiples are strong.

SMACMS module uses the Taylor terms stored in header files to subtract the predicted signals from the original shot gather.

### 3.2.6. Stacking

Stacking process sums all the traces along a horizontal line to produce a single representative trace of a given CDP. A NMO corrected data with stretched trace muted is used as an input. Two methods have been experimented for stacking traces. Mean stacking algorithm computes the mean average amplitude of all the traces within a single CDP while in alpha-trim median stacking, the lowest 15% and the highest 15% amplitudes are excluded in the summation of the traces.

## 3.3. Estimation of velocity at the seafloor

When the angle of incidence at the seafloor exceeds the critical angle, some of the energy is refracted and travel along the surface (Fig3.6). This phenomenon is observed with long offset streamers in relatively shallow water. Fig 3.7, shows a single CDP gather from profile AWI-95060, where refracted seismic signals can be observed.
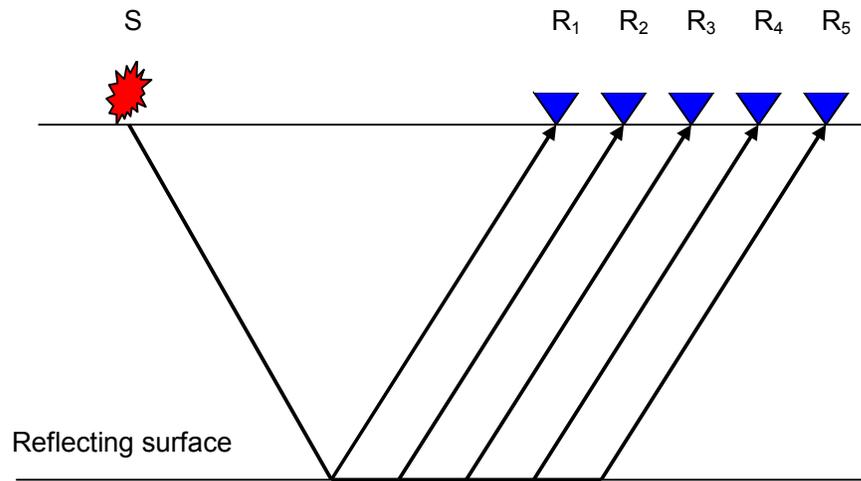


Figure 3.6: Refracted seismic waves at the seafloor recorded at receivers R2-R5.
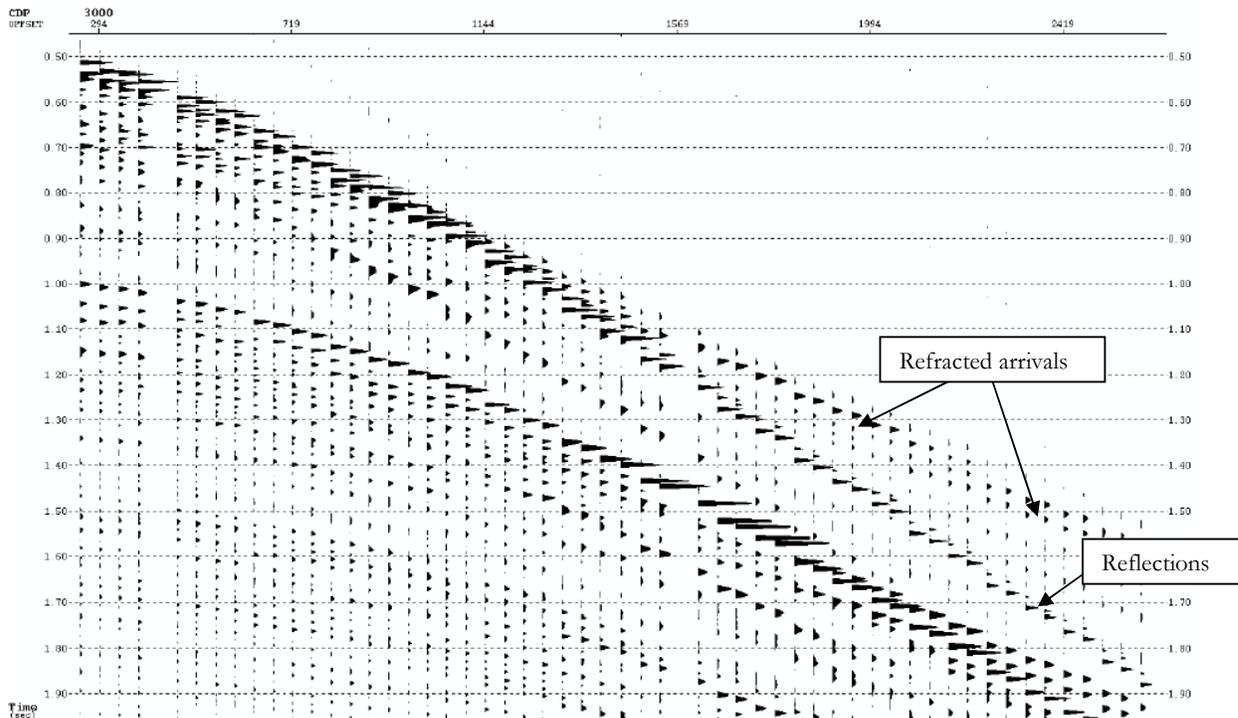


Figure 3.7:  Single CDP gather from profile AWI-95060 showing refracted arrivals at the far offsets.

The difference in travel path is equal to the receiver interval as illustrated in Fig 3.6. The velocity v at the seafloor is calculated as

$$v = \frac{X_2 - X_1}{T_2 - T_1}$$

Where , $X$ = Offset distance

$T$ = two-way travel time

Velocities are calculated every 50 CDPs or 1250 m using the average of 7 time-offset pairs.

# Chapter 4.    Results and Discussions

All the profiles, in general, display a similar pattern of strong surface related multiples originating from the seafloor and the subsurface. The sea-bottom multiple is much stronger than neighbouring primaries, in some cases comparable to the primaries from the seafloor. Subsurface features also show a repeating charateristic with the period equal to water depth suggesting these multiple are a result of reverberation in the water column. Internal multiples are not observed or are very weak to be identified. In addition, signals from a bubble pulse are also recorded which can be distinctly observed with a lag of approximately 180 ms. In some parts, the multiples resulting from bubble pulse are also observed.

## 4.1. Intermediate depth with weak to moderate dipping events:

Profile AWI 95060:
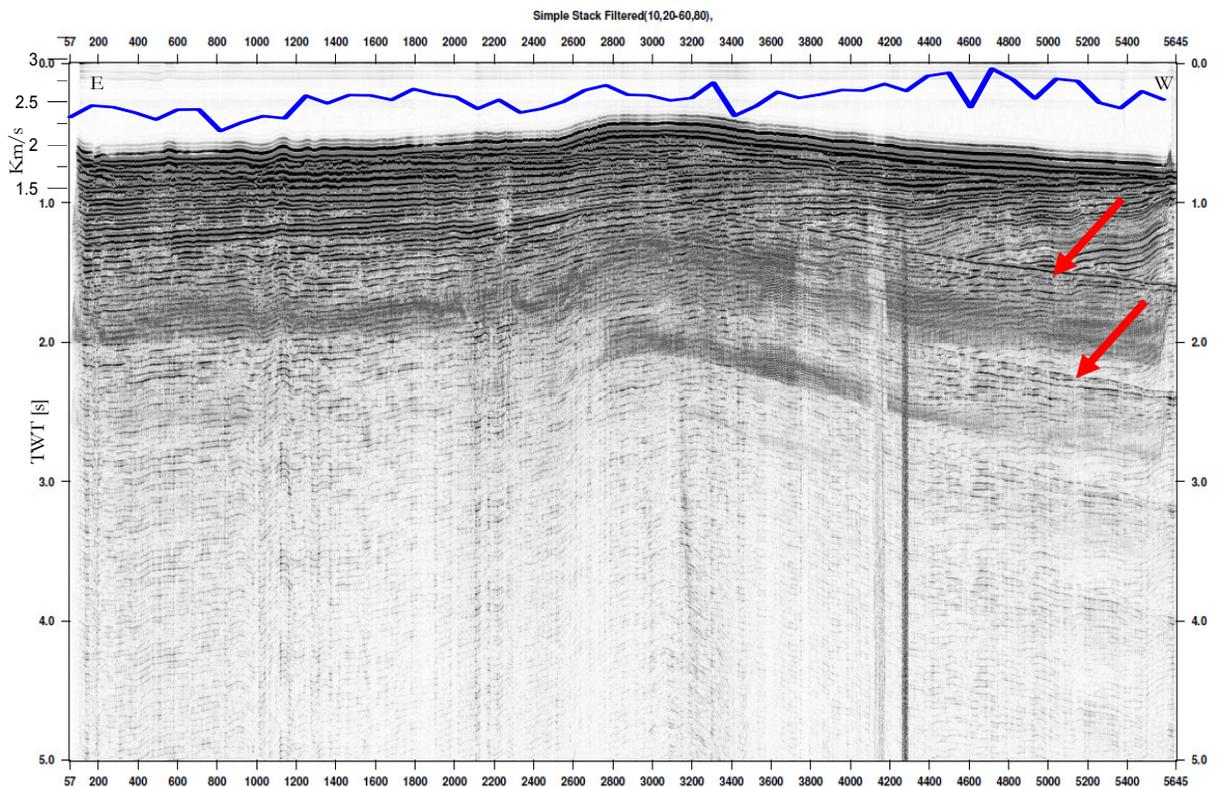


Figure 4.1: Stacked profile of AWI-95060 without any multiple suppression and velocity at the seafloor derived from refracted arrivals. Red arrows indicate multiples.

Profile AWI 95060 (Fig4.1) is a east-west trending profile with a topographic high in the middle of the profile. The seafloor gentle gradient away from the topographic high. The subsurface is characterized by a group of parallel events dipping east towards the middle of the basin with occasional undulations. The events toplap with seafloor, an indicator for truncation due to erosion that is most likely glacial related. The surface velocity ranges from 2.1 km/s to 2.8 km/s and shows a decreasing trend from west to east implying higher consolidation towards the west.
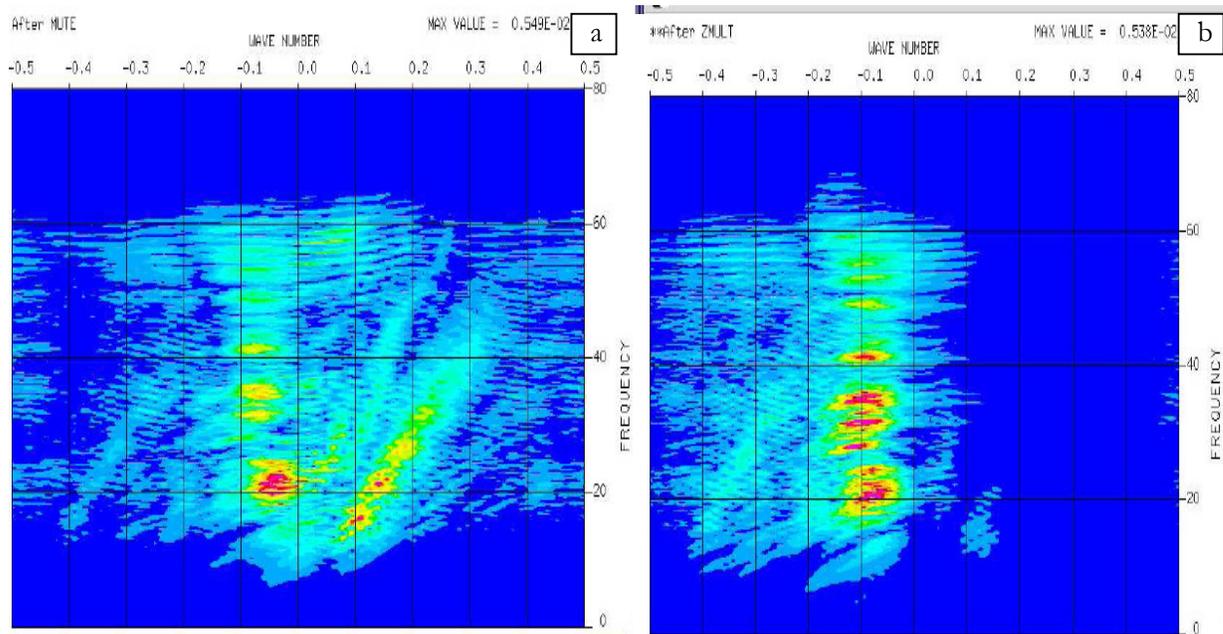


Figure 4.2: Transformation of over corrected cdp gather between 1.0 and 2.0 s into F-K domain . 3 distinct zones can be identified that are located between -0.1 and 0.2 . After Filtering, all the energy in the positive quadrant is suppressed.

Fig 4.2 shows the result of F-K transform to CDP 2000 after applied overcorrection . Three regions with strong coherent energy related to primary, first order multiple and second second multiple can be identified. Fig 4.2b shows the result of filtering out energy of multiples that lie in the positive quadrant. Almost all the energy in the positive quadrant is attenuated whereas the energy in the negative quadrant related to primaries is almost unaffected.

Corresponding results in X-T domain for multiple suppression with F-K filter is shown in Fig 4.3. After applying overcorrection to a NMO corrected gather, it is possible to identify primaries from multiples by their different move-out time between 1.0 and 2.0 ms. After ZMULT, the under corrected events are filtered out leaving the over corrected events untouched. Seismic events that were masked by multiples are now clearly visible. In the far offset region, a group remnant energy that are poorly suppressed are discontinuous and align with intersecting primary events post filtering.
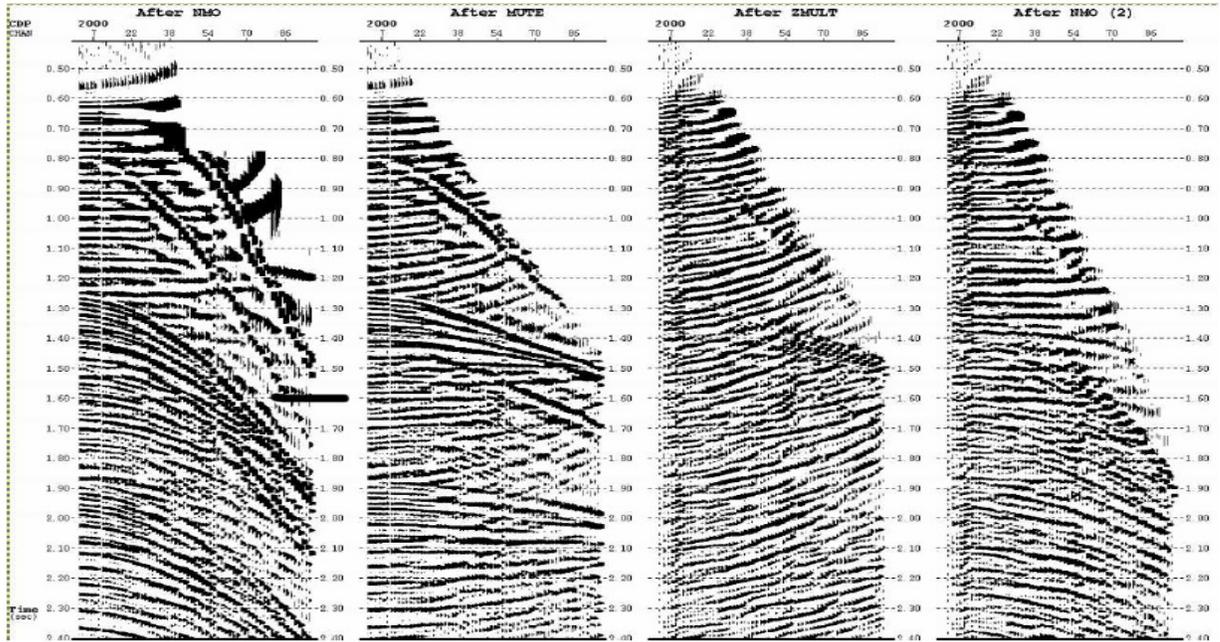
Figure 4.3: Steps for multiple suppression with F-K filtering. After ZMULT, multiples in the far offset align with the primaries that influence the final stack.

Fig 4.4 shows the results of profile AWI-95060 with mean stack of multiple suppressed CDP gather. Dipping events in the subsurface continue dipping eastwards with occasion undulation. The first multiple, characterized by a single sharp coherent event, cuts through primary events. However it should be noticed that the multiple has been shifted deeper by roughly 200 ms. This multiple is a contribution from the remnant energy of poorly suppressed multiples in the far offset regions The remnant energy is still very strong to influence the stacking results. . This problem can be alleviated by using an alpha-trimmed stacking algorithm. In Figure 4.4b that shows the result of alpha trim stack, the multiples are very well suppressed.
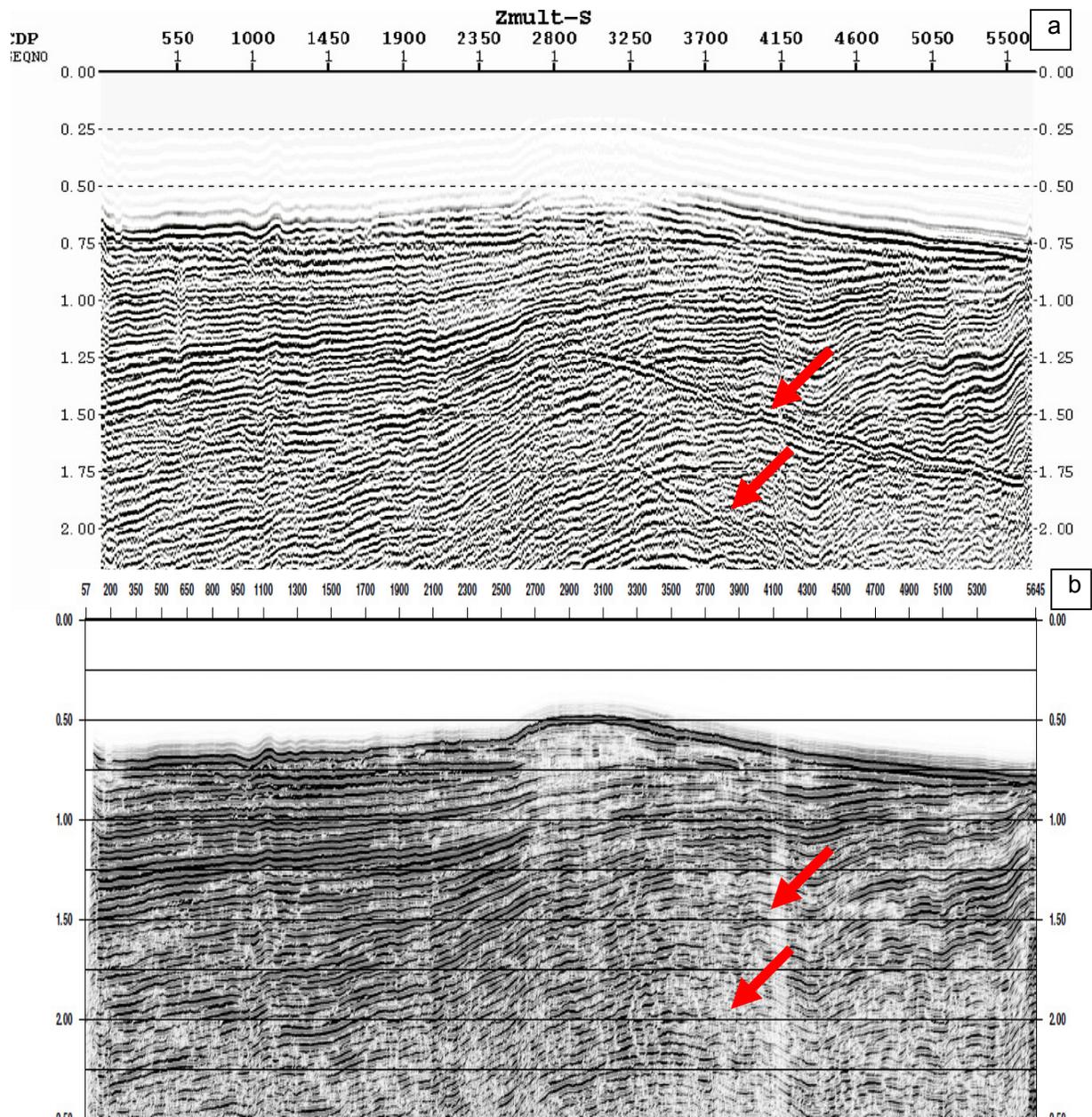
Figure 4.4: Results of F-K filtering with a) mean stack and b)alpha-trim stack. Note the shift in multiples by ~200ms with a mean stack. Red arrows indicate multiples or suppressed multiples

Filtering in Parabolic Radon domain is shown in Fig 4.5. Although not well delineated, theoretically primaries should be modelled by very low parametric values (near zero). Seabottom multiples can be identified by the high energy modelled by large parametric values that decrease for higher order multiples. The effect of bubble pulse is modelled by high parameters at 800 ms TWT. Filtering out the flattened out curves corresponding to primaries leaves behind only multiples and other noise which is then transformed and subtracted from the original input (Fig 4.5a). The signals after subtraction corresponds to primaries with flattened events (Fig 4.5c).
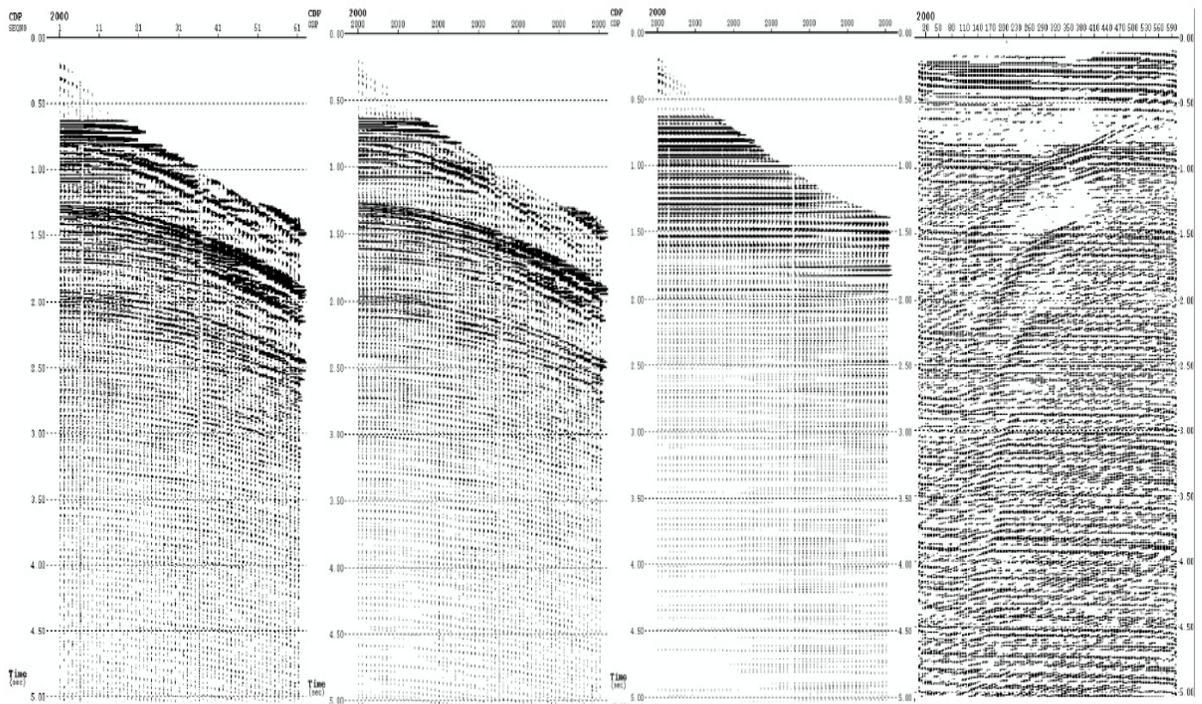
Figure 4.5: Multiple suppression of a single CDP gather in Parabolic radon domain. a) NMO- corrected CDP gather. b) Predicted multiples that are modelled by filtering out horizontal events (Primaries). c) Result of subtraction of modelled multiples (b) from original input (a). d) Result of Parabolic transformation of a) with 500 parabolas modelled between -20 ms and 1000 ms .

Post parabolic Radon multiple suppression, a sharp and strong multiple of the seafloor can be observed in the stacked profile (Fig 4.6). Multiples from the subsurface are significantly suppressed. The strong seafloor multiple might be a result of imperfect inverse transformation. Very strong multiples have a significant contribution to the traces in the parabolic radon domain which should theoretically be dominated by primaries. In the inverse transformation, the energy is imperfectly mapped to horizontal reflectors, thereby, reintroducing multiples in the stacked profile. Using a higher number of parabolas can reduce this effect but it drastically increases the computation time.
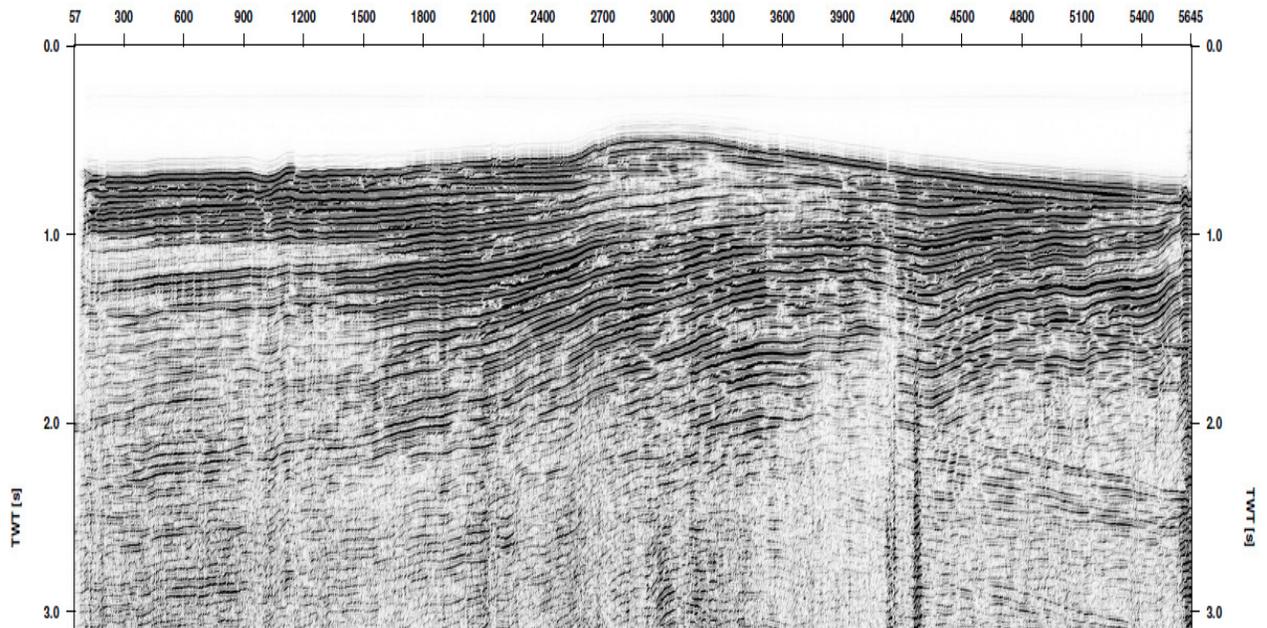
Figure 4.6: Result of multiple suppression with parabolic Radon transformation.

Profile AWI-95070:

In profile AWI-95070, the water depth ranges from 400 ms to 750 ms TWT with a gentle gradient in most parts (Fig 4.7a). The subsurface is characterized by nearly horizontal reflectors that are truncated at the seafloor. It indicates an erosional regime that are mostly due to ice sheet grounding. The subsurface show a mixture of horizontal to weakly dipping events with some diverging and sidelap structures. While the deeper events are relatively smooth, the shallow events show ripple structures with smaller transparent to chaotic packages inbetween. The velocity at the seafloor does not show any increasing or decreasing trend but has a strong variation with dip.

A simple stacked profile shows a weak first order multiple (Fig 4.7). The second order multiple gives a noise-like effect and with incresing depth the effect of multiples begin to dominate. With F-K filtering, the first and second order multiples are well suppressed but not the multiples in deeper parts. Multiple suppression with parabolic Radon transformation can suppress higher order multiples, enhancing primary events between 2.0 and 3.0 s TWT that were masked by multiples. In contrast to the results of multiple suppression in profile AWI-95060, the seafloor multiple is not observed as they are not strong enough to leak back in to the X-T domain during inverse transformation.
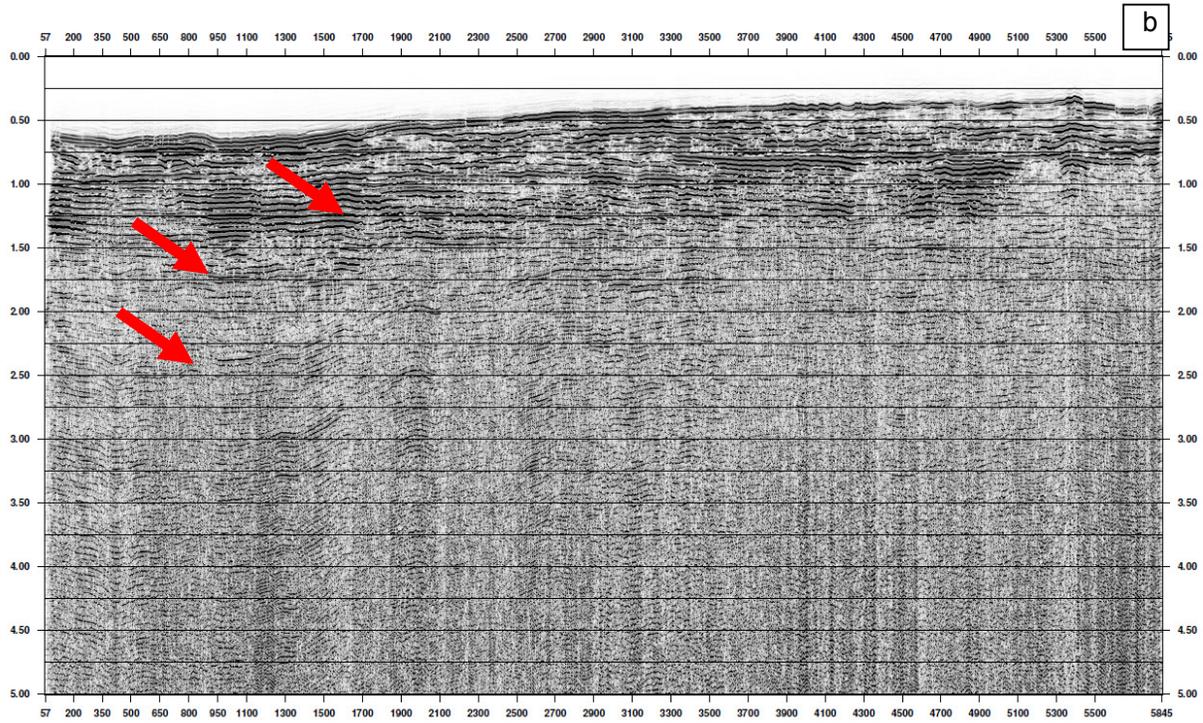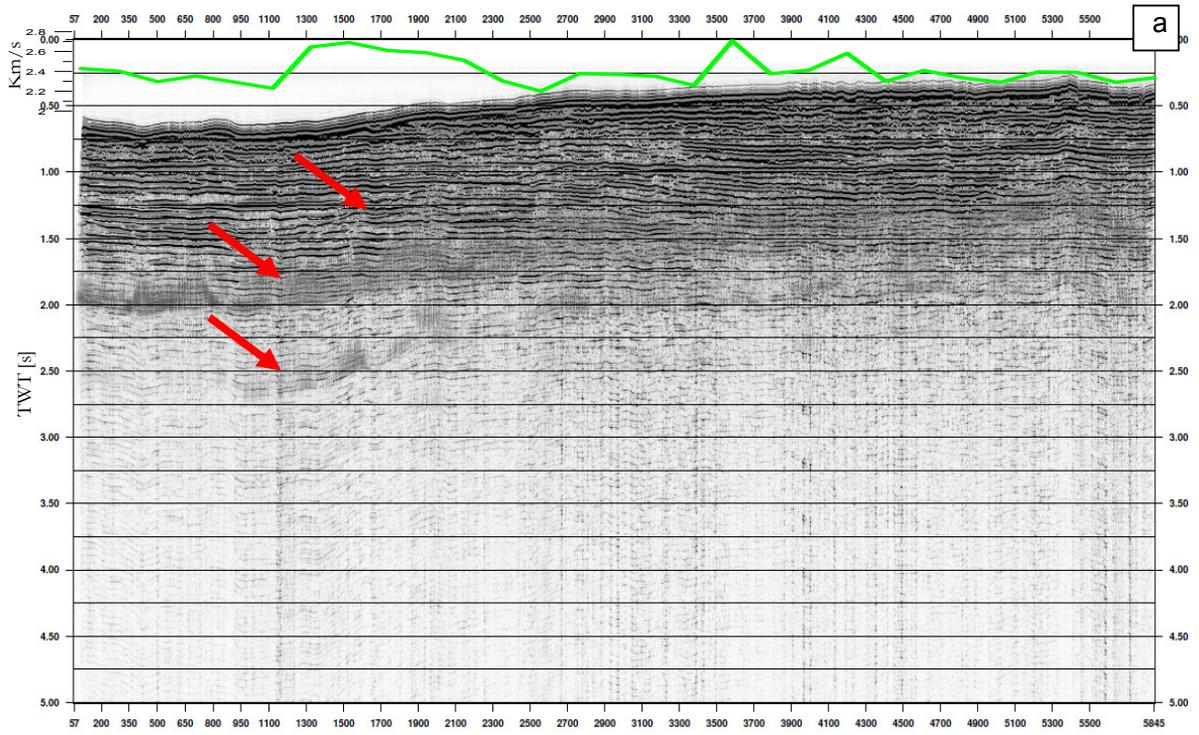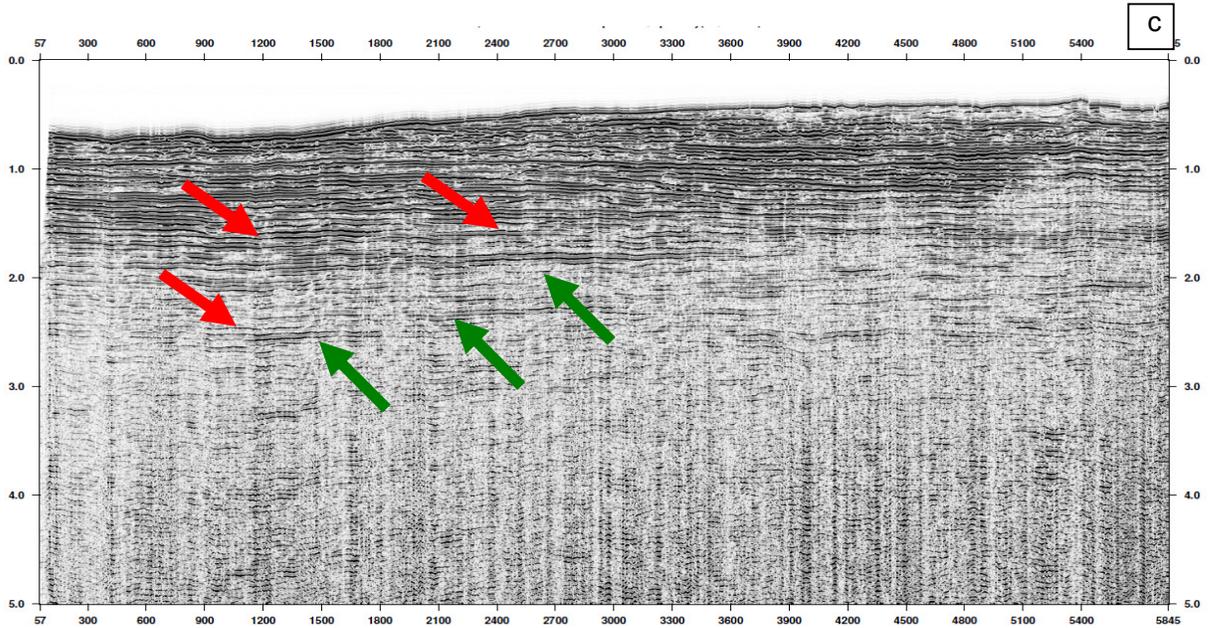
Figure 4.7: Profile 95070 a) without multiple suppression and velocity at the seafloor derived from refracted arrivals b) with F-K filtering c) Parabolic radon Transformation. Note the events between 2.0 and 3.0 s that are enhanced. Red arrow indicates multiples or suppressed multiples and green arrow indicates primaries.

## 4.2. Intermediate depth with folded sediments and weak dipping events:

Profile AWI-95062:
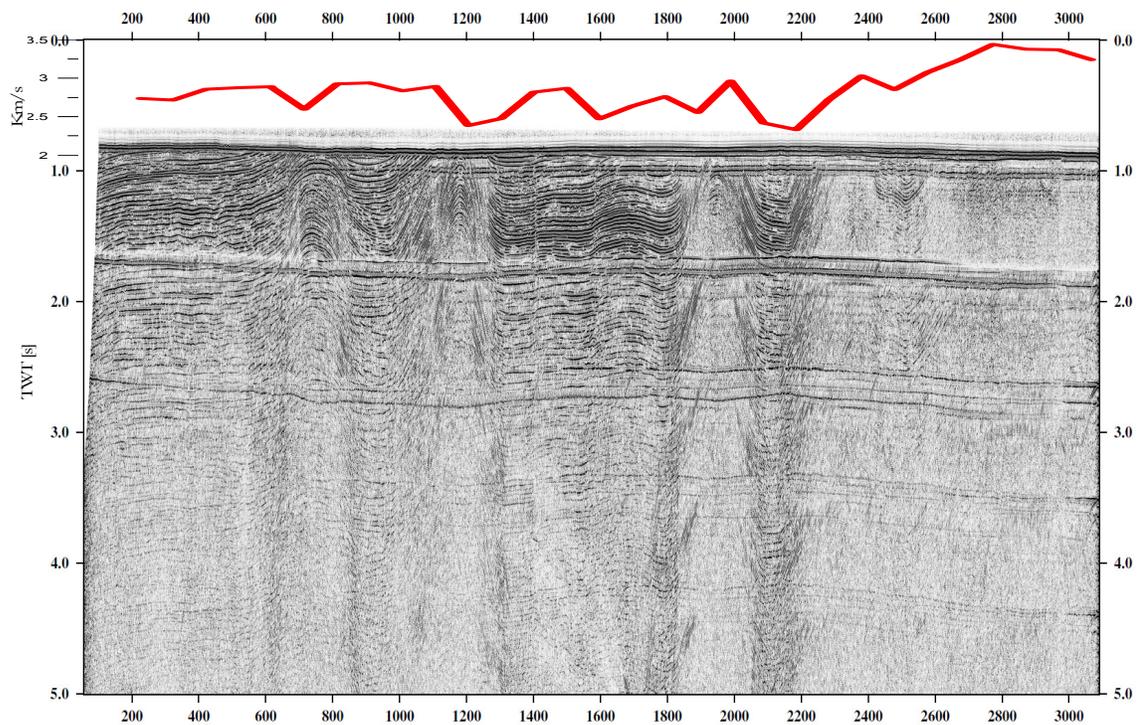


Figure 4.8: Stacked profile of AWI-95062 without any multiple suppression and velocity at the seafloor derived from refracted arrivals.

Profile AWI-95062 (Fig4.8) is located close to the Antarctic Peninsula, has almost horizontal seafloor reflector across the profile with little or no undulations or dip . On the west side of the profile there are no strong reflections from the subsurface except for multiples. It may be acoustic basement or highly consolidated sediments . The velocities at the surface exceed 3.3 km/s while velocity in the subsurface are found to exceed 5.0 km/s (Jokat et al 1996). The profile is charaterized by 3 strongly folded sediment structures . The fold sediments are separated by strongly reflecting parallel sediment package with alternating weak to transparent packages that dip eastward. The sediment packages onlap on to the flanks of the anticline. Between CDP 1800 and 1200, the sediment package have a wave-like pattern starting just under the seafloor continuing downwards. At CDP 1600 and 1400 the wavelike sediments packages are show a strong dip and discontinuity respectively with a downward offset in west-east direction which might be related to faults located in deeper structures. At the extreme east end of the profile the sediments show a much steeper gradient that continue into profile AWI-95060.

The parallel east dipping events show either truncation or top lap at the seafloor. It could be result of erosion from ice stream A (Fig 1.4) flowing possibly in the North to North east direction followed by erosion.

F-K filtering can suppress multiples but the underlying primaries are masked by the noise that are remnants of the multiples (Fig 4.9a). The frequency of the noise is the same as the bandwidth of primary signals and therefore cannot be filtered out by frequency filters. Using a coherence filter enhances the effect of multiples.

Seafloor multiples are poorly suppressed because of very strong amplitudes that leak in to the X-T domain as explained previously. Multiple suppression in the parabolic Radon domain strongly suppresses surface related multiples (Fig 4.9b). Events from the subsurface show repeating trend. It is difficult to comment if all the events are primary or a multiple from the subsurface (SRM). No events can be resolved under the folded sediments.
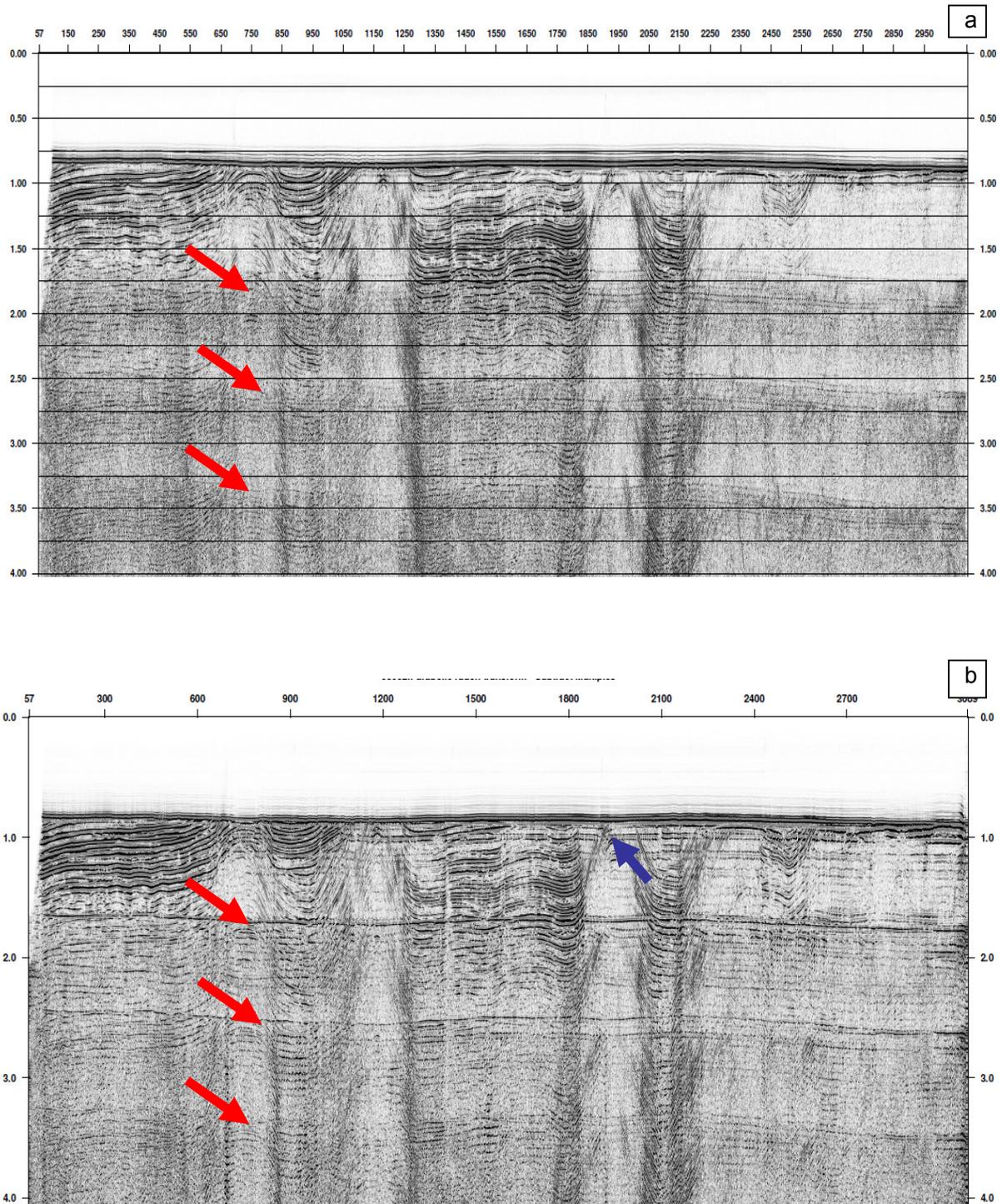
Figure 4.9: Results of multiple suppression with a) F-K filtering and b) parabolic radon transformation. The multiples are replaced with random noise bands after F-K filtering. Red arrow indicates multiples or suppressed multiples and blue arrow indicates bubble pulse.

For predictive deconvolution, CDP gathers are first transformed to Tau-P domain (Fig 4.10a). Multiples are now located at periodic intervals of the seafloor for every parameter value. After predictive deconvolution the effect of bubble pulse is suppressed. Multiples are not suppressed.

Transforming back into the X-T domain it can be seen that near-offset multiples are well suppressed and with increasing depth the offset range of well suppressed multiples also increase (Fig 4.10b). The suppressed multiples are not a result of predictive deconvolution but a result of inverse transformation.
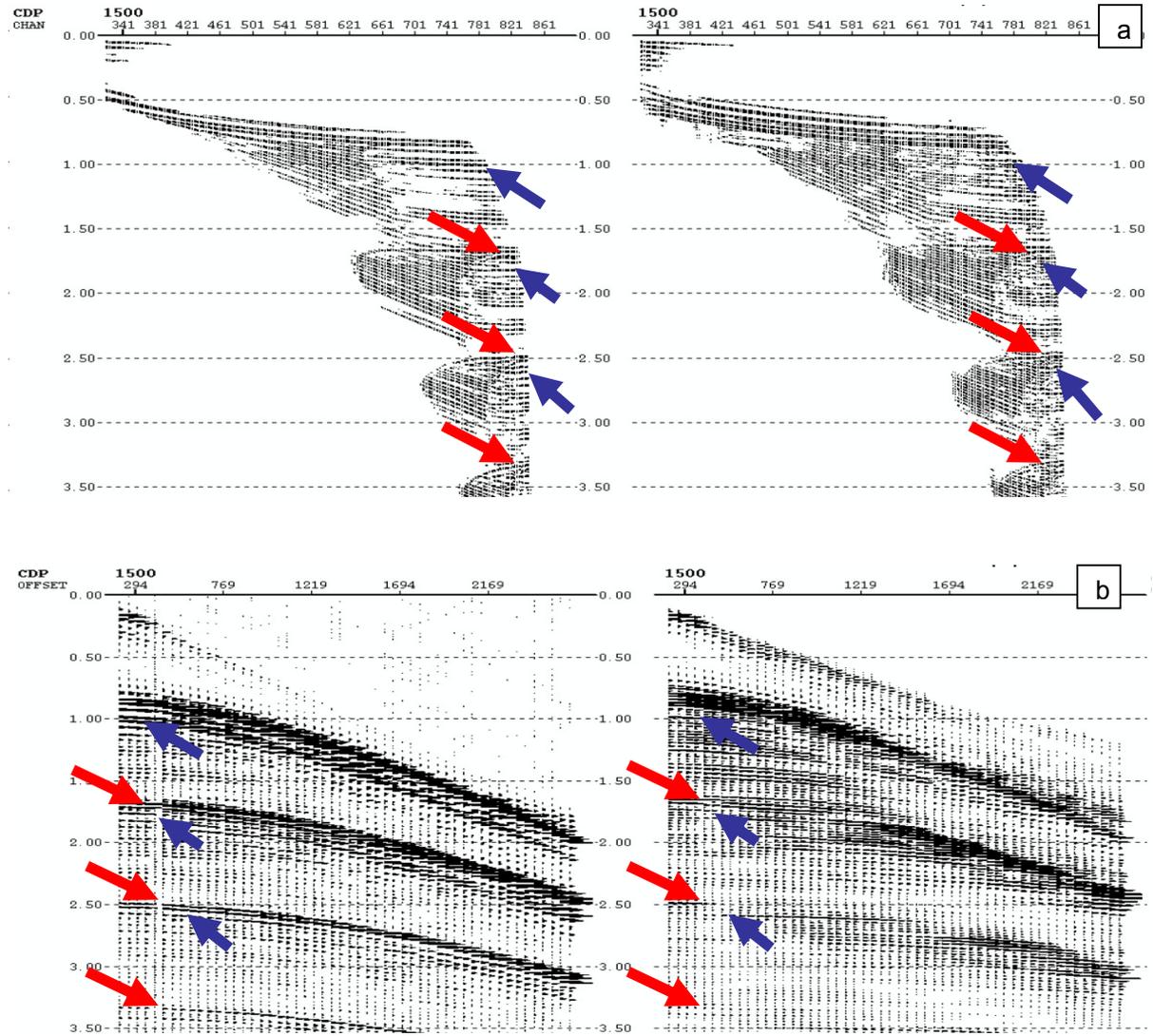


Figure 4.10: Predictive deconvolution in a) Tau-P domain and b) the corresponding results in X-T domain. Note suppression of bubble effect from primaries of the seafloor and the multiples. Suppression of multiples in the near offset is a result of transformation. Red arrow indicates multiples or suppressed multiples and blue arrow indicates bubble pulse.

Well suppressed bubble pulse effect and its related multiples in comparison to poor results of multiple suppression can be explained by distortion of signals travelling much larger distances through the water column that results in poor correlation of deconvolutio process. Increasing the white noise to 0.3 does not improve the image significantly but instead suppresses the primaries close to the seafloor.
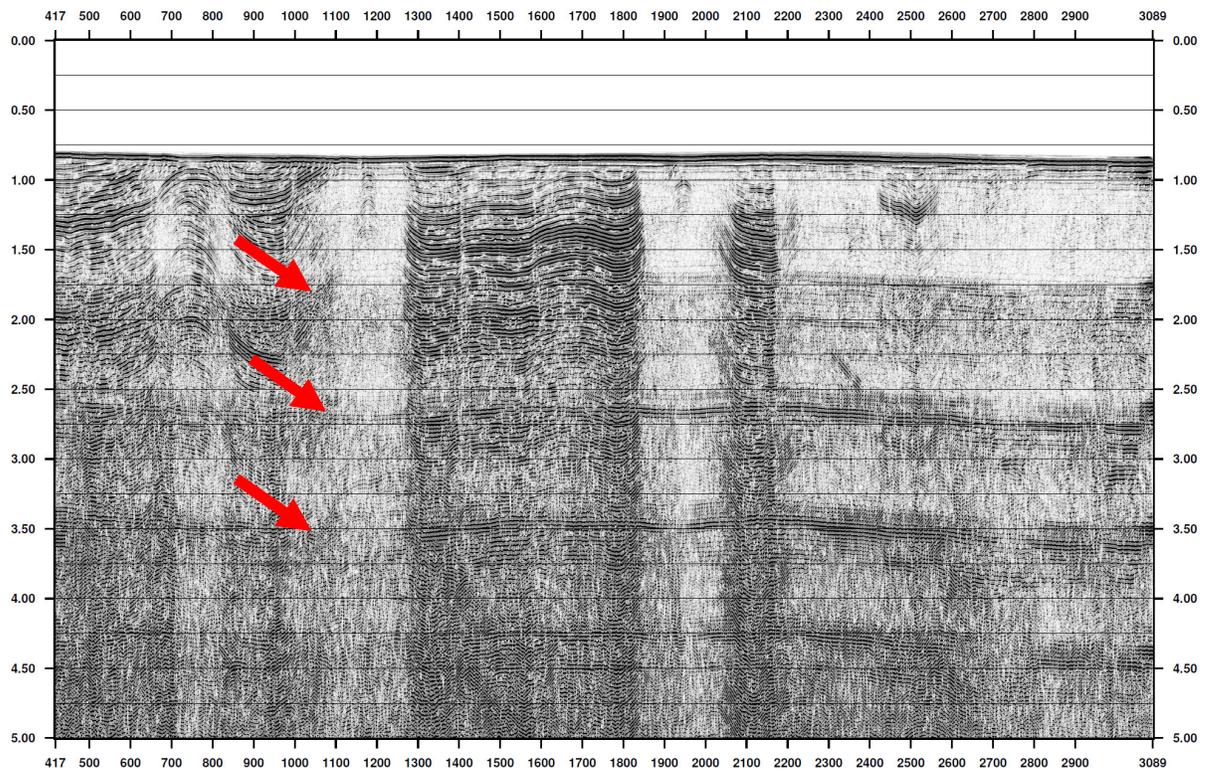
Figure 4.11: Result of stacking after predictive deconvolution in Tau-P domain. Reflectors under the seafloor are also weakened.

In SRME, the output of Predictive deconvolution is as an input. Using predictive deconvolution before reduces the source wavelet length which facilitates multiple prediction and adaptive subtraction. Also predictive deconvolution suppresses the effect of bubble pulse that is not addressed by SRME. Fig 4.12a is shot ordered gather that has been precisely muted at the first break. The interpolation of traces in the first step has a good correlation to the input gather (Fig 4.10). The extrapolation of the traces to its multiples correlates well with the interpolated trace (Fig 4.12b). The adaptive subtraction process weakly suppresses the first and second order multiples of the seafloor and higher order multiples are almost completely eliminated. The stacked profile is free from sea bottom multiples but the subsurface multiples are similar to the primaries and therefore the interpretation is still ambiguous.
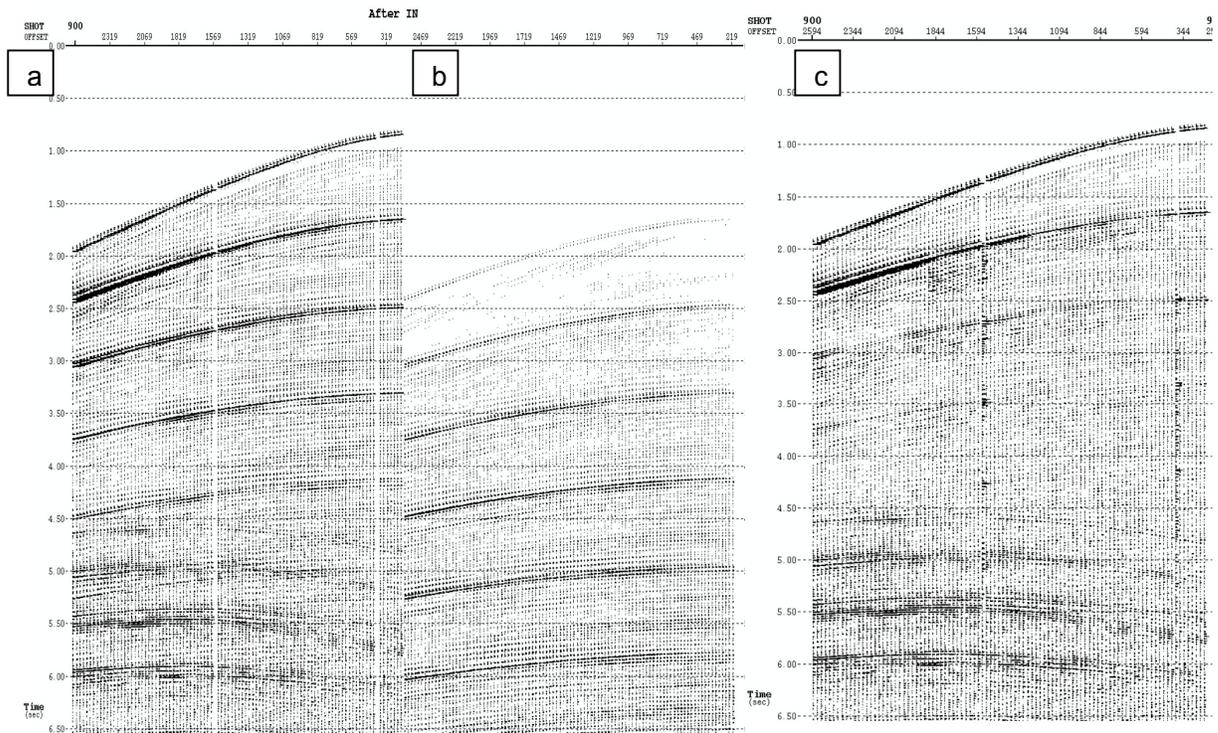
Figure 4.12: Results of SRME (shot gather). a) Interpolated shots (only the traces from the input shot gathered are displayed). b) Extrapolated first order multiples, note the good correlation of extrapolated multiples to the imput multiples c) Shot gather after adaptive subtraction of the traces. Strong reflections in deeper structures are from the ice-edge.
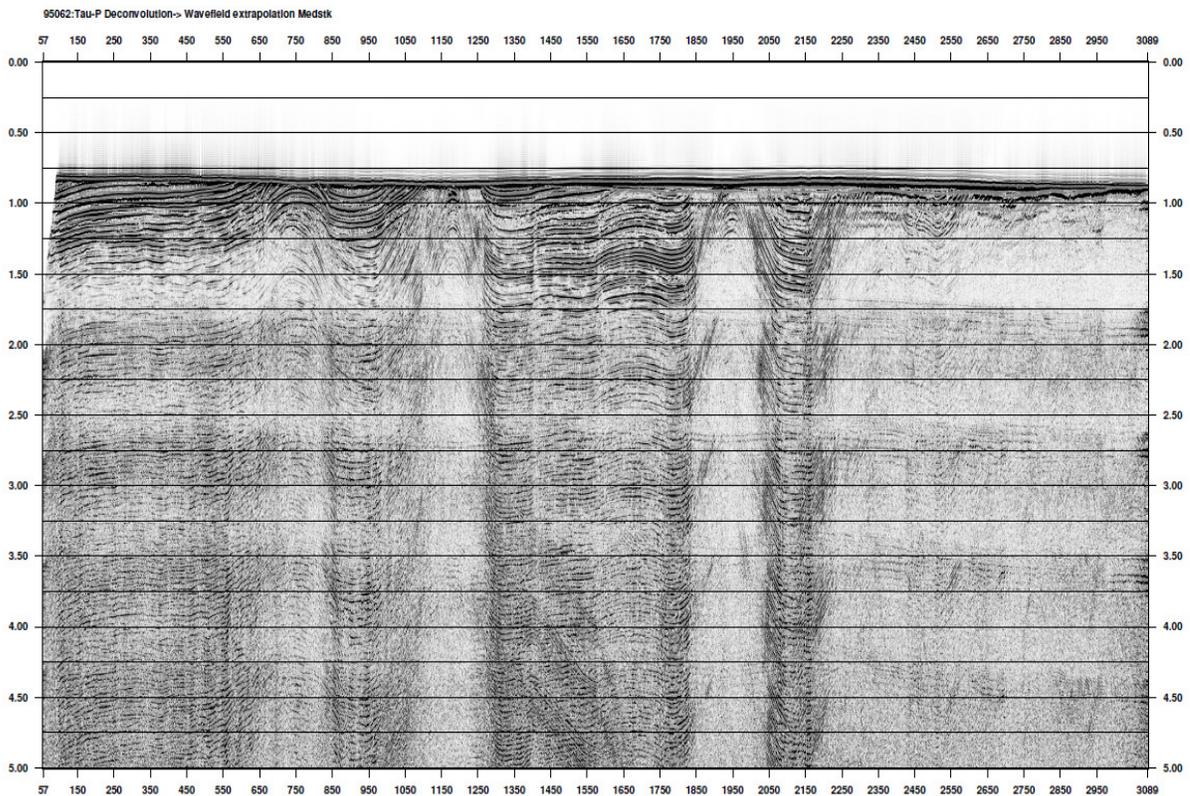


Figure 4.13: Results of SRME (stacked) after predictive deconvolution in Tau-P domain.

In order to image the area around the folded sediments, an attempt to migrate the events is made. Two migration strategies are employed viz., Prestack time migration (PSTM) and post stack migration. Fig 4.14 shows the results of PSTM after ZMULT processing. The top of the fold is well migrated but deeper structures under the fold and the flanks are still not imaged correctly after PSTM. Post stack migration does not improve the flanks and introduces artifacts in the lower structure which resemble typical results of migrating random noise. Migrating such structures may not be possible or needs advanced expertise that is outside the scope of this master thesis. The results, nevertheless, imply that multiple suppression with F-K filtering can be done prior to PSTM without having adverse effects.
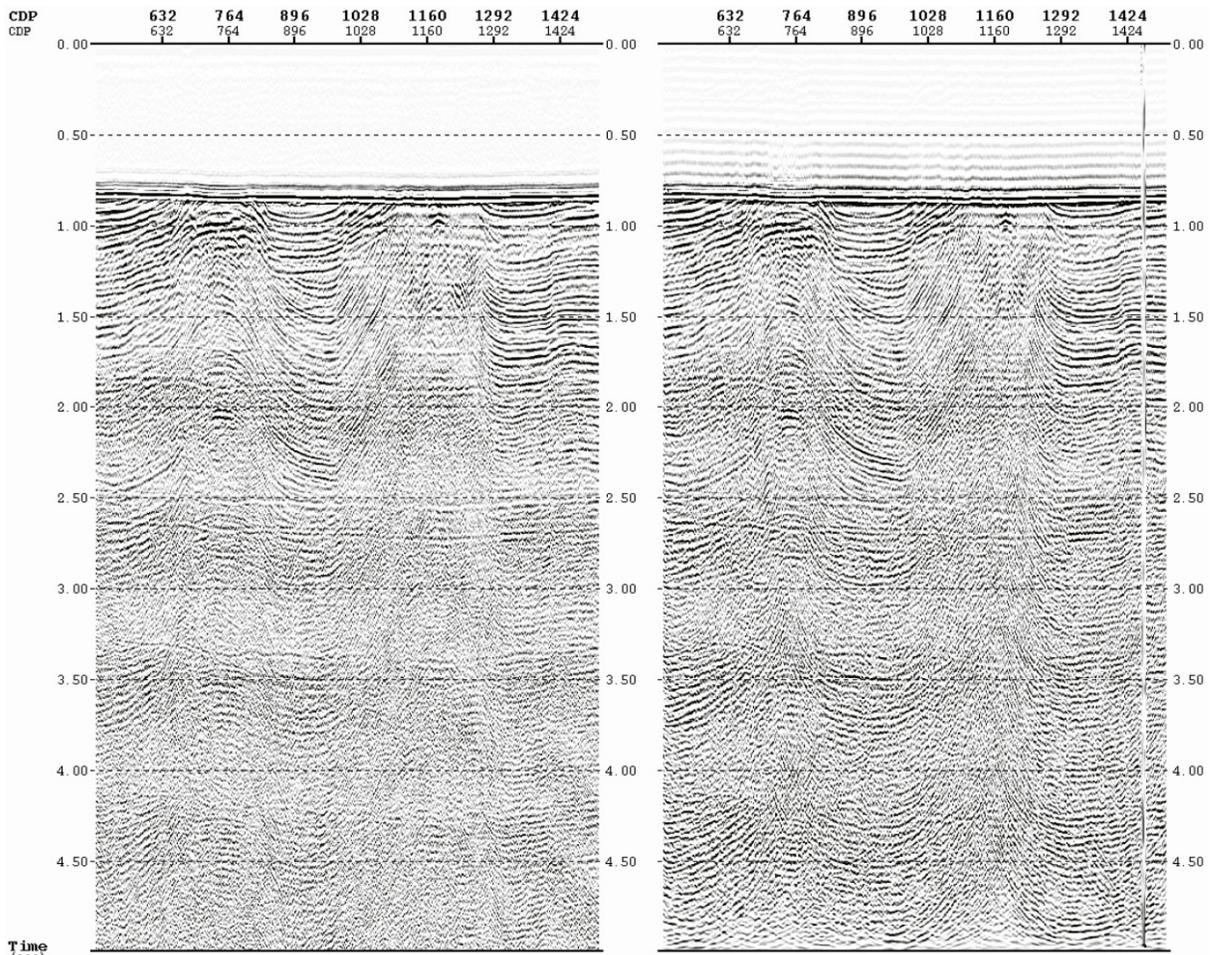


Figure 4.14: Result of pre-stack migration (left) and post stack migration on PSTM (right) CDP gather. Note that the top of the anticline is imaged well. Post stack migration introduces artifacts in deeper structures

## 4.3. Strong dipping events and hummocky structure

Profile AWI- 95090
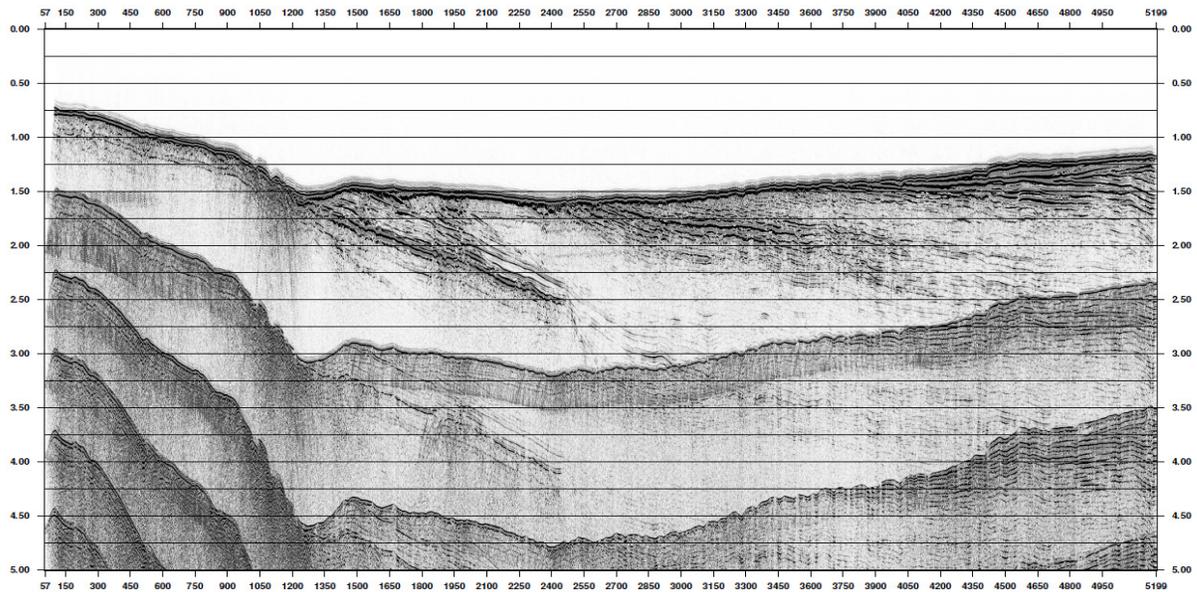


Figure 4.15: Profile AWI-95090 stacked without suppressed multiples.

Profile AWI 95090 is located in the Filchner trough (Fig 4.15) . The maximum water depth in the profile is 1.5 TWT (~1100 m) at CDP 1300. On the landward side, the seafloor reflector is underlain by acoutically transparent basement. A basin like structure is seen between CDP 1200 and 1400. It may relate to ice sheet grounding and extend several kilometers on to the shelf . This has been described by Stolldorf (2012) as scouring related to sluggish flow of ice stream from originating from EAIS. The profile west of the basin displays alternate packages of  seaward dipping well stratified and chaotic sediments that are truncated at the seafloor. At CDP 2500 at 2.5s TWT, the dip of, what maybe, the basement-sediment boundary reflector is very steep (~30°) overlain by divergent  reflectors. The package of stratified sediment deposits that lay above it also show stronger dip than at other sections of the profile.

Multiple suppresion with F-K filtering and parabolic Radon is not very effective because the water depth is larger than in the previous profiles. Separating primaries from multiples at larger depth is much more difficult owing to smaller NMO difference. Multiples with F-K filtering (Fig 4.16) and parabolic Radon filtering (Fig 4.17)are replaced by a strong random noise band. Predictive deconvolution  (Fig 4.18) and SRME (Fig 4.19) give much better results and primaries can be traced even under second order multiple. However, the underlying primaries are weak and cannot be easily distinguished from the multiples. The basement can be delineated under the first multiple albeit with some uncertainty which was not possible previously. As in previous profiles strong

suppression with deconvolution is achieved at the cost of primaries close to the seafloor. Using a coherence filter to filter events dipping in different direction significantly improves the image but it has to be used cautiously as it involves assumption based on visual interpretation.
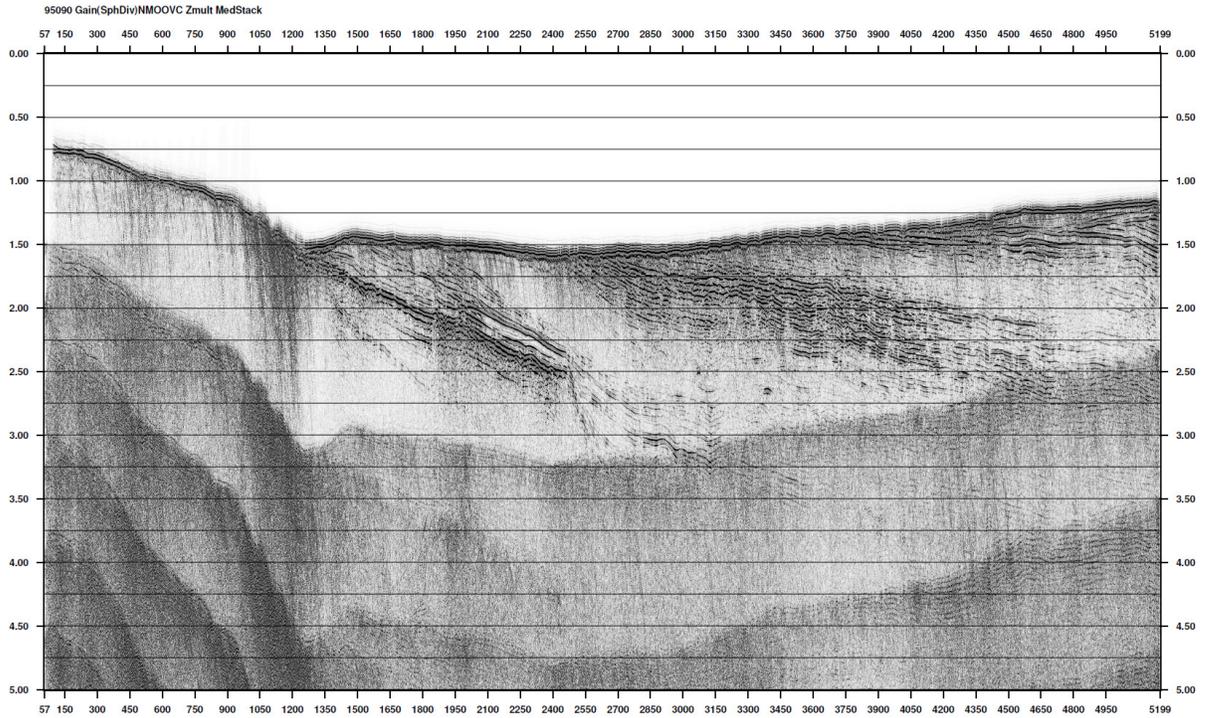


Figure 4.16: Result of Multiple suppression with F-K filtering. Note that the multiples are replaced by a band of random noise
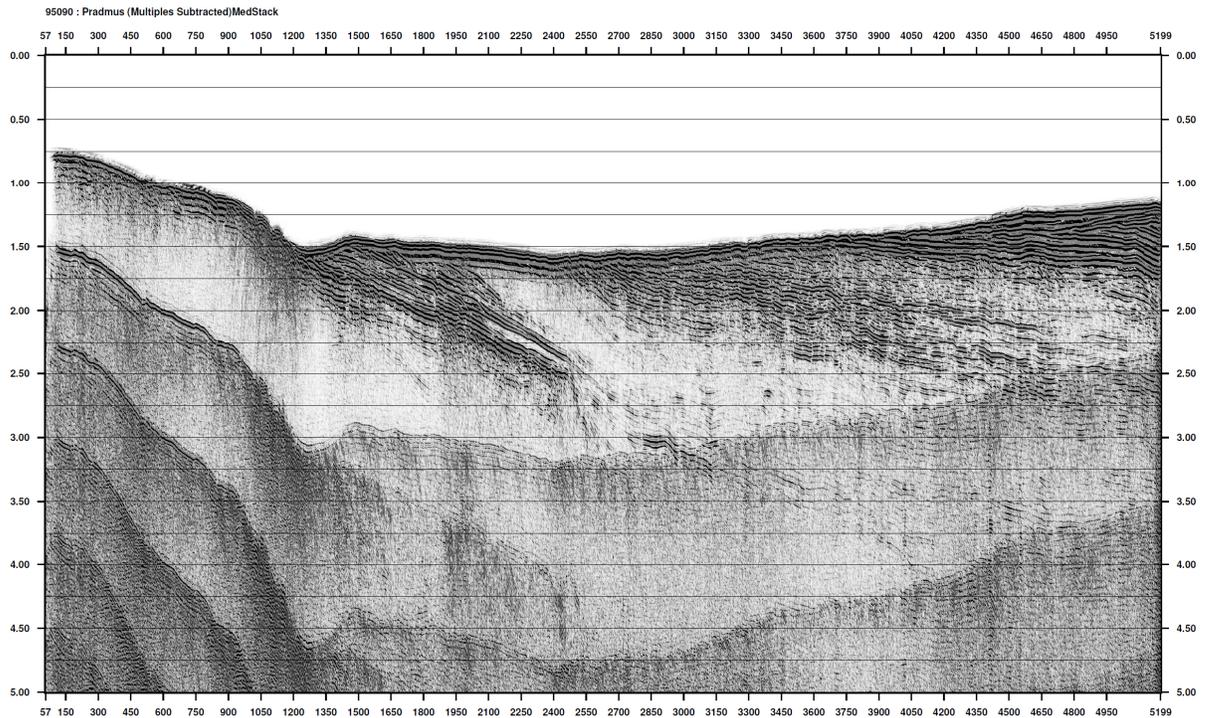


Figure 4.17: Result of multiple suppression in Parabolic radon domain.
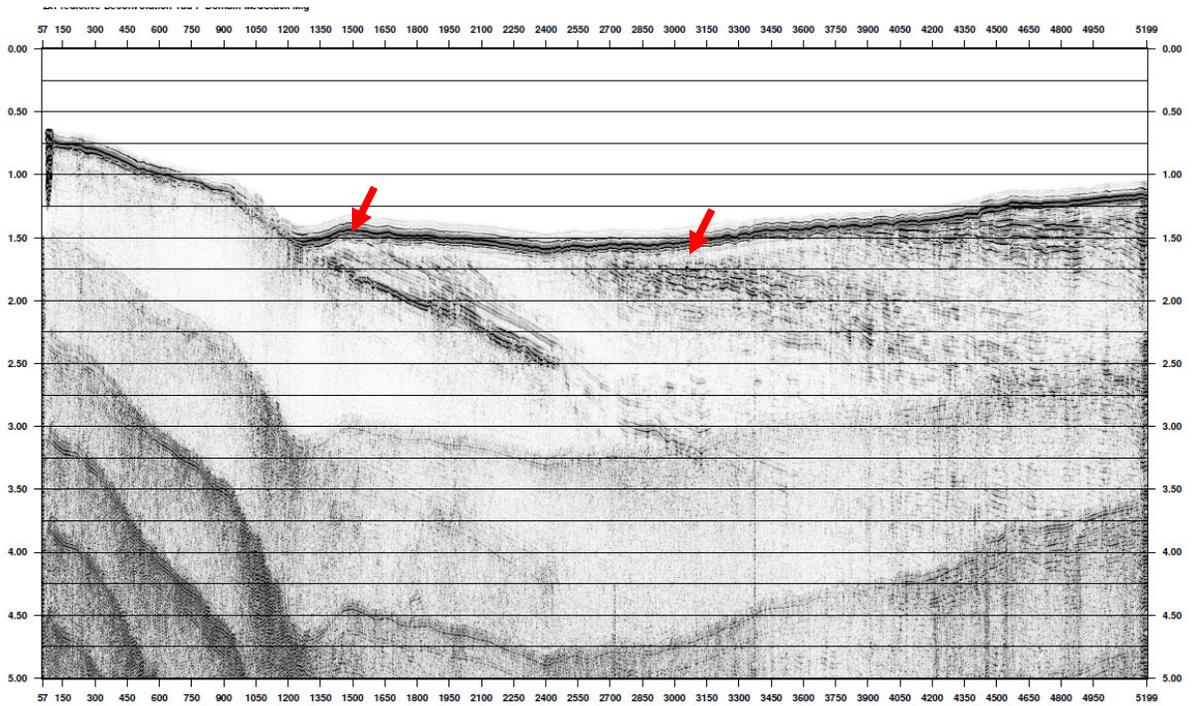
Figure 4.18: Result of Predictive deconvolution in linear Radon domain. Arrows indicate suppressed primaries under the seafloor.
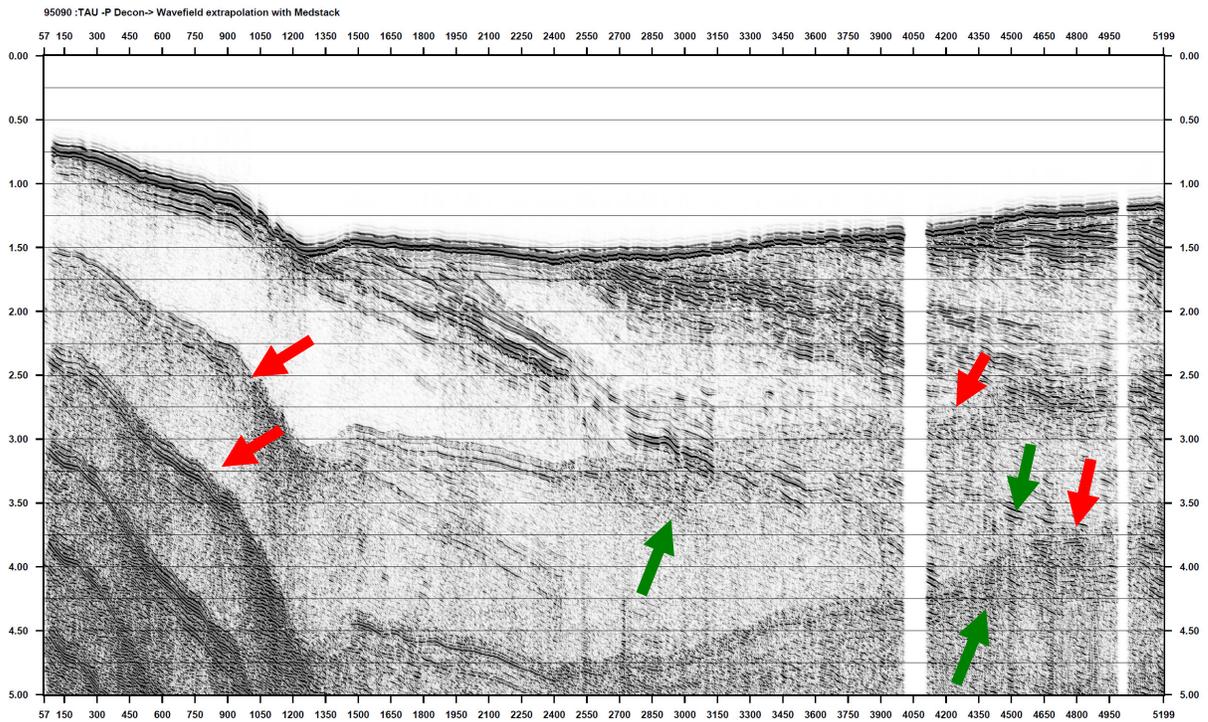


Figure 4.19: Result of SRME after predictive deconvolution. Red arrow indicates multiples or suppressed multiples and green arrow indicates primaries.

A comparison of amplitude gain after multiple suppression with ZMULT, PRADMUS and SRME (Fig 4.20) show that all the methods significantly suppress multiples (more than 10 dB for first

order). With ZMULT and PRADMUS, the underlying primary signals are not very well enhanced consequently the primaries continue to be masked under the noise band of suppressed multiples. With SRME, not only are the multiples suppressed but also the primary signals well preserved.
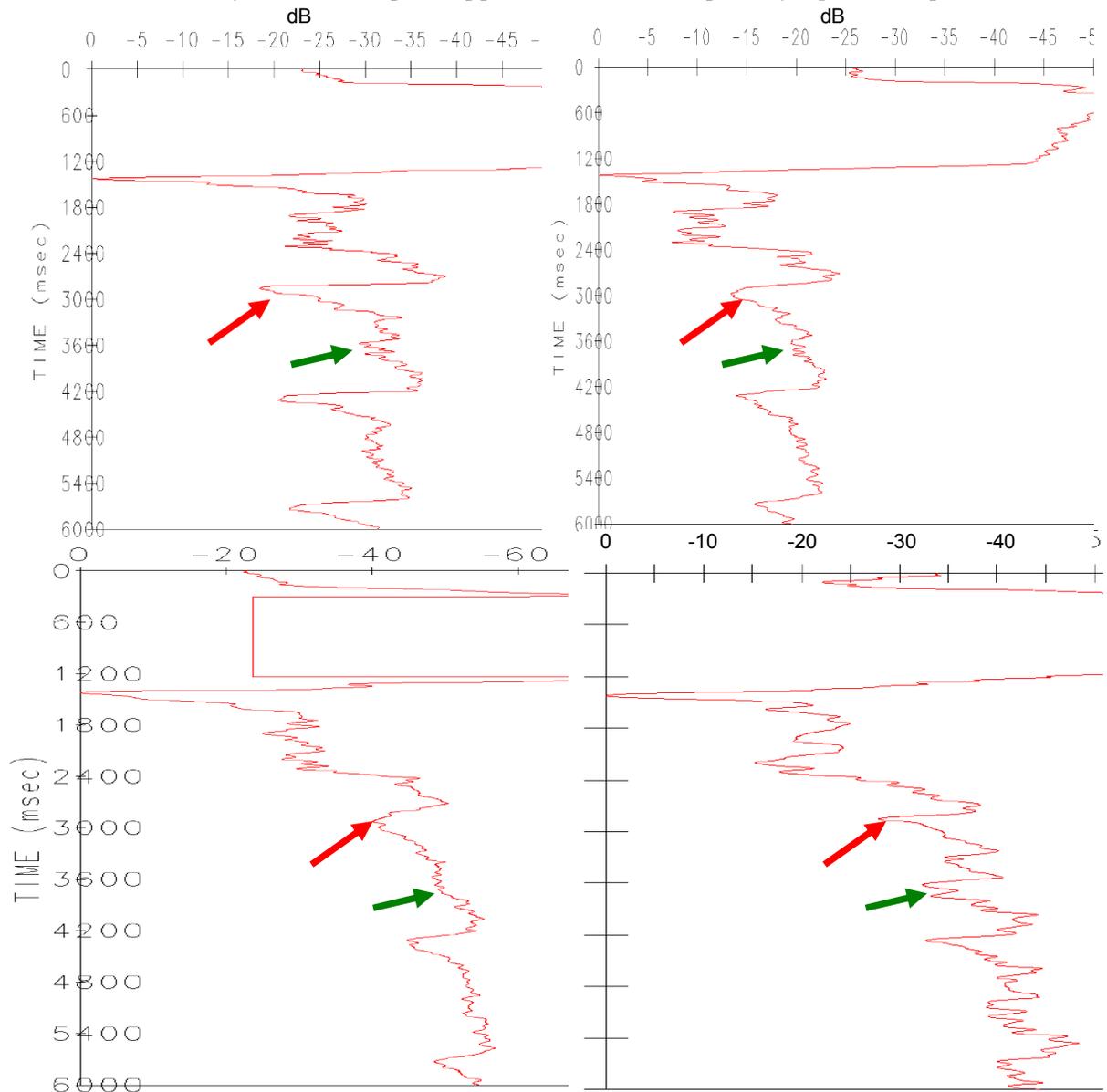


Figure 4.20: Comparison of amplitude gain of stacked traces after multiple suppression from CDP 3800 to CDP 3900 in profile AWI-95090. a) without multiple suppression b) after ZMULT c) after PRADMUS d) after SRME. Red arrows indicate multiples and green arrow indicate primaries.

## 4.4. Influence of Signal to Noise Ratio (SNR)

A comparison of amplitude from traces of poorly suppressed is done against traces where multiples are well suppressed. A sample of individual traces are shown in Figure 4.21. CDP 1500 and 2700 from profile AWI-95060 where the multiples are well suppressed show exponential damping of

amplitude again that one would expect to see of signals from deeper structures with occasional sharp  excursions that are related to seafloor multiples.

In CDPs 500 and 5400, subsurface multiples have large footprint and are much stronger than the primaries just above it by at least 10 dB if not more. In profile AWI-95062, CDP 900 and 1800 does not display an exponential decrease with depth, rather a weak linear decrease in amplitude with depth. The linear decrease is a result of  convolution of strong multiples from the subsurface (SRM) with weak primaries. The primary reflector of the seafloor shows a strong amplitude which is more than twice as in CDP 1500 and 2700 of profile AWI-95060 implies that most of the icident energy is reflected at the seafloor.

In profile AWI-95090, the amplitude in CDP 2800 and 4200 show a rapid decrease with depth and are almost equal to the noise in the water column.  With a low signal to noise ratio, multiple suppression is not very effective.
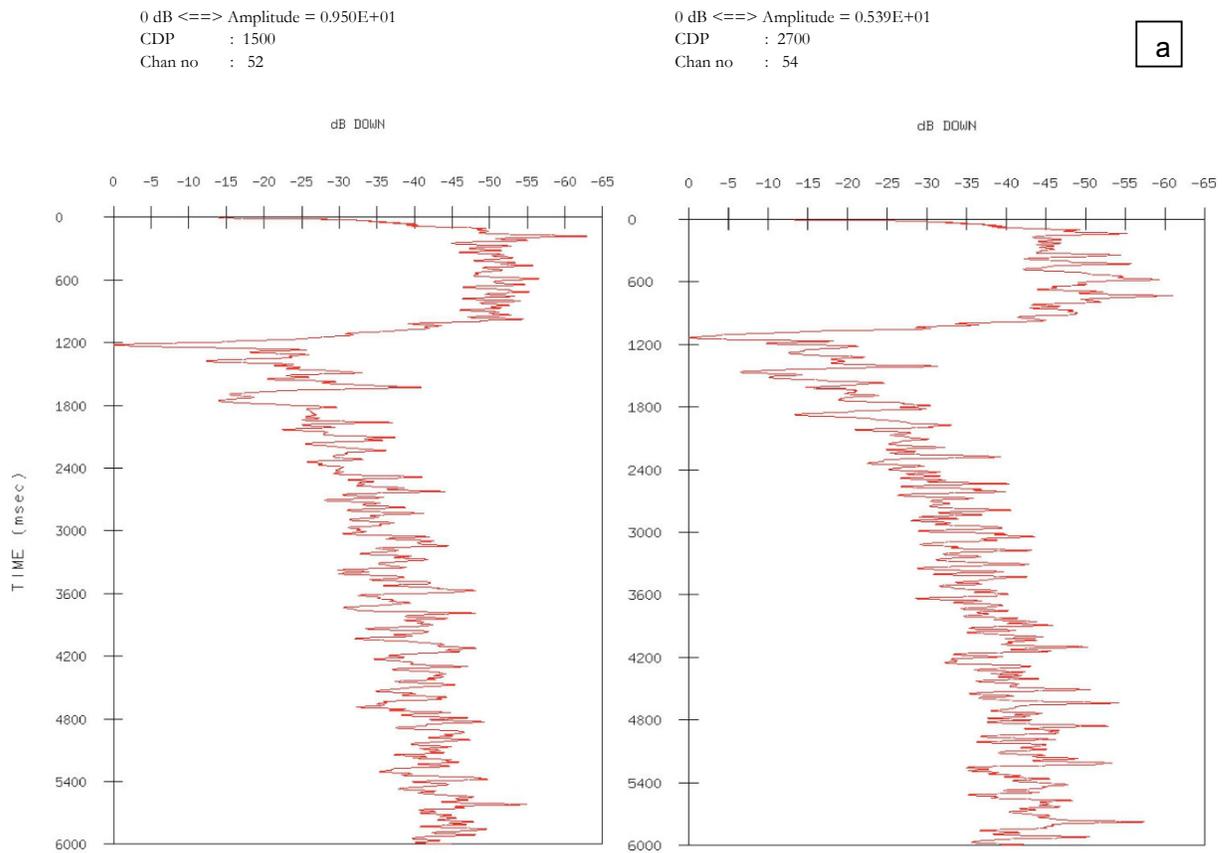
0 dB <==> Amplitude = 0.558E+01
CDP        : 500
Chan no   : 52

0 dB <==> Amplitude = 0.907E+01
CDP        : 5400
Chan no   : 52

dB DOWN

dB DOWN
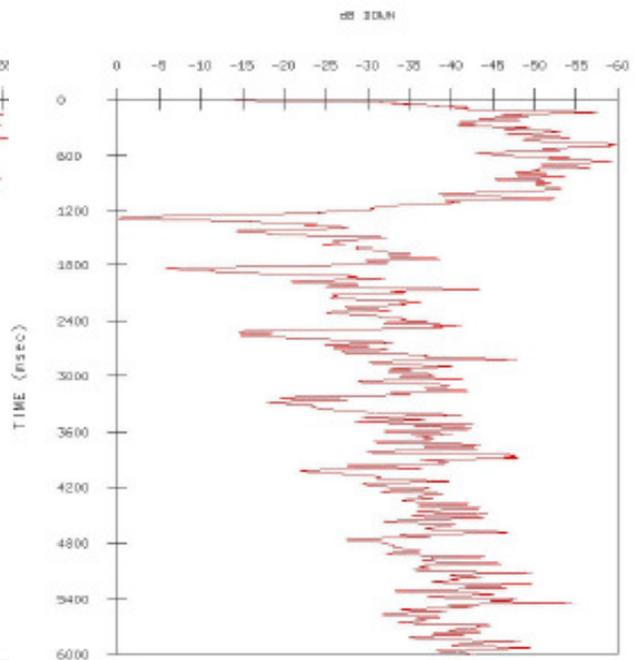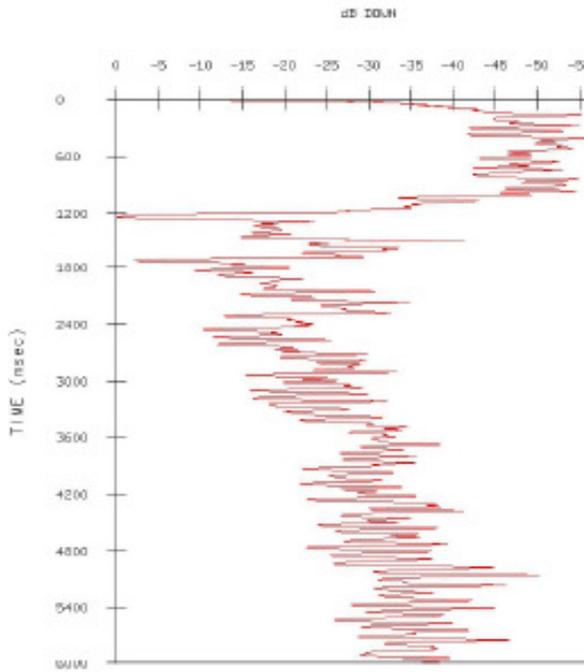
0 dB <==> Amplitude = 0.124E+02
CDP        : 900
Chan no   : 50

0 dB <==> Amplitude = 0.106E+02
CDP        : 500
Chan no   : 52

dB DOWN

dB DOWN
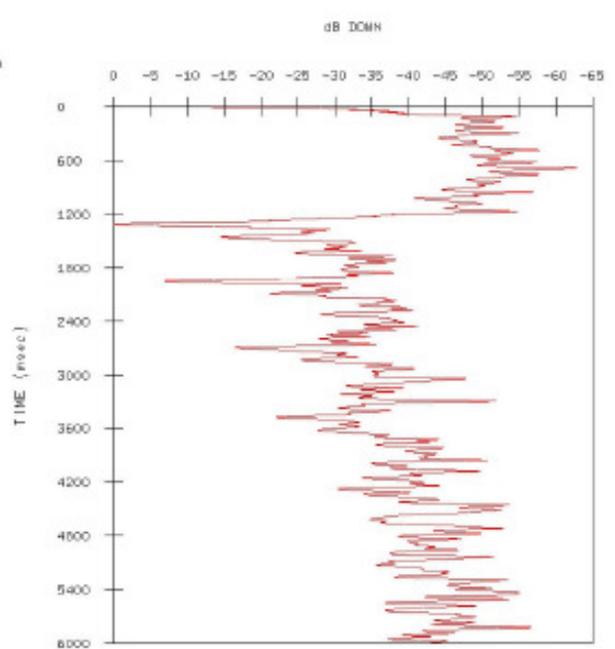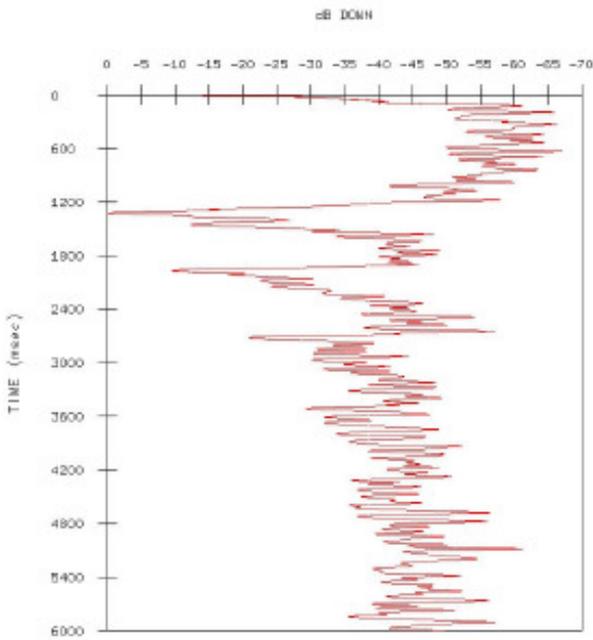
0 dB <==> Amplitude = 0.418E+01
CDP : 2800
Chan no : 51

0 dB <==> Amplitude = 0.828E+01
CDP : 4800
Chan no : 52
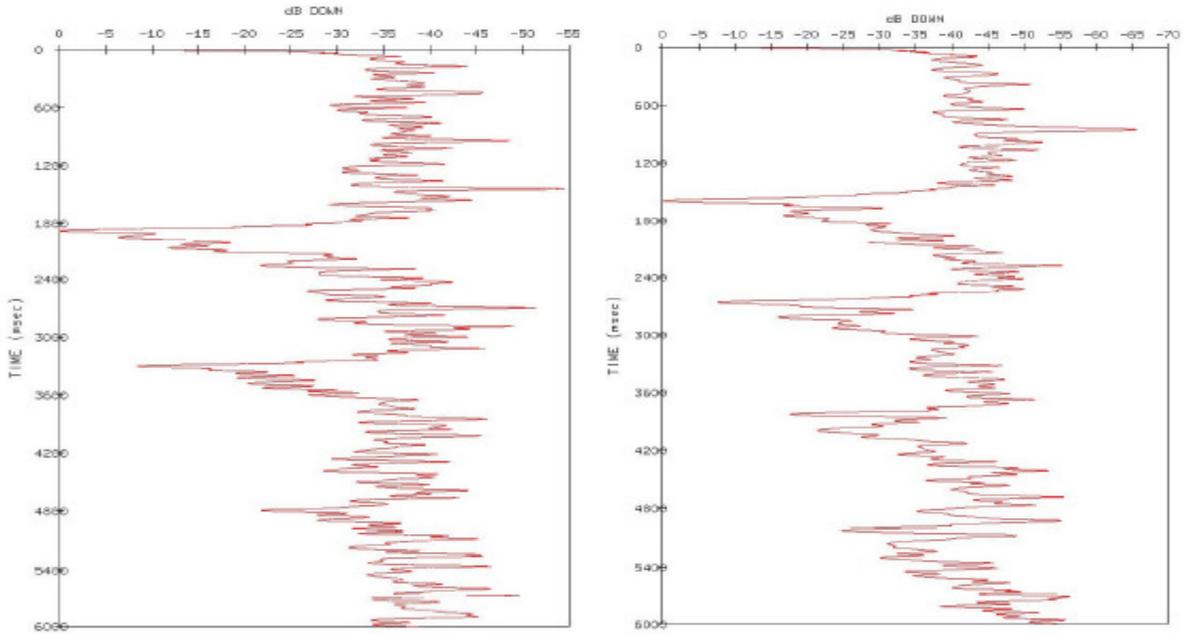


Figure 4.21: Amplitude gain funtion of sample traces from unprocessed seismic gather. A) gain function of traces where multiples are well suppressed in profiles AWI-95060. B), C) and D) are traces with poorly suppressed multiples. (Note: All traces have approximate same offset of 1544 m)

## 4.5. Bathymetry

Weddell sea is characterized by 3 troughs namely, Ronne trough, Filchner trough and Hughes trough that are located at either sides and middle of the shelf. Fig 4.21 shows the bathymetry of the Weddell Sea embayment obtained from Gebco. The ship bathymetry is similar to the Gebco but lacks coverage of the entire area. The troughs are a result of erosion from ice streams originating in WAIS and EAIS. Multibeam beam data from the ship has been analysed by Stolldorf and others (2012). They observe mega scale glacial lineations (MGSL) that are 200-500 m wide with an amplitude of 4-10 m in the Ronne trough. In Hughes trough, MGSL are 300 - 600 m wide with an amplitude of 3-7 m. There are similar geomorphologic features in the Filchner trough but are confined to the exposed basement and are not considered to be MGSL. Iceberg furrows, charaterised by their random orientation, are found in the Southern and Eastern part of the Weddell sea (Stolldorf et al, 2012).
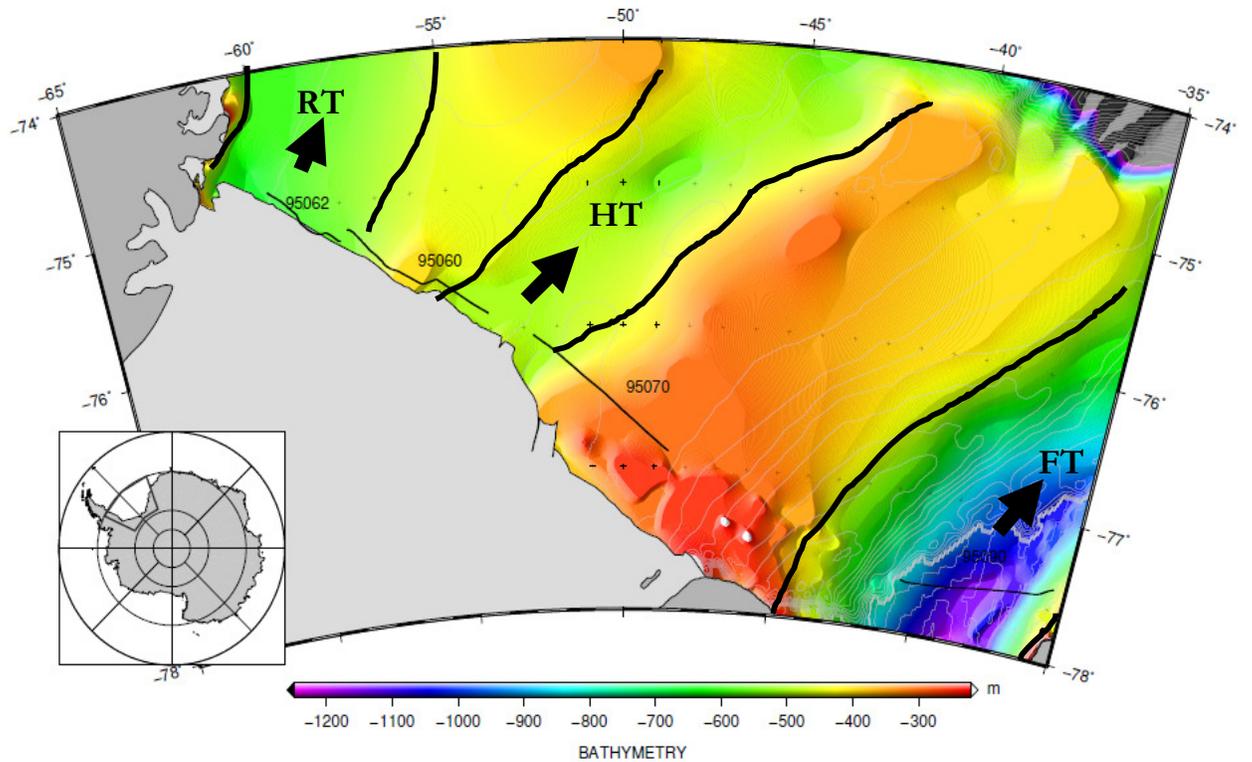
Figure 4.22: Bathymetry map of the Weddell Sea showing Ronne (RT), Hughes (HT) and Filchner (FT) troughs. Processed seismic lines (thin black line) are acquired in the troughs. Arrows indcate flow direction of ice streams

In general, it is observed that multiple suppression results are rather poor in the troughs. Analysis of surface velocities with local bathymetry show higher velocity in the trough, which indicates a harder seafloor while the surface velocity decreases away from the trough (Fig 4.23). The degree of multiple suppression inversely correlates to the surface velocities and can be clearly seen by comparing the results in Ronne trough (Profile AWI-95062) to the bathymetric high between Hughes and Filchner trough (Profile AWI-95070).
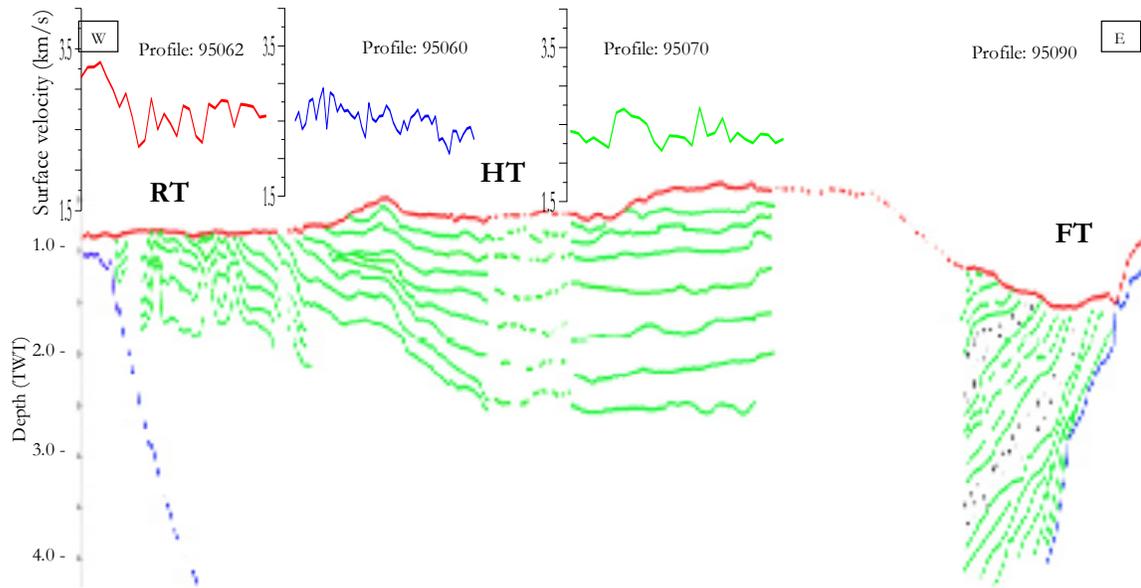
Figure 4.23: Basin profile model and surface velocities of Weddell Sea as interpreted from seismic lines AWI-95060, AWI-96062, AWI-95070 and AWI-95090. The seafloor is shown in red, sedimentary sequence in green and acoustic basement in blue. Broken lines between profiles are approximations ( note: model is not to scale in horizontal direction)

## 4.6. Evolution Of Weddell Sea Embayment

In lieu of a technical nature of this thesis, only a brief description of subsurface features and its likely interpretation is done. There is a prominent listric fault in the Filchner trough close to the East Antarctic craton (Profile 95090 ~CDP 2400). There maybe other similar faults in the region (CDP 5100? ). This indicates a extensional regime in the crust and supports the model of a stretched continental crust suggested by various authors (Storey et al 1991; Huebscher et al, 1996; Studinger & Miller, 1999). Across the Weddell Sea, west of Berkner Island, sediment deposition show almost horizontal stratification. Refraction Seismic data indicate sediment thickness exceeding 15-25 km (Huebscher et al, 1996).

On the Eastern margin of the Antarctic Peninsula, the shelf is characterized by at least 3 Mesozoic folded sediment packages. The folding extends further onto the shelf and has been observed in seismic data acquired further down the shelf during an expedition in 1990 (Huebscher et al, 1996). These structures maybe related to compressional tectonics as weak zones that failed to accomodate the change in tension. The steps or wave-like structure observed between CDP 100 of profile 95062 and CDP 2000 could be related to listric faults in regions where sedimentation rate is not as

fast as extension/subsidence (see Fig 4.24). Velocity models derived from refraction seismics also show evidence of listric faults located at ~ 10 km depth (see appendix A.1) that look similar to the illustration in Fig 4.23. However, the result of folding in the back-arc region creating wave-like structures may not be excluded. The dipping of layers towards the basin and almost horizontal layers in the centre of the basin support the presence of rifts under the Ronne shelf. There is no information to comment on the timing of the folds or the faults.
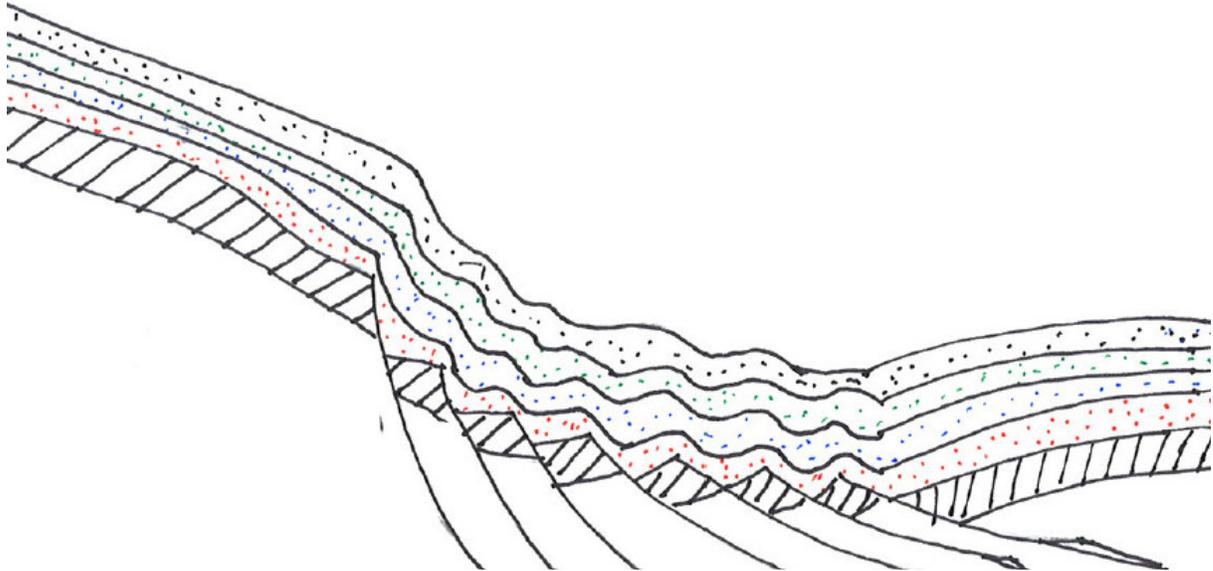


Figure 4.24: Schematic diagram of listric faults in an extentional tectonic regime. The sedimentation rate is less than the extension / subsidence rate.

Alternating well-stratified units and transparent units dipping seawards in the Filchner trough is a typical feature that has been observed around the Antarctic (Fig 4.25), for example, in Amudsen Sea (Weigelt et al )and Ross Sea (Anderson 1999). As suggested by the authors, this typical structure might relate to glacial-interglacial periods when the region was subjected to alternate periods of glacial and open ocean conditions. Sediment cores in this region display distal glacial sediments underlain by proximal glacial sediments (Stolldorf et al, 2012). In a depositional regime, transparent or weaky reflecting units are an indicator for poorly sorted homogenous units and /or strong reflection from point sources, in this case , till. The source for glacial deposition is found to be of East Antarctic origin (Stolldorf et al, 2012).
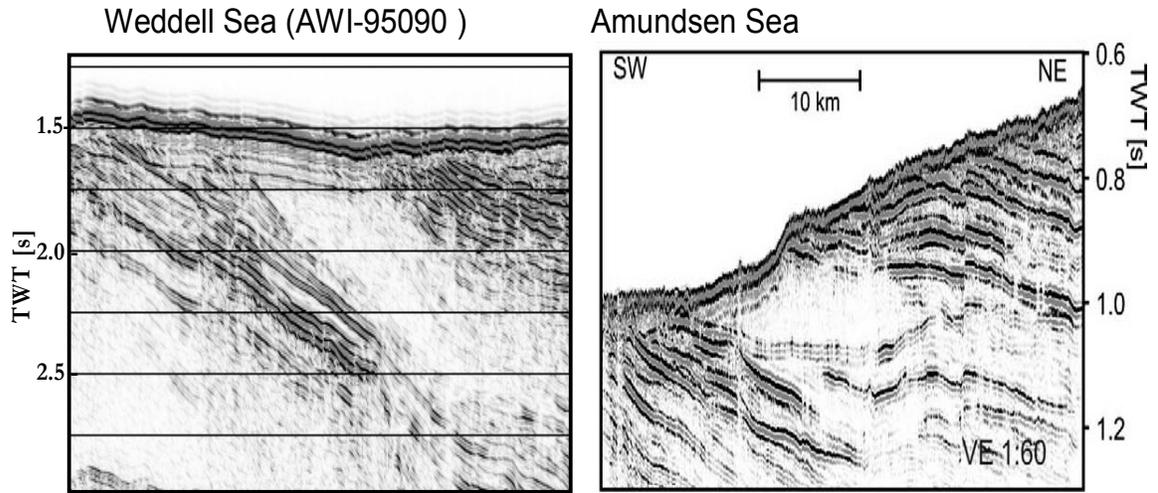
Figure 4.25: Comaprison of seismic profiles from Weddell Sea (AWI-95090) and Amundsen Sea (Weigelt et al, 2009). Both profiles show alternating well stratified and reflection poor units

# Chapter 5.    Conclusions

The multiple suppression methods applied have a been fairly successful in achieving their objectives. The success of multiple suppression is dependent on several conditions. Signal to noise ratio (SNR) and depth of multiples are the primary parameters that determines the suppresion of multiples and enhancing the underlying primary events. SNR ultimately depends on physical properties of the medium and geometry of the features. The Weddell Sea shelf consists of highly consolidated sediments that reflect most of the incident seismic energy.  Strong attenuation of primaries in the subsurface convolved with strong multiples have been primary reason for poor multiple suppression results in some sections of the processed data. Limited far-offset range restricts move-out based methods to distinguish primary and multiple reflectors in deeper structures.

For shallow to intermediate depths, F-K filtering is the most efficient method in terms of computational time and quality. It is effective for suppressing first and second order sea bottom multiples and surface related multiples from the subsurface. It fails however to suppress higher order multiples and deep water multiples where the NMO difference is not very large.

Parabolic radon transformation is a very effective method to suppress multiples that are not very strong. As observed in profile AWI-95060 and  AWI-95062, strong multiples leak in to the X-T domain because of imperfect transformation. An advantage of this method is that the random noise is also filtered out because of the transformation to the Radon domain.  A major drawback of this method is the exceptionally long computation time required to achieve good quality results. The degree of suppression is also relies on the accuracy of the velocity model. However, the transformation cannot be done several times as the approximations made during the process result in traces to have a wiggle worm like appearance. Like other move-out time difference method, it is also restricted with streamer length but, unlike F-K filtering, it can differentiate even small difference as long as a good velocity model is available.

Predictive deconvolution in Tau-P domain is a good solution to suppress multiples when move-out time based methods do not work. It suppress multiples very well in the near offset efficiently. It is not very effcient however for  long period multiples as the correlation with

primaries is significantly reduced. Using a large value for white noise results in strong suppression of primaries near the seafloor which results from strong correlation of signals .

SRME although very promising method  is a very much restricted by it is constraints. It is severely limited by acquisition set up and depends heavily on subsequent shot gathers and receiver interval. Sparse density of shots and traces have a significant influence in the outcome of multiple predicition (see appendix C). When all the conditions are satisfied, the reconstruction of multiples is excellent. The adaptive subtraction part, however, is not very efficient for first and second order multiples. This problem maybe solved in the future as successful applications with custom designed algorithms have been published to accomodate this shortcoming (e.g. Berkhout, 1981; Zhou & Greenhalgh, 1996; Guitton, 1999; Dragoset, 1999; Verschuur, 1999) albeit they may address specific situations.

It can be concluded that the choice of multiple suppression method depends on the target subject to the fulfillment of constraints of the method ( example streamer length, shot/receiver interval). A combination of different  methods, with respect to the principle used, may improve the results in some cases when individual methods do not yield sufficient results, like predicitive deconvolution and SRME demonstrated in this thesis.

# Bibliography

Anderson, J. B., 1999, Antarctic marine geology, Vol. 289. Cambridge, UK: Cambridge University Press.

Anderson, J. B., Shipp, S. S., and Siringanf, P., 1992. Preliminary seismic stratigraphy of the northwestern Weddell Sea continental shelf. In YOSHIDAY,. ,K AMINUMKA., & SHIRAISKH.,I , eds. Recent progress in Antarctic earth sciences. Tokyo: Terra Scientific Publishing Company, 603-612.

Bentley, M. J., and Anderson, J. B., 1998. Glacial and marine geological evidence for the ice sheet configuration in the Weddell Sea–Antarctic Peninsula region during the Last Glacial Maximum. Antarctic Science,10, pp 309325 doi:10.1017/S0954102098000388

Cooper, A., Brancolini, G., Escutia, C., Kristoffersen, Y., Larter, R., Leitchenkov, G., O'Brien, P., and Jokat, W., 2009. Cenozoic Climate History from Seismic Reflection and Drilling Studies on the Antarctic Continental Margin. In: F. Florindo and M. Siegert (eds), Developmentsin Earth & Environmental Sciences, 8, Antarctic Climate Evolution, Elsevier B.V., p. 144-161. doi: 10.1016/S1571-9197/(08)00005-0.

Dalziel, I. W., and Grunow, A. M., 1992. Late Gondwanide tectonic rotations within Gondwanaland. Tectonics, 11(3), 603-606.

Denton, H., PRENTICEM, L. and BURCKLEL, H., 1991. Cainozoic history of the Antarctic Ice Sheet. In TINGEV, R.J., ed. Thegeology of Antarctica. Oxford: Clarendon Press, 365-433.

Dragoset, W. H., and Jericevic, Z., 1998. Some remarks on surface multiple attenuation: Geophysics, 63, no. 02s, 772-789.

Weigelt, E., Gohl, K., Uenzelmann-Neben, G. and Larter, R. D., 2009. Late Cenozoic ice sheet cyclicity in the western Amundsen Sea Embayment—Evidence from seismic records. Global and Planetary Change, 69(3), 162-169.

Fahrbache, T., Schroderm, L., and Klepikova, 1998. Circulation and water masses in the Weddell Sea. In: Lepparantma., (ed.) Physics of Ice-Covered Seas. Lecture notes from a summer school in Savonlinna,Finland, Helsinki University, 569-603.

Fechner, N., and Jokat, W., 1996. Seismic refraction investigations on the crustal structure of the western Jameson Land Basin, East Greenland. Journal of geophysical research, 101(B7), 15867-15.

Grunow, A. M., Kent, D. W., and Dalziel, I. W. D., 1987. Mesozoic evolution of the West Antarctica and the Weddell Sea Basin: New paleomagnetic constraints, Earth Planet. Sci. Lett., 86, 16–26.

Grunow, A. M., 1993, New paleomagnetic data from the Antarctic Peninsula and their tectonic implications. Journal of Geophysical Research 98(B8):13815–13833

Huebscher, C., Jokat, W., and Miller, H., 1996. Structure and origin of southern Weddell Sea crust; results and implications, edited by Storey, B. C., King, E. C., and Livermore, R. A., Weddell Sea tectonics and Gondwana break-up: Geological Society Special Publications: London, Geological Society of London, p. 201-211.

Hughes, T., 1973. Is the West Antarctic ice sheet disintegrating?. Journal of Geophysical Research, 78(33), 7884-7910.

Hughes, T. J., 1977. West Antarctic ice streams : Reviews of Geophysics, v. 15, p. 1-46.

Hughes, T. J., 1981. The Weak Underbelly of the West Antarctic Ice-Sheet: 518.Earth Science Faculty Scholarship. Paper 156.

Jokat, W., N. Fechner, and M. Studinger, 1997, Geodynamic models of the Weddell Sea embayment in view of new geophysical data, in The Antarctic Region: Geological Evolution and Processes, edited by C. A. Ricci, pp. 453–459, Terra Antarct., Siena, Italy.

Jokat, W., T. Boebel, M. König, and U. Meyer (2003), Timing and geometry of early Gondwana breakup, J. Geophys. Res., 108, 2428, doi:10.1029/2002JB001802.

Jokat, W., and Oerter, H., 1997. The Expedition ANTARKTIS-XII of RV Polarstern in 1995: Report of Leg ANT-XII/3. Berichte zur Polarforschung, 219, 1. Alfred-Wegener-Institut fuer Polar-und Meeresforschung, Bremerhaven (Germany)

King, E. C., and Bell, A. C., 1996. New seismic data from the Ronne Ice shelf, Antarctica. Geological Society, London, Special Publications, 108(1), 213-226.

Mayne, W. H., 1962. Common reflection point horizontal data stacking techniques. Geophysics, December 1962 v. 27 no. 6 p. 927-938

Nicholls, K. W., Østerhus, S., Makinson, K., Gammelsrød, T., and Fahrbach, E., 2009. Ice-ocean processes over thecontinental shelf of the southern Weddell Sea, Antarctica: A review, Rev. Geophys., 47, RG3003, doi:10.1029/2007RG000250

Maslanyj, M. P. and Storey, B. C., 1990. Regional aeromagnetic anomalies in Ellsworth Land: crustal structure and Mesozoic microplate boundaries within West Antarctica. Tectonics, 9(6), 1515-1532.

Michels, K., Kuhn, G., Hillenbrand, C., Diekmann, B., Fütterer, D., Grobe, H. and Uenzelmann-Neben, G. 2006 The southern Weddell Sea: combined contourite-turbidite sedimentation at the southeastern margin of the Weddell Gyre: Stow, D A V; Pudsey, C; Howe, J C; Faugères, J-C & Viana, A R (eds.), Deep-water contourite systems: modern drifts and ancient series, seismic and sedimentary characteristics. Geological Society of London, Memoirs, London .hdl:10013/epic.32118

Millar, I. L., and Pankhurst, R. J., 1987, Rb-Sr geochronology of the region between the Antarctic Peninsula and the Transantarctic Mountains: Haag Nunataks and Mesozoic granitoids, in McKenzie, G. D., ed., Gondwana Six: Structure, tectonics, and geophysics: Washington, D.C., American Geophysical Union, Geophysical Monograph 40, p. 151–160.

Pankhurst, R. J., 1982. Rb-Sr geochronology of Graham Land, Antarctica. Journal of the Geological Society, 139(6), 701-711.

Robinson, E. A., 1954, Predictive decomposition of time series with application to seismic exploration: reprinted in Geophysics, 1967 , 32, 418–484.

Schopf, J. M., 1969. Ellsworth Mountains: position in West Antarctica due to sea-floor spreading. Science, 164, 63-66.

Sloan, B. J., Lawver L.A . and Anderson J. B, . 1995. Seismic stratigraphy of the Palmer Basin. Antarctic Research Series, 68, 235-260.

Stolldorf, T., Schenke, H., and Anderson, J. B., 2012 . LGM ice sheet extent in the Weddell Sea: evidence for diachronous behavior of Antarctic Ice Sheets. Quaternary Science Reviews, Volume 48, p. 20-31. DOI: 10.1016/j.quascirev.2012.05.017

Storey, B. C., Pankhurst, R. J. and Johnson, A. C., 1994. The Grenville Province within Antarctica: a test of the SWEAT hypothesis. Journal of the Geological Society, 151(1), 1-4.

Storey, B. C., Vaughan A. P. M. and Millar I. L., 1996. Geodynamic evolution of the Antarctic Peninsula during Mesozoic times and its bearing on Weddell Sea history. Geological Society, London, Special Publications January 1, 1996, v. 108, p. 87-103 , doi: 10.1144/GSL.SP.1996.108.01.07

Storey, B. C., Hole, M. J., Pankhurst, R. J., Miller, I. L., and Vennum, W., 1988. Middle Jurassic within-plate granites in West Antarctica and their bearing on the break-up of Gondwanaland: Journal of the Geological Society of London, v. 145, p. 999-1007.

Studinger, M., and Miller, H., 1999. Crustal structure of the Filchner-Ronne Shelf and Coats Land, Antarctica from gravity and magnetic data: implications for the breakup of Gondwana, J. Geophys. Res., 104(B9), 20379-20394.

Weber, W., 1982. Beitrag zu Geologie des Pensacola-Gebirges (Antarktika): Freiberger Forschungshefte, Reihe C, v. 371, p. 41–96.

Weertman, J., 1972. General theory of water flow at the base of a glacier or ice sheet. Reviews of Geophysics, 10(1), 287-333.

Verschuur, D. J., 2006, Seismic Multiple Removal Techniques: Past, Present and Future, EAGE publications

Yilmaz, O., 1987. Seismic Data Processing. SEG.

# Appendix

## A. Velocity Models
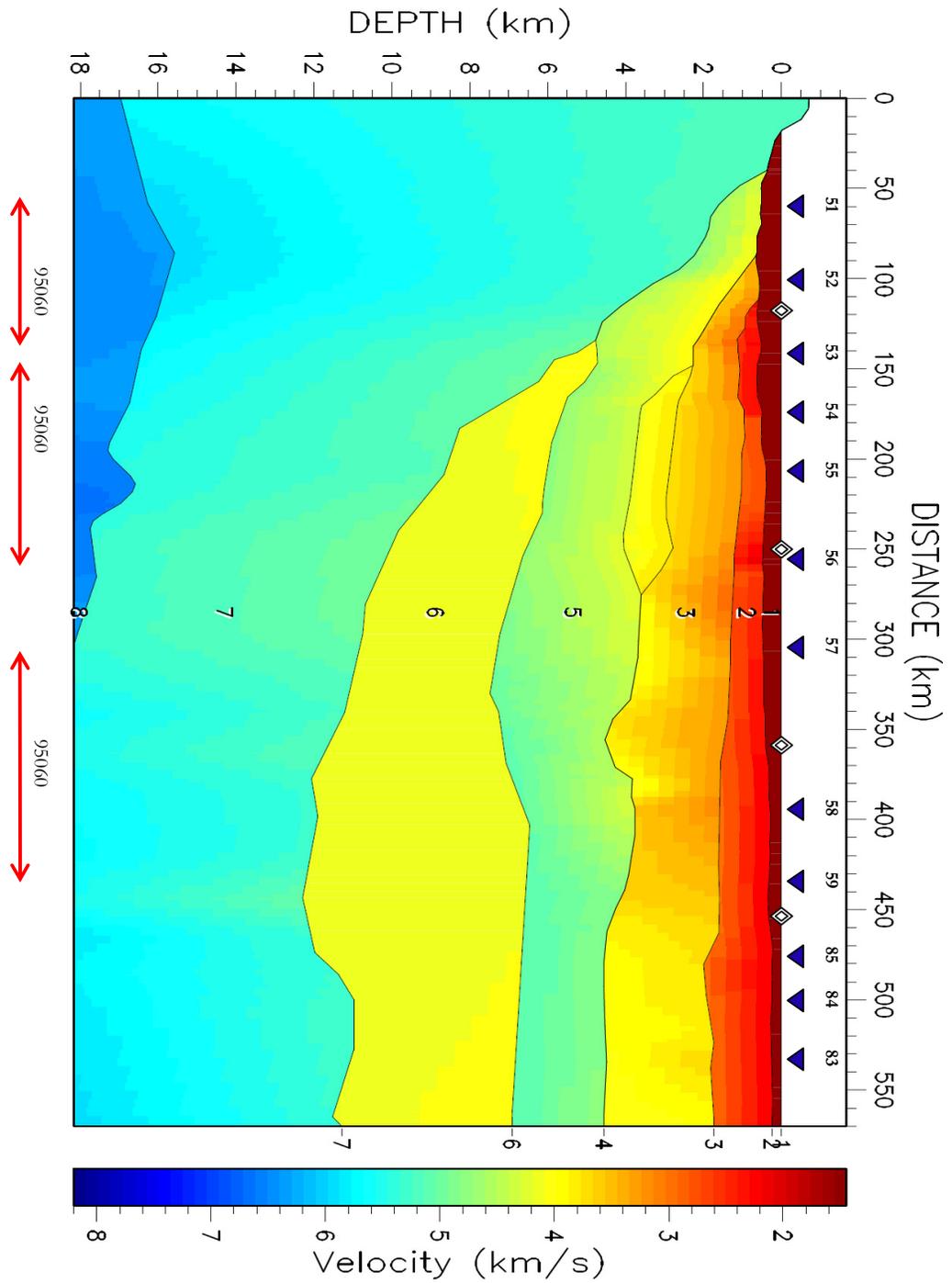


Figure A.1: Velocity model derived from refraction seismics. (Figure contribution: U. Herter)
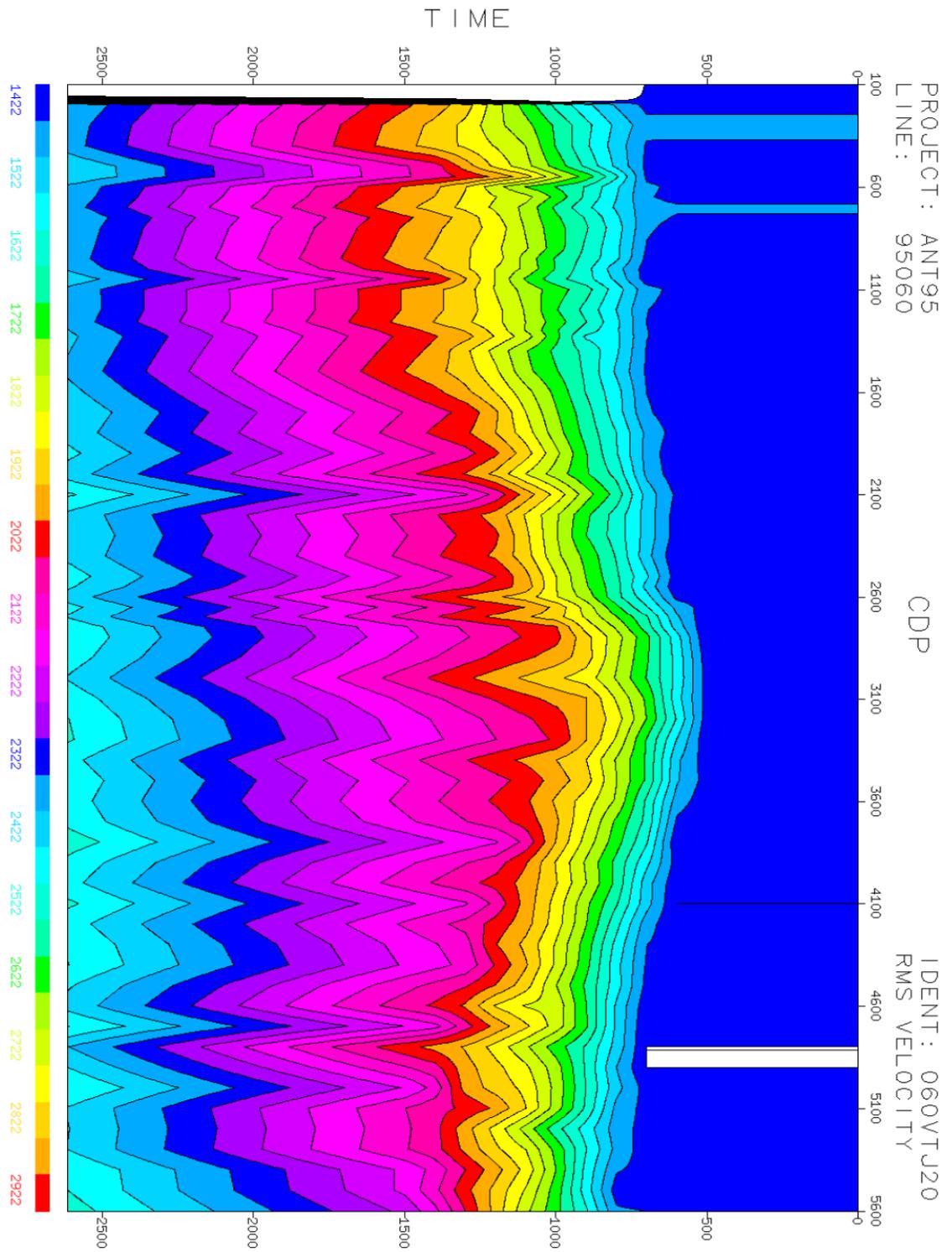
Figure A.2 : Velocity model (rms) of profile AWI-95060
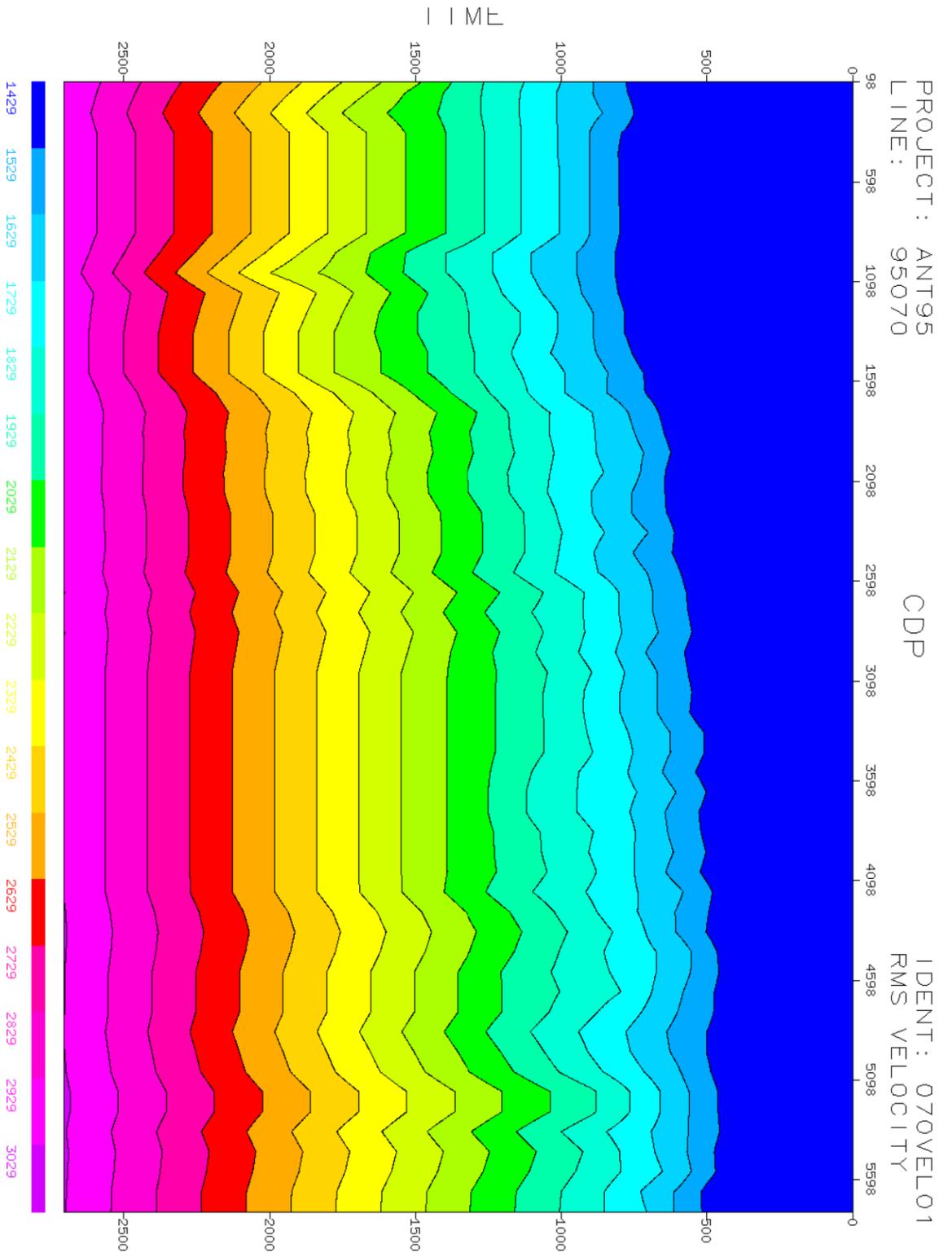
Figure A.3 : Velocity model (rms) of profile AWI-95070
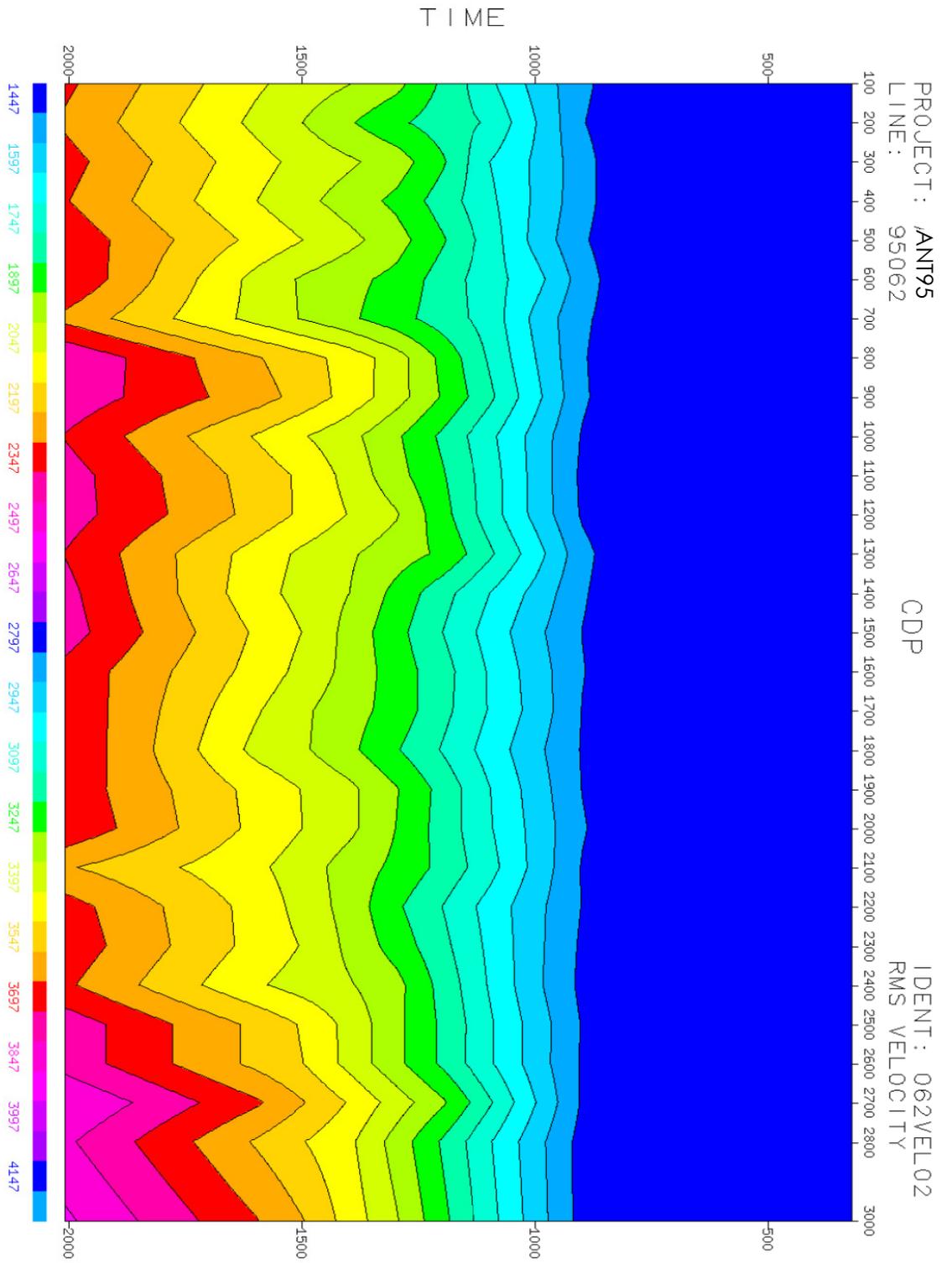
Figure A.4 : Velocity model (rms) of profile AWI-95062
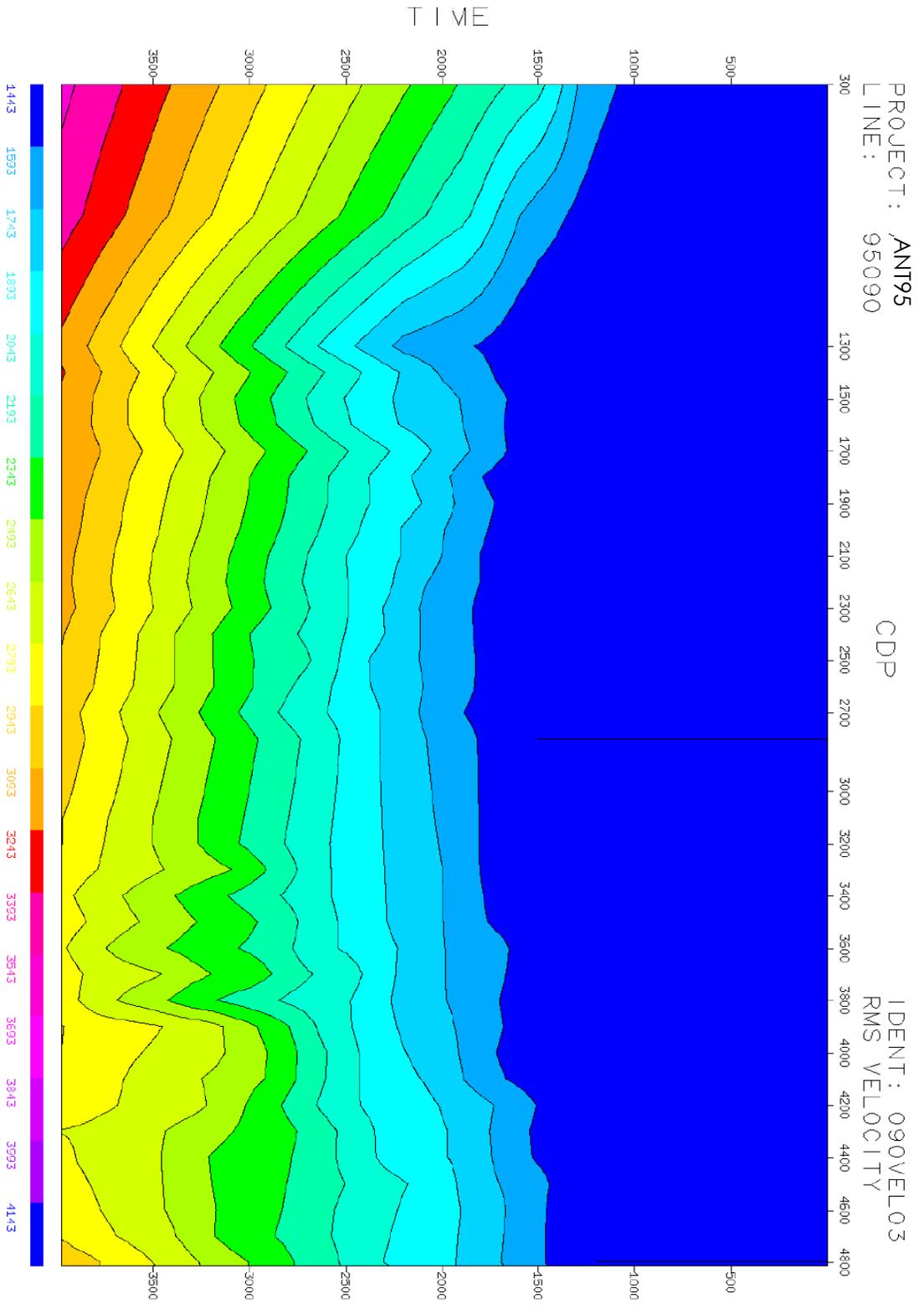
Figure A.5 : Velocity model (rms) of profile AWI-95090

## B. Seismic data processing scripts for DISCO

1. Multiple suppression with ZMULT for profile AWI-95060

```
*JOB    ANT95   95060
*CALL   IN      11776
SRCHSTR
/seissrv1/projects/ant95/95060/*
FILNAM
(ieee)/seissrv1/data/ju_95060_InputMute
CATNAM
ju_95060_InputMute
ORDER
RANGE   3000    4645    1       1
**
*CALL   FILTER  CDP
BAND
        5000    10      20      50      60
5000    8000    10      20      40      50
*CALL   EDIT    CDP     CHAN
SEL     57      5199    KILL
8       55
**
*CALL   NMO     060VTJUF
**
*CALL   NMO     060VTJUF        OVCAPP
OVERC   100
600     2594    250
5500    2594    120
OVERC   3000
450     2594    250
5500    2594    120
OVERC   5600
750     2594    250
5500    2594    120
**
*CALL   ZMULT   500     20              2       500     11000
**
*CALL   NMO     060VTJUF        OVCREM
OVERC   100
600     2594    250
5500    2594    120
OVERC   3000
450     2594    250
5500    2594    120
OVERC   5600
750     2594    250
5500    2594    120
```

```
*CALL    FILTER  CDP
BAND
        11000   10      20      50      60
**
*CALL   DSKWRT  /seissrv1/data/ju_95060_OVC_ZMULT_unstk_Zmult
*CALL   MEDSTK
TRIM
**
*CALL   DSKWRT  /seissrv1/data/ju_95060_OVC_Zmult_stk
**
*CALL   PSPLOT          VDEN    14      8
FILE
/seissrv1/projects/ant95/95060/plots/OVC_Zmult_medstk.ps
VAWGPRM         1
MAXTR   100000
SETAMP
GAIN
VDENPRM LINEAR
TRANGE          5000
PGPARM  1       1       LAND    8
TITLE
95060 Gain(SphDiv)NMOOVC Zmult MedStack
TRLABEL
TLABEL  0.5
TLGRID  0.25
*END
```

2. Multiple suppression with PRADMUS for profile  AWI -95062

```
*JOB     ANT95   95062
*CALL    IN      11776
SRCHSTR
/seissrv1/projects/ant95/data-proc-rfl/*
FILNAM
/seissrv1/projects/ant95/data-proc-rfl/062cdpsort
ORDER
RANGE    57      3089    1
**
*CALL    FILTER  CDP
BAND
         5000    10      20      50      60
5000     8000    10      20      40      50
**
*CALL    NMO     062VEL03
*CALL    MUTE    CDP
STRETCH 20       062VEL03
**
***CALL   MUTE    cdp     chan
**STRETCH 25
**
*CALL    PRADMUS                         5       600     2594
FORWARD 450      6000    -10     600     2594
FILTER
         -10     35
INVERSE SUBTRACT
**
*CALL    DSKWRT  /seissrv1/data/ju_95062_pradmus_RWP_unstk
**
*CALL    FILTER  CDP
BAND
         5000    10      20      50      60
5000     8000    10      20      40      50
**
*CALL    GAIN    CDP
SPHDIV                           062VEL03
*CALL    MEDSTK
TRIM
**
*CALL    DSKWRT  /seissrv1/data/ju_95062_pradmus_SUB_stk
**
*CALL    PSPLOT          VDEN    14      8
SETAMP
```

```
FILE
/seissrv1/projects/ant95/95062/plots/ju_95062_pradmus_SUB.ps
VDENPRM LINEAR
GAIN    1
TRANGE  0       5000
PGPARM  1       2       LAND    11
TITLE   10                      CENTER
95062:Parabolic Radon transform - Subtract Multiples
TRLABEL CDP     300             10
TLABEL  1       10                      1
TLTEXT  10
TWT [s]
MAXTR   100000
**TLGRID        0.2
***RESET
*END
```

3.  Multiple suppression with predictive deconvolution in Tau-P domain for profile
AWI -95062


```
*JOB     ANT95   95062
*CALL    IN      11776
SRCHSTR
/seissrv1/projects/ant95/data-proc-rfl/*
FILNAM
/seissrv1/projects/ant95/data-proc-rfl/062cdpsort
ORDER
RANGE    57      3089    1       1
**
*CALL    EDIT    CDP     CHAN
ALL
8        55
**
*CALL    FILTER  CDP
BAND
                 15      20      45      55
*CALL    RADFOR  1       -800    850
VELFUN   062VEL03
*CALL    DECONA  CDP
KEYDEF   1       1       96
GAP      200              60      0.1
100      8000    200     8000
*CALL    DECONA  CDP
KEYDEF   1       1       96
GAP      1200             60       0.1
100      8000    200     8000
*CALL    FILTER  CDP
BAND
                 15      20      45      55
*CALL    RADINV  1       -800    850
VELFUN   062VEL03
*CALL    FILTER  CDP
BAND
                 15      20      45      55
*CALL    DSKWRT  /seissrv1/data/ju_95062-TP-DeCona-unstk
*CALL    GAIN    CDP
SPHDIV                           062VEL03
**
*CALL    NMO     062VEL03
**
*CALL    MEDSTK
TRIM     0.2              50
```

```
**
*CALL    DSKWRT   /seissrv1/data/ju_95062-TP-PreDeCona-Medstk2
**
*CALL    PSPLOT            VDEN    14       8
FILE             /seissrv1/projects/ant95/95062/plots/TP-Decona-
Medstk2.ps
VAWGPRM         1
MAXTR   100000
SETAMP
GAIN
VDENPRM LINEAR
TRANGE           5000
PGPARM  1        1       LAND     8
TITLE
Double Predictive Deconvolution Tau-P Domain MedStack Mig
TRLABEL
TLABEL  0.5
TLGRID  0.25    0.25
*END
```

4.  Multiple suppression with SRME for profile  AWI -95062

```
*JOB     ANT95    95062
*CALL    IN       11776
SRCHSTR
/hs/userf/projects/ant95/data-proc-rfl/*
FILNAM
(ieee)/seissrv1/data/ju_95060_shotDecon
CATNAM
ju_95060_shotDecon
ORDER
RANGE    650     1300     1        1
*CALL    SORT    96       5000
MAJOR    SHOT
MINOR    CHAN
*CALL    FILTER  CDP
BAND
                15      20       50       55
*CALL    GAIN    SHOT     LINEAR
SPHDIV                            062VEL03         PRENMO
**
*CALL    SMACTRM 60       2        20
SPREAD  -2600   -200     25       1000     1
HANDVEL
0       1450    800     1450    1600    1450    5000    1450
*CALL    DSKWRT  /seissrv1/data/ju_95062_TPDeconSmt_smactrm
*CALL    SMACMS  SOFFSET 100      PONLY   2        1
*CALL    NMO     062VEL03         NMOREM
*CALL    DSKWRT  /seissrv1/data/ju_95062_TPDeconSmt_shotsort
```

```
*CALL    SORT    96        5000
MAJOR    CDP
MINOR    CHAN
**
*CALL    NMO     062VEL03
**
*CALL    MEDSTK
TRIM     0.2               50
*CALL    DSKWRT  /seissrv1/data/ju_95062_TPDeconSmt
*END
```

## C. SRME with synthetic profile.
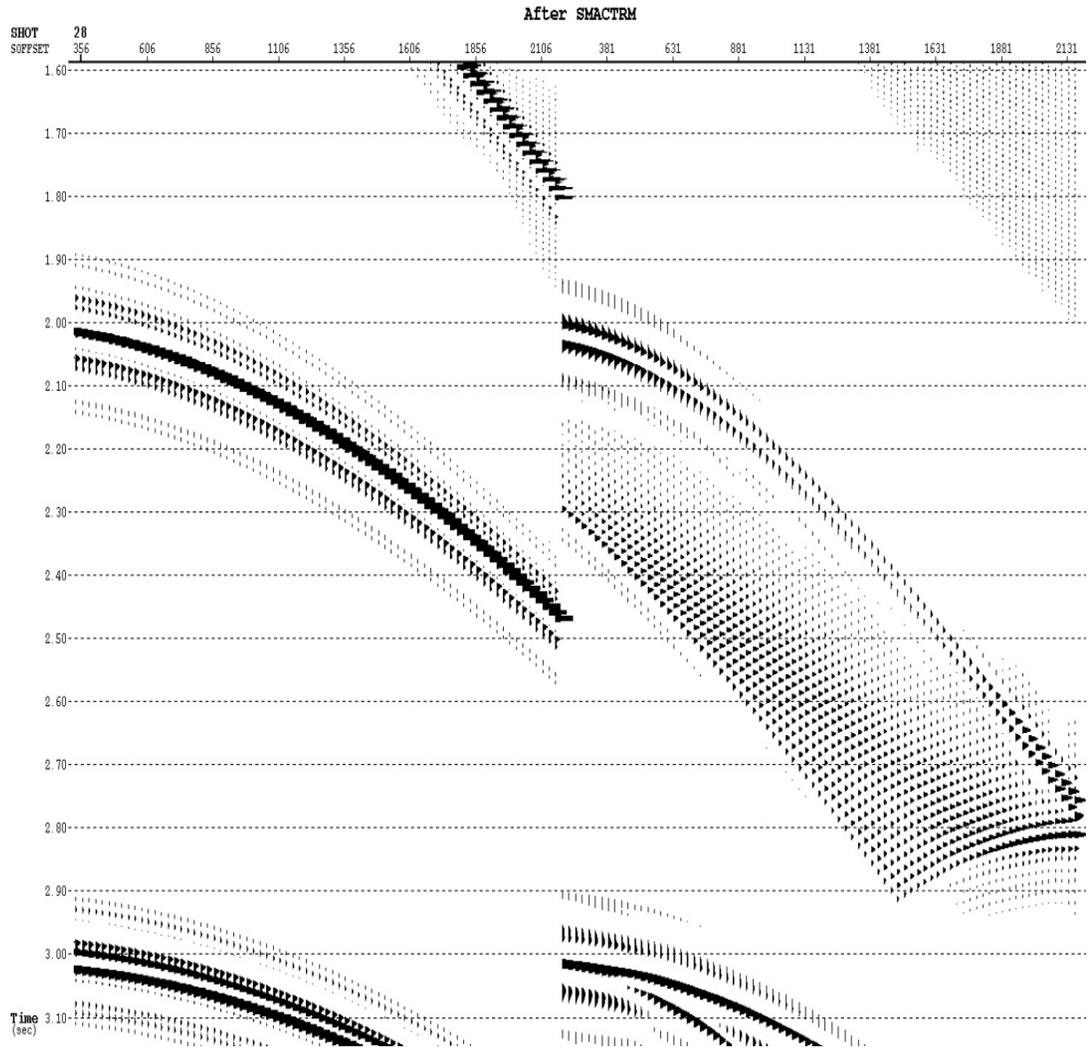


Figure C.1: Multiple prediction  of shot number 28 from a synthetic profile with 30 shots and receiver interval of 25 m. Note, the increasing difference in time of predicted multiples from actual multiples with increasing offset (300 ms at 2594 m offset). Lack of subsequent shots result in wrong prediction.